Development of near real-time assessment system for cancer cells

By

Nahrizul Adib Kadri

A thesis submitted in partial fulfilment for the
degree of Doctor of Philosophy
in the
Faculty of Engineering and Physical Sciences
Centre for Biomedical Engineering

December 2010

Abstract

Dielectrophoresis (DEP) is an electrical phenomenon that occurs when a polarisable particle is placed in non-uniform electrical fields, generating DEP force (F_{DEP}) that is dependent upon the electrophysiological make-up of the particle in use. In cell cytometry studies, DEP offers the advantage of conducting various cell manipulations *in vitro* without the need of specific surface markers. Its drawbacks, namely the time-consuming processes involved and the inability to conduct large batch cell assays, had limited its usage.

This thesis presents the work that offered solution to the said obstacles, by developing a system capable of conducting DEP experiments within a very short period of time, thus allowing DEP effects to be recorded close to real-time; and conducting the DEP experiments in parallel, thus allowing the DEP effects to be recorded concurrently on multiple cell samples. This is achieved with the design and development of programmable, multiple output waveform generator using (capable of producing up to eight signal outputs, and extendable in multiples of four channels); improvement of planar microelectrode device design (capable to be energised individually); design and fabrication of the microfluidic gasket (better solution flow without localised cell collections), and design and development of alternative DEP image analysis algorithms (capable of handling near real-time DEP events data, and quantifying initial conditions for the light intensity).

Results from the validation studies showed that the waveform generator is capable of producing stable, individually addressed channel outputs of up to 10 MHz at 15 Vp-p with the DEP effects observed when the signal is supplied at a minimum of 10 seconds. The system is also capable of handling highly conductive suspending media (up to 1.4 S/m). Validation studies using leukemic cell lines showed the system is capable of producing near real-time DEP spectra that were consistent with published data at a minimum temporal resolution of 60 seconds. DEP effects of the said cell population when treated with valinomycin, a K^+ ionophore, were also recorded and showed a decrease of both membrane conductance and capacitance values as apoptosis was induced and progressed.

Declaration of Originality

This thesis and the work to which it refers are the results of my own efforts. Any ideas, data, images or text resulting from the work of others (whether published or unpublished) are fully identified as such within the work and attributed to their originator in the text, bibliography or in footnotes. This thesis has not been submitted in whole or in part for any other academic degree or professional qualification. I agree that the University of Surrey has the right to submit my work to the plagiarism detection service TurnitinUK for originality checks. Whether or not drafts have been so-assessed, the University reserves the right to require an electronic version of the original document (as submitted) for assessment as above.

Acknowledgements

In the Name of Allah, the Most Gracious, the Most Merciful

I would like to extend my gratitude to all members of the Centre for Biomedical Engineering, University of Surrey, particularly to Mike, Fatima, Henry, Kai, David, Hayley, Ruth, Rula, Mohammed, Nazim, Sabry, and Azhar; the University of Malaya, Malaysia; and the Ministry of Higher Education, Malaysia; all of whom played a significant part in ensuring the project and this thesis reach its final destination.

And I would love to dedicate this work to my family and friends, especially those dearest to me: my parents, Mak and Abah; and my family, Ayang, Hakimi and Luqman. Without their support and encouragement this work may not see to its fruition.

Nahrizul Adib Kadri

Contents

List of Figures

List of Tables

Glossary of Terms

AC	Alternating current
ATP	Adenosine triphosphate
dc	Direct current
DEP	Dielectrophoresis
DNA	Deoxyribonucleic acid
dpi	Dots per inch
ER	Endoplasmic reticulum
FBS	Fetal bovine serum
ITO	Indium tin oxide
K562	Myelogenous leukaemia cell line
KCl	Potassium chloride
PCB	Printed circuit board
RMS	Root mean squared
rpm	Revolutions per minute
RNA	Ribonucleic acid
UV	Ultraviolet
YPD	Yeast Peptone Dextrose

1 Introduction

1.1 Background

Dielectrophoresis (DEP), one of the phenomena commonly grouped as part of AC electrokinetics, has been used for physically manipulating and characterising various types of cells and particles ever since its discovery by Herbert Pohl in 1951. Following the successful separation and the subsequent preliminary DEP analysis of viable and non-viable yeast cells (Pohl and Hawk, 1966; Crane and Pohl, 1968), a multitude of DEP-based studies have ensued.

The technique received a boost in the 1980s and 1990s following advancements in microfabrication technology, and many studies have incorporated DEP as a markerless cell cytometry assay in developing numerous variations of lab-on-a-chip (LOC) applications and/or micro-total analysis systems (μTAS). Despite the aforementioned advantages and the discovery of the DEP phenomenon by Pohl in 1951, the technique has yet to enjoy worldwide acceptance by the biotechnology industry. This most probably is down to two related factors, namely the time-consuming processes involved, thus allowing experiments only to be conducted serially; and the lack of detecting techniques and/or hardware to conduct large batch cell assays (Hoettges *et al.*, 2008). Nevertheless, advances in microfabrication techniques, along with the general increase of interest in microfluidics and BioMEMS as emerging trends towards personalised diagnostic and healthcare, has helped to push efforts towards solving these inherent predicaments. In addition, there is also a need for non-invasive techniques to monitor and observe drug-cell interactions *in situ* to be developed. The majority of drug interaction studies rely on either computerised pharmacokinetics simulations of cellular and molecular interactions, or recorded observations of known inhibitor and/or inductor to the particular drug in use or the expected cellular responses (e.g. Lehmann *et al.*, 1998; Thummel and Wilkinson, 1998). Of particular interest is the role that cellular surface markers play in drug discovery studies, since up to 60% of current drugs in the market today are targeted towards the receptors of the plasma membrane (Christopoulos, 2002). Since DEP experiments allow cellular characterisation studies based on the characteristic membrane and cytoplasmic electrophysiological make-up (Hughes, 2002), it would be highly desirable therefore to explore the advantages of employing DEP as a complementary and non-invasive technique in drug interaction studies.

The current project aims to advance the solution by providing a means to observe and record cellular electrophysiological changes in real-time by conducting multiple DEP experiments in parallel, based on the dot microarray electrode system developed by Fatoyinbo *et al.* (2008). The DEP effects of selected cell populations, namely K562 and Jurkat cells, will be observed and recorded in real-time; both in a typical DEP environment and when treated with a chemical reagent with known effects on the plasma membrane. This will be achieved by the development of a programmable, multiple output waveform generator that is capable of producing stable outputs within a range of 1 kHz-50 MHz (10-15 V_{p-p}); and to use it in conjunction with a parallel version of the dot microarray electrode. Each of the dots will receive a different signal frequency, thus enabling multiple experiments to be conducted concurrently and real-time data to be collected. This will hopefully address the aforementioned large-batch assay drawback of DEP, and at the same time propose a prototype DEP analysis system that is capable of conducting near real-time electrophysiological analyses. The system could be of benefit as a complement to drug discovery studies by being capable of proposing possible mechanisms of action of any chemical reagents that affect the physical morphology of the plasma membrane and/or the cytoplasm.

1.2 Thesis objectives

The objective of this project is to document the outcome of the efforts in establishing the feasibility of developing a robust, programmable, multiple output system to conduct a series of DEP experiments concurrently (using a parallel version of the dot microarray electrodes proposed by Fatoyinbo *et al.*, 2008), in order for it to produce the desired DEP spectrum of the chosen cell populations within a period of time considered to be 'near real-time'. The project will also outline the best experimental conditions and software settings to be used in order to produce consistently reliable DEP spectra. For this project, the cell populations of choice are K562 and Jurkat cells.

1.3 Thesis structure

This thesis will include the following topics:

a) A concise literature review on the topics of BioMEMS; the use of AC electrokinetics in cell electrophysiological analyses, particularly DEP; mammalian cell anatomy and physiology and its relation to cancer; and an introductory note on digital image processing.

b) A description of the design and development of the system, including the multiple output waveform generator, the microelectrode device, the additional analysis modules, and the proposal of new algorithms for DEP spectra analysis.

c) A description of the work undertaken in validating the developed system, including cell culture and analysis, and the outcome of the system at various parameter differences (cell concentrations, media types and conductivities, electrode diameters and geometries, and input supply voltages).

d) A discussion on the results attained from the various tests conducted for the developed system, using DEP experiments to observe changes in the electrophysiological properties involving K562 and Jurkat cells, both normal and when treated with apoptotic agents.

e) An overall conclusion based on the work undertaken for the project, including a brief summary of future work that needs to be completed.

1.4 Summary of novel work undertaken

The following is a list of original undertakings undertaken towards the completion of this thesis:

a) Design and development of a four-channel waveform generator, employing AD9833 waveform generator chip controlled by PIC16F877 microcontroller with a MATLAB graphical user interface.

b) Improvement of gasket design and fabrication to be used in the microelectrode device, based on simulation analyses using COMSOL Multiphysics software.

c) Design and development of PCB platform to be used in the microelectrode device.

d) Completion of DEP experiments involving the K562 and Jurkat cells using the newly developed system, both untreated and treated with an apoptotic agent (valinomycin).

e) Improvement of the automatic detection of dots within the current analysis algorithm.

f) Design and development of additional analysis modules to indicate the optimal initial light intensity.

g) Design and development of two new algorithms for the analysis of DEP spectra and the subsequent extraction of biophysical properties.

2 Literature review

2.1 Introduction

This section will cover relevant background information that relates to the three primary aspects of the project, namely; the design and development of the programmable, multiple output signal generator; the conducting of the near real-time experiments; and the design and development of the analysis algorithm.

The review will start with a brief outline of the biological microelectromechanical systems (BioMEMS), amongst which the 'lab-on-a-chip' is one of the research areas; followed by a brief description of DEP, along with a concise review of the relevant literature, including electrode geometry and the extraction of cell biophysical properties. A short review of the mammalian cell structure and the types of cells used in the project, namely K562 and Jurkat cells, will be subsequently included; along with a review of the relevant theoretical considerations in designing and developing the analysis algorithm, including a brief overview on digital image processing.

2.2 BioMEMS

The ability to physically manipulate particles has long been the fascination of scientists and researchers; be it in the field of medicine, engineering, and biotechnology. Along with the advancement of the microfabrication techniques in the semiconductor industry, researchers are now being presented with a possibility of developing technology capable of separating, collecting and conducting analysis on particles with a high level of efficiency and accuracy. In addition to the low production cost, this method also has the advantage of being modular, making it highly extensible with the addition of other lab-on-a-chip applications and/or techniques, and thus further reducing the impact of destructive procedures normally employed in handling cells and particles (Gravesen *et al.*, 1993; Whitesides, 2006).

Also due to the ever-increasing move towards evidence-based medicine in the healthcare industry, there is an almost perpetual demand for personalised and automated diagnostic and prognostic systems to be developed (Pethig and Markx, 1997; Hughes, 2003). The combination of these demands

and technological know-how invariably leads to the birth of BioMEMS as a promising approach towards the development of the said systems.

One of the widely employed group of techniques are known as the AC electrokinetics, which include dielectrophoresis (DEP), electro-rotation (ROT), travelling-wave dielectrophoresis (tw-DEP), electro-osmosis, and electro-orientation (Jones, 1995; Pethig and Markx, 1997; Hughes, 2003). Although these methods offer a number of advantages over routine cell assay methods, the uptake has been generally low. Most of its usage is confined within research institutions, due to the time-consuming processes involved. This predicament is due primarily to the limitation imposed on the number of cell assays that can be performed at any one time (Hughes, 2002; Hoettges *et al.*, 2008). Previous experience of conducting DEP experiments at the Centre for Biomedical Engineering, University of Surrey have shown that the time taken to complete the whole processes of recording and analysing the data was between 40-120 minutes, in order to produce statistically acceptable DEP spectra from a single cell sample. This is primarily due to the time taken to complete the manual processes involved in the recording of DEP events at pre-determined frequencies (limited to one frequency at a time) for a specific period of time (between 60-120 seconds), and the required analysis stage to produce a single DEP spectrum.

The Centre for Biomedical Engineering at the University of Surrey is addressing the need to overcome this problem by focusing its effort towards developing DEP-based techniques that may allow faster DEP analyses to be conducted and/or multiple analyses to be conducted simultaneously (Broche, 2005; Chin *et al.*, 2006; Fatoyinbo *et al.*, 2008; Hoettges *et al.*, 2008). The current project endeavours to offer a solution in the latter, by providing a way of conducting a single set of experiments within a very short period of time with the use of a programmable multiple output waveform generator, enabling any physical changes to the cell populations in use to be analysed as close to real-time as possible.

2.3 Dielectrophoresis

The DEP force, and its possible applications in manipulating cells, was first described by Pohl in 1951, and was later used in separating dead and living yeast cells (Pohl and Hawk, 1966; Crane and Pohl, 1968). A decade later, Pohl published what is widely regarded as the key definitive documentation of the DEP force, in his book entitled “Dielectrophoresis” (Pohl, 1978).

As alluded to in the previous subsection, DEP has the capability to differentiate different populations of particles based on its relative polarisibility ‘strength’, which may be demonstrated in a DEP

spectrum plot. Different populations of cells, for example, will display different crossover values, and thus making it highly useful in cell characterisation studies. DEP has been employed, among others, to separate live and dead cells (Pohl and Hawk, 1966; Mason and Townsley, 1971), different strains of bacteria (Inoue *et al.*, 1988; Washizu *et al.*, 1993; Markx *et al.* 1994a; Markx *et al.*, 1996; Goater *et al.*, 1999; Gascoyne *et al.*, 2002, Suehiro *et al.*, 2003), viruses (Schnelle *et al.*, 1996; Green *et al.*, 1997; Hughes and Morgan, 1998; Hughes *et al.*, 1998; Morgan *et al.*, 1999; Archer *et al.*, 1999), DNA molecules (Washizu *et al.*, 1995), parasites (Dalton *et al.*, 2001), spores (Archer *et al.*, 1999, Fatoyinbo *et al.*, 2007), and algae (Hübner *et al.*, 2003). Other types of molecules have also been the subject of DEP characterisation studies, including nano-sized latex spheres (Green and Morgan, 1997; 1999; Qiu *et al.*, 2002) and biopolymers (Washizu *et al.*, 1994).

In addition, numerous studies focused on the use of DEP in characterising the myriad of mammalian cells, including yeasts (Crane and Pohl, 1968; Asami *et al.*, 1976; Pohl *et al.*, 1981; Huang and Pethig, 1991; Hölzel and Lamprecht, 1992; Huang *et al.*, 1992; Wang *et al.*, 1993; Markx *et al.*, 1994b), neurons (Heida *et al.*, 2001; Heida *et al.*, 2002; Prasad *et al.*, 2004), leukocytes (Yang *et al.*, 1999; Wang *et al.*, 2000; Yang *et al.*, 2000), erythrocytes (Krishna *et al.*, 1989; Auerswald and Knapp, 2003; Hübner *et al.*, 2005), platelets (Rhoads *et al.*, 1976; Pommer *et al.*, 2008), and even human spermatozoa (Fuhr *et al.*, 1998). Although this in itself provides a much needed alternative method for cell detecting and sorting assays, a worthier cause of DEP usage would be in detecting and collecting abnormal particles from a given cell population. And as expected, similar studies in separating these cells have been conducted as early as the recognition of DEP as an advantageous marker-less cell sorting technique back in the 1980s. Mischel *et al.*, for example, had successfully separated malignant melanocytes from normal cell populations in 1983. The study showed that the electrical behaviour of malignant melanocytes is markedly dependent upon the type of cell line, age, and drug treatment (e.g., chlorpromazine) and thus can be separated from normal cells using DEP.

The advancement of DEP research has not come about without concurrent progress in research of the relevant hardware to conduct the experiments. Incidentally the innovation in microfabrication techniques and the increasing demand for better diagnostic methods, particularly using lab-on-a-chip techniques, to provide personalised care, have also helped to push the research field further.

One of the most prolific DEP-based research groups is the one based at the Institute of Molecular and Biomolecular Electronics, University of Wales. The Institute was under the direction of Ronald Pethig, one of the collaborators of Herbert Pohl, widely accepted as the pioneer of DEP. In 1977, they described a technique to determine the dielectric properties (permittivity and conductivity) of materials as a function of applied signal frequency (Pohl and Pethig, 1977).

In 1989, the group proposed an optical DEP spectrometer for measurements on colloidal suspensions (Burt *et al.*, 1989), and used it for the characterisation of erythroleukaemic cells (Burt *et al.*, 1990; Gascoyne and Becker, 1990). In 1991, the Institute successfully designed a microelectrode, based from a Laplacian polynomial, which was capable of collecting yeast cells using negative DEP (Huang and Pethig, 1991). The group has also been able to quantify the AC electrodynamics differences (using 'smeared-out sphere' modelling) between viable and non-viable yeast cells in terms of the membrane and cytoplasm conductivity changes using DEP and electrorotation (Huang *et al.*, 1992; Markx *et al.*, 1994b), and successfully incorporated time-dependent conductivity gradient into the DEP analysis (Markx *et al.*, 1996). Collaborations with other research groups yielded one of the earliest studies in employing computerised image analysis in quantifying the rate of particle motion (Gascoyne *et al.*, 1992). The group also developed the interdigitated (Becker *et al.*, 1994) and castellated (Markx *et al.*, 1994a) microelectrode designs; both of which became the basis of many studies conducted later at the Centre for Biomedical Engineering, University of Surrey.

Another research group, based at the Humboldt Universität zu Berlin, Germany, developed a technique to physically move and rotate selected particles using negative DEP (50 MHz and above; high medium permittivity) within a specially designed microchamber (Fuhr *et al.*, 1992). The so-called 'field cage' technique was documented, along with the testing of several microelectrode designs at high AC frequency (up to 400 MHz), and the position and trajectories of particle motion were measured (Schnelle *et al.*, 1993). The group subsequently showed that a specific planar quadrupole electrode configuration (fabricated by electron-beam lithography; gaps down to 500 nm; field strength up to 56 MV/m at MHz frequency range) was capable of trapping, aggregating and concentrating micrometer particles using positive and negative DEP (Müller *et al.*, 1996). The group later developed miniaturised electrode arrays (made using ITO) that are capable of trapping mammalian cells in a laminar flow (up to 10 mm/s) (Fiedler *et al.*, 1998). The hardware was further improved, and a 3D microelectrode system to focus, trap and separate eukaryotic cells with a diameter of 10-30 μm using negative DEP (5-11 V; 5-15 MHz; PBS as conductive medium) was developed (Müller *et al.*, 1999, Schnelle *et al.*, 1999).

Similar studies were also conducted by other groups at around the same time, including the Bioelectronic Research Centre at the University of Glasgow. One of their earliest efforts involved the separation of latex spheres (Green and Morgan, 1997), followed by the development of a large-area (capable of incorporating up to 25,000 electrodes) travelling-wave DEP design to separate components of whole blood (Morgan *et al.*, 1997) and nano-scaled particles (Morgan *et al.*, 1999). The group also managed to achieve a controlled separation of submicron bioparticles (tobacco mosaic virus and herpes simplex virus) in a heterogeneous mixture using microelectrode arrays fabricated

using electron beam lithography (Morgan *et al.*, 1999). A specific coplanar plate microelectrode array geometry was later employed and detailed experimental measurements of the resultant fluid flow (velocity as a function of signal frequency and potential, and medium conductivity) over the electrodes was made (Green *et al.*, 2000), and an analysis based on linear double-layer model was proposed (González *et al.*, 2000).

2.3.1 Theory

As previously mentioned, a DEP force is generated when a polarisable particle is placed in a conductive medium, and a non-uniform electric field is applied. Depending on the overall alignment of the induced dipole moments, the particle will either move towards or away from the area of the highest electrical gradient (Jones, 1995; Hughes, 2003). The alignment of the dipoles is determined in turn by the relative polarisability compared with the surrounding medium. The actual direction of the electric field does not affect the direction of the overall force. Figure 2-3 illustrates an example of positive DEP in a typical arrangement. In this example, the particle is more polarisable than its surrounding medium, and thus dipole moments will be induced on its surface. Due to the high electrical gradient towards the negative end, the particle will experience a net force towards it. Negative DEP, on the other hand, will occur if the surrounding medium happens to be more polarisable than the particle, and thus repelling the particle towards the positive end of the gradient. The effective movement of the particle is entirely dependent on the polarisability of the particle and its medium, rather than the direction of the electrical gradient, thus fundamentally differentiating the DEP phenomenon against another related electrical phenomenon, electrophoresis.

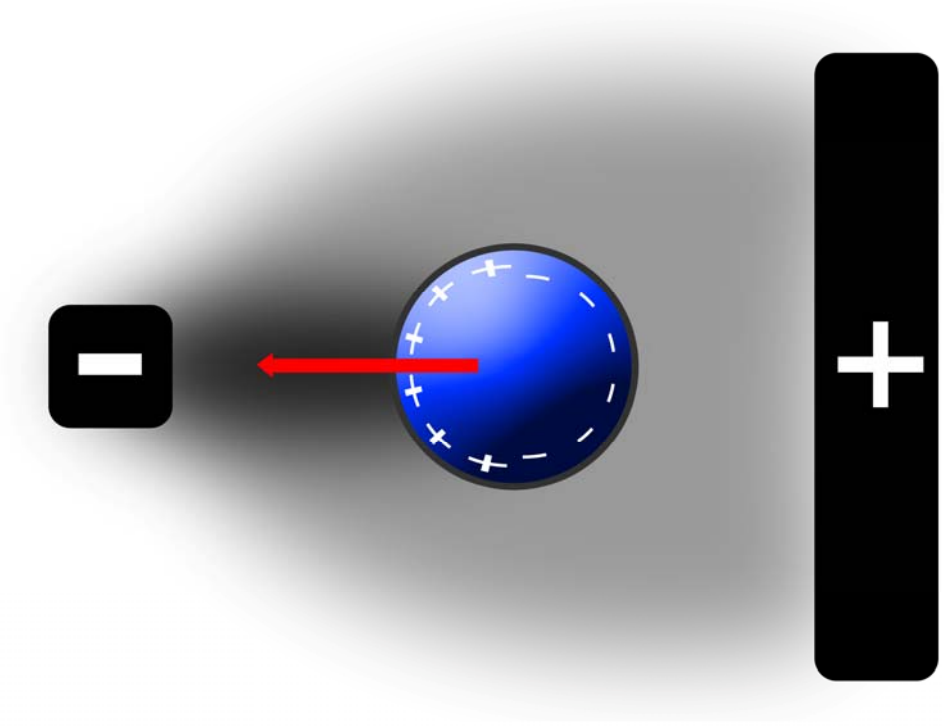

Figure 2-1 A schematic diagram of a positive DEP effect (particle is more polarisable than surrounding medium). Arrow indicates net movement of the particle

The DEP force, F_{DEP}, exerted on a homogeneous sphere may be modelled as:

$$\langle F_{DEP} \rangle = 2\pi r^3 \varepsilon_m \, \mathrm{Re}[K(\omega)] \nabla E^2 \tag{2.1}$$

where r is the cell radius, ε_m is the permittivity of the medium surrounding the cell, $K(\omega)$ is the complex Clausius-Mossotti factor, ∇ is the Del vector operator, and E is the electric field strength, expressed in its RMS value. The Clausius-Mossotti factor is a measure of the strength of the effective polarisability and may be shown as:

$$K(\omega) = \frac{\varepsilon_p^* - \varepsilon_m^*}{\varepsilon_p^* + 2\varepsilon_m^*} \tag{2.2}$$

where ε_p^* and ε_m^* are the complex permittivities of the cell and the medium, respectively. In addition,

$$\varepsilon^* = \varepsilon - \frac{j\sigma}{\omega} \tag{2.3}$$

where σ is the conductivity, ε is the permittivity, and ω is the angular frequency of the applied AC electric field.

From 2.1, due to the presence of the Clausius-Mossotti factor that is frequency-dependent, it is clear that F_{DEP} varies depending on the frequency of the applied electric field. The magnitude of the Clausius-Mossotti factor, in turn depends on the relative polarisability "strength" between the particle and its surrounding medium. If the factor is positive (i.e. particle is more polarisable than medium), then the particle will move towards the region(s) with the highest electrical gradient; also known as positive DEP. A negative DEP will be produced if the opposite occurs, i.e. the medium is more polarisable than the particle, thus effectively repelling the particle towards the region(s) of lower electrical gradient.

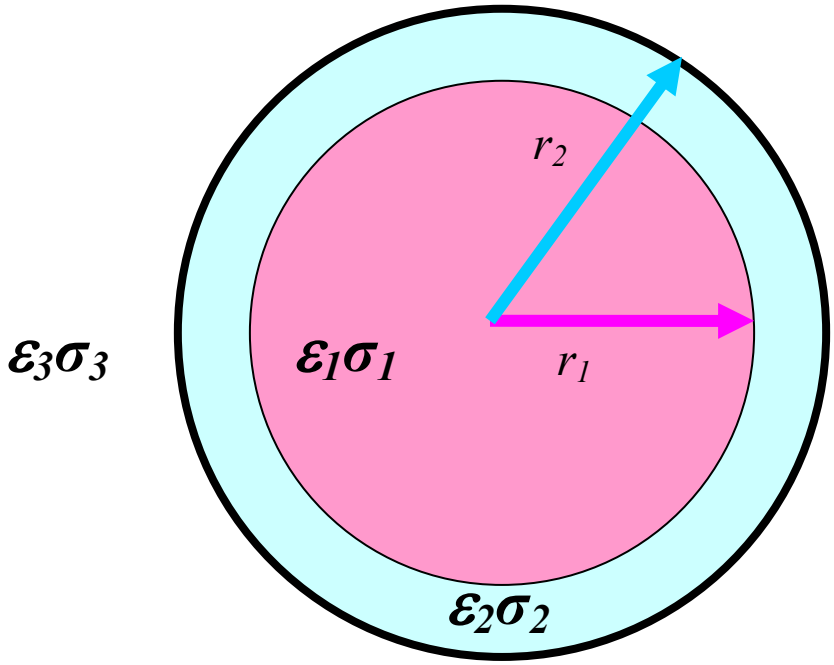

Figure 2-2 A schematic diagram of the single shell model

For the purpose of the analysis of DEP data, however, Equation 2.3 may be simplified into an effective value, subsequently transforming the Clausius-Mossotti factor into an effective value, and thus easily allowing the determination of F_{DEP} using numerical methods, if the conductivity of the dielectric medium and particle size is known. In order to achieve this simplification, a generic single shell model (Benguigui and Lin, 1982) must be employed (Figure 2-4). The model assumes that a particle consists of a homogeneous spherical core and surrounded by a homogeneous shell, such that:

$$\varepsilon_{1eff}^{*} = \varepsilon_{2}^{*} \frac{\left(\frac{r_2}{r_1}\right)^3 + 2\frac{\varepsilon_1^{*} - \varepsilon_2^{*}}{\varepsilon_1^{*} + 2\varepsilon_2^{*}}}{\left(\frac{r_2}{r_1}\right)^3 - \frac{\varepsilon_1^{*} - \varepsilon_2^{*}}{\varepsilon_1^{*} + 2\varepsilon_2^{*}}} \tag{2.4}$$

where subscripts 1 and 2 refer to the properties of the core and shell of the model, respectively. This will effectively transform the Clausius-Mossotti factor into:

$$K(\omega) = \frac{\varepsilon_{1eff}^{*} - \varepsilon_3^{*}}{\varepsilon_{1eff}^{*} + 2\varepsilon_3^{*}} \tag{2.5}$$

where subscript 3 refers to the surrounding dielectric medium. Along with the use of numerical methods, a polarisability (or DEP) spectrum may then be plotted for a given population of particles suspended in a conductive medium. If the said shell has a comparatively lower conductivity than both the inner core and the surrounding medium, it will be expected that the DEP plot will show a characteristic change from a negative to a positive $K(\omega)$ value at a certain low frequency, and from a positive to negative value at a much higher frequency value (Figure 2-3).

Although the above analytical expressions may have been satisfactory in explaining the DEP behaviour of spheres in a given solution, it is generally considered to be too complex to be expanded in order for the dielectric properties to be directly calculated and correlated in a useful manner (Jones, 1995). The common method of correlating the relevant cellular electrical parameters with the DEP behaviour is by making an estimate of the electrophysiological properties performed by best-fit numerical analysis (Huang *et al.*, 1996), and has been successfully used in numerous DEP characterisation studies (e.g. Labeed *et al.*, 2003; Chin *et al.*, 2006; Labeed *et al.*, 2006; Duncan *et al.*, 2008). The estimation method has also been shown to be useful in characterising multiple cell populations within a heterogeneous cell sample (Broche *et al.*, 2005).

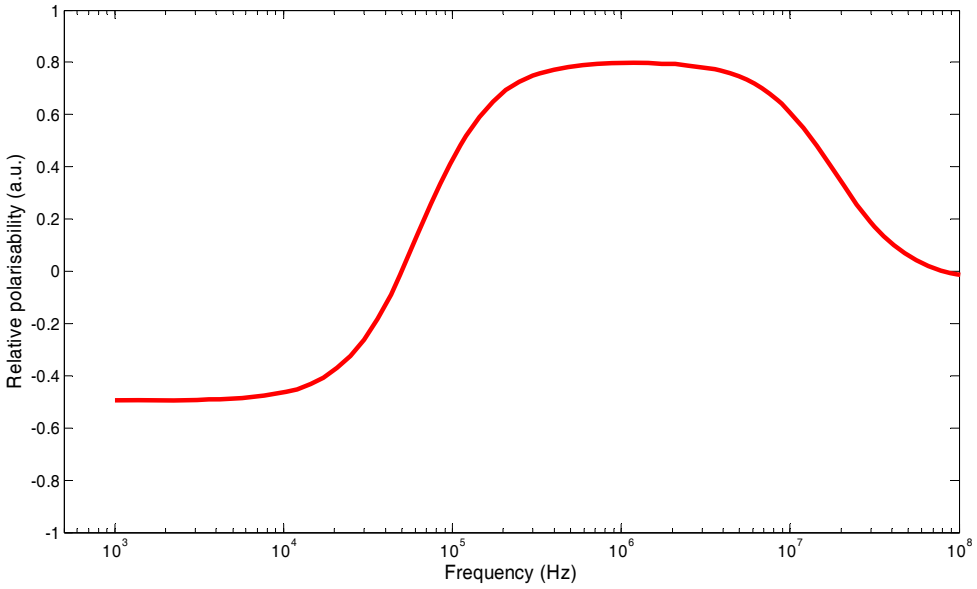

Figure 2-3 A typical shape of the DEP spectrum based on the single shell model

It must be noted however, that the single shell model may not be useful for all types of cells. Cells or particles with prominent inner compartments, and thus considered to be having additional 'shells', will require the multishell model in order for the electrical properties to be inferred from using the curve-fitting method. Theoretically, the closer the number of shells used to the number of actual compartments that a cell has, the more accurate the estimate will be (Gimsa *et al.*, 1991). Nevertheless, it will also become more difficult to fit a model plot with higher number of shells because the number of features to be fitted is exceeded by the number of parameters, leading to non-unique solution sets. Furthermore, the multishell model was limited to particles in the regions of micrometers only (Hughes *et al.*, 1999). Generally, the shape of the DEP spectrum will typically determine which model will be used (i.e. double shell, or triple shell, etc) in the analysis.

The extraction of electrophysiological properties from the acquired DEP spectra is highly beneficial because it provides an estimate of the state and the environment the cells were experiencing. If the said changes were caused by the presence of an external reagent, one can safely assume (in the absence of other external factors) that the changes were solely caused by the offending reagent and may help to explain its mechanism of action on the cellular membrane and the effect it has on the cytoplasm. Ionophore molecules for example, when attached to the cellular membrane will allow additional amount of ions to pass through the cellular membrane and ultimately disturb the membrane and/or cytoplasmic conductivity values because of the disturbance to the total ionic distribution, thus

affecting the Clausius-Mossotti factor value. This change will be expressed by the changing of the shape of the DEP spectra. From Equation 2.3 it can be predicted that if say, the particle conductivity were to be increased at a given frequency value, the permittivity will correspondingly decrease, and the resultant Clausius-Mossotti will also be decreased. This will be shown by a general shift of the DEP spectrum to the right, in the absence of other compounding factors.

By having a system that is capable of recording these DEP changes very close to real-time, it would allow researchers to have an additional tool to be used in predicting and explaining the mechanisms of action of any reagents that are responsible for causing the said ionic and morphological disturbances as it happens. Such a system would be useful as a complementary tool in drug discovery studies, for instance.

2.3.2 DEP electrode design

In order to actually observe the movement of the particles, the generation of non-uniform electrical field that is of desirable strength is essential. In addition, it is also required that the generated field is of a specific shape, such that the difference between the effects of negative and positive DEP may be clearly distinguished. Therefore, a suitable electrode design must be prepared to fulfil the particular needs of a study, preferably at the lowest voltage possible.

For the purpose of this project, the types of electrodes that will be focused upon are the ones grouped as planar microelectrodes and fabricated using common lithography techniques within the regions of microns. Examples of such electrode designs include the interdigitated electrodes (Qiu *et al.*, 2002; Suehiro *et al.*, 2003; Ermolina *et al.*, 2005), castellated inter-digitated electrodes (Price *et al.*, 1988; Gascoyne *et al.*, 1992; Becker *et al.*, 1995; Markx *et al.*, 1996), spiral electrodes (Müller *et al.*, 1996; Wang *et al.*, 1997) and polynomial electrodes (Huang and Pethig, 1991; Hughes and Morgan, 1998). The use of 3D electrode designs have also been explored, namely field cage technique (Fuhr *et al.*, 1992; Schnelle *et al.*, 1993; Fiedler *et al.*, 1998; Müller *et al.*, 1999), grid electrodes (Suehiro and Pethig, 1998), microwells (Jaber *et al.*, 2009) and DEP-well (Broche *et al.*, 2005; Hübner *et al.*, 2005; Labeed *et al.*, 2006; Hoettges *et al.*, 2008). Figure 2-4 shows a selection of these electrode designs.

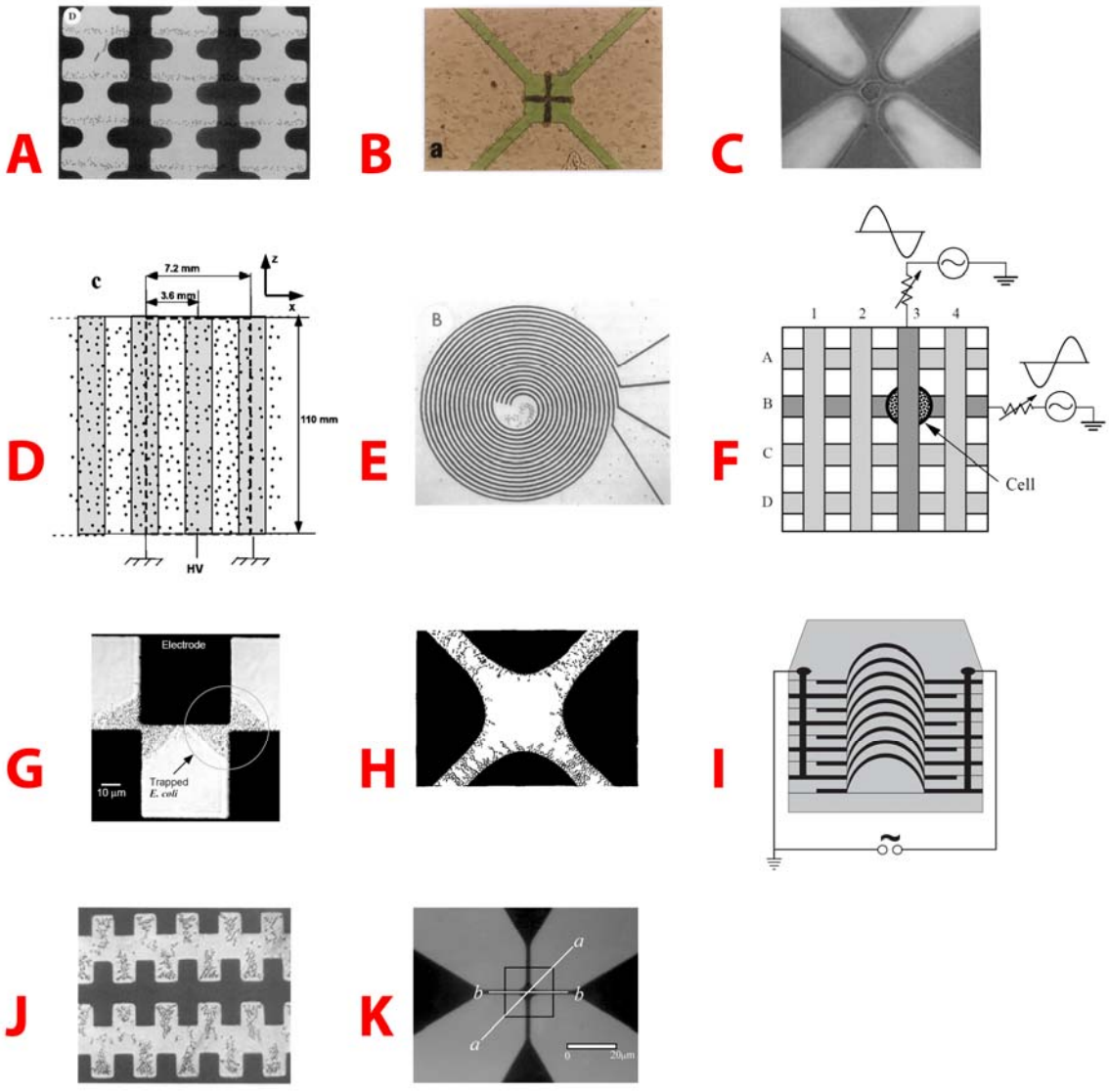

Figure 2-4 A selection of electrode designs used in the literature: a) Becker *et al.*, 1995; b) Müller *et al.*, 1996; c) Fiedler *et al.*, 1998; d) Qiu *et al.*, 2002; e) Wang *et al.*, 1997; f) Suehiro and Pethig, 1998; g) Suehiro *et al.*, 2003; h) Huang and Pethig, 1991; i) Hübner *et al.*, 2005 and Labeed *et al.*, 2006; j) Gascoyne *et al.*, 1992; k) Hughes and Morgan, 1998

All of these different electrode designs have been designed to address a specific task or issue at hand. The interdigitated electrode design for example (Figure 2-4(a), Figure 2-4(d), Figure 2-4(g), Figure 2-4(j)), was designed for the purpose of separating specific population of cells on the basis of the characteristic electrical properties, while the grid electrode (Figure 2-4(f)) on the other hand, allows the movement of a single cell to be physically manipulated with a high degree of precision. In addition, a three-dimensional electrode design, such as the DEP-well electrode (Figure 2-4(i)), allows

characterisation studies to be conducted on larger populations of homogeneous cells. The overall objective of the study dictates the final geometry and design of the electrode in use.

In the context of the current project, the most suitable electrode design would be a planar electrode type, with circular 'dots' to create the chamber for the DEP effects to be observed and recorded. The circular nature of the electrode should create a three-dimensional axisymmetrical electrical gradient over the electrode surface; small enough for the DEP effects to be created and for multiple dots to be seen under the microscope for the images to be recorded concurrently. The dots must also be designed such that it can be supplied individually by the multiple output waveform generator, and will only uses small number of cells (in comparison to the DEP-well electrode).

2.3.3 Biophysical properties

Apart from the ability to physically manipulate particles, an additional advantage of using DEP-based techniques is the ability to determine a number of biophysical properties of the said particles based on the acquired DEP spectra. This is quite clear-cut since the DEP force is directly affected by the surface charge, and thus any morphological changes to the membrane will inevitably affect the movement of the particles within the electric field and will produce corresponding observable changes in the DEP spectra. This, in turn, enables the biophysical properties to be determined. Of particular interest is the electrical properties of the membrane, namely the conductance and capacitance, since these properties may indicate the overall state and functioning of the cell, depending on the type of ionic and morphological changes that are occurring on the membrane surface and cytoplasm. As briefly mentioned in the previous Theory section, the two commonly used models in DEP-based experiments are the single-shell (Benguigui and Lin, 1982) and multi-shell (Irimajiri *et al.*, 1979) models. The choice of model depends on the type of particles used, although the multi-shell model generally is considered too complex to provide useful analysis for many cell types, and is not applicable to particles smaller than in the region of microns.

Using the single shell model, Gascoyne *et al.* (1993) found significant drops in membrane conductivity and capacitance between different cell lines of Friend murine erythroleukemia cells that were treated with various terminal differentiation inducers. Huang *et al.* (1996) also found that there was a significant reduction in both the specific membrane conductance and capacitance values in a population of rat kidney cells that were subjected to a temperature change from 33°C to 39°C in 24 hours. The correlation between the reduction and the morphological changes on the membrane surface was made using scanning electron microscopy. In a related study, the acquired DEP spectra of two leukemic cell lines, namely K562 and K562AR, were analysed to determine the differences in

cytoplasmic conductivity, and the changes following modulation therapy with a multidrug resistance (MDR) reversal agent. The outcome helped the subsequent understanding on the role of MDR modulators in preventing drug efflux in MDR cancer cells (Labeed *et al.*, 2003). It was later found that both the cytoplasmic conductivity and capacitance also rises significantly in K562 cells undergoing apoptosis following the delivery of staurosporine; suggesting the role of ion efflux in the apoptotic process (Labeed *et al.*, 2006).

A number of studies have also looked into the possibility of automating the DEP-based experiments, such that the changes in cellular electrical properties may be observed and recorded in real-time. Based on the electrorotation (ROT) technique, Gasperis *et al.* (1998) developed a real-time PC-based system that was capable of measuring cell rotational motion and analysing the acquired spectra for a single cell. The system was found to be as accurate as manual measurements, and a complete ROT spectrum of a cell in the range of 1 kHz to 200 MHz was obtained in less than 5 minutes, representing an increase in speed of about threefold compared to the previous laborious manual timing measurements. A similar system that was capable of analysing electrorotation spectra of single cells in real time, without the need of image storage, was developed by Hölzel (1998). The study monitored the membrane and the cytoplasmic changes of Saccharomyces cerevisiae treated with nystatin, at a temporal resolution of 3 minutes. Prasad *et al.* (2005) on the other hand, used a specialised motion-based segmentation algorithm to successfully track single yeast and cancerous cells. Physical characteristics, including cell count, velocity and size, were individually extracted. A semi-automated well-based assay system, utilising a laminated 3D electrode design, allowed parallel DEP experiments to be conducted (Hübner *et al.*, 2005). Dielectric properties of red blood cells, treated with saponin and valinomycin, were extracted using an ellipsoidal multi-shell model. The system was further developed to allow combination with simultaneous measurement of conventional fluorimetric well-based assays (Hoettges *et al.*, 2008). The study reported rapid determination of the effects of ion channel blockers on cancer cells, and antibiotics on bacteria; and simultaneous determination of the biophysical properties of multiple cell subpopulations within a single well.

Optical- or image-based analyses of particle movement in producing DEP spectra have also helped in the development of the aforementioned automated DEP systems. Price *et al.* (1988) for example, developed a system capable of measuring dielectrophoretic behaviour of three types of bacteria by monitoring the decrease in optical absorbance of a cell suspension. The experiments were conducted within the frequency range of 20 Hz to 4 MHz, and suspending medium conductivity of 0.2 S/m. In a further development of the system, particle surface charge and surface conductivity of silicon powder, yeast and a bacteria were also measured (Burt *et al.*, 1989). A computerised image analysis was developed by Gascoyne *et al.* (1992) to quantify the rate of motion of cells in a DEP experiment using

an interdigitated electrode array. The system was capable of measuring the dielectrophoretic properties of normal and leukemic mouse erythrocytes in the range of 500 Hz to 500 kHz; and was also successful in separating different cell types in a given cell mixture. Using the single-shell model, the system was further developed to be capable of determining the reduction in membrane conductivity and capacitance of Friend murine erythroleukemia cell lines when treated with hexamethylene bisacetamide and dimethylsulfoxide (Gascoyne *et al.*, 1993).

2.4 Mammalian cells

A typical mammalian eukaryotic cell structure contains three primary components, namely plasma membrane, cytoplasm and nucleus. Other components may also exist, depending on its function and the role it plays within the organism (Figure 2-5). Table 2-1 summarises the functions of the common intracellular components.

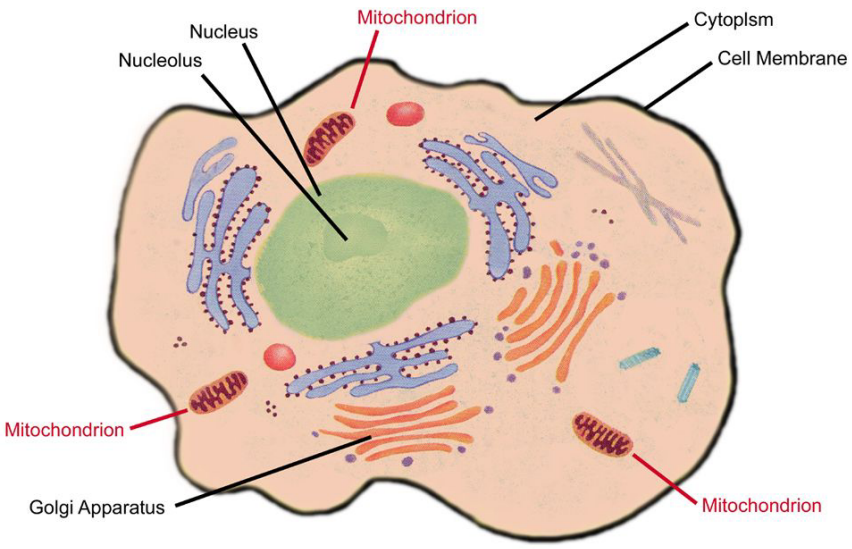

Figure 2-5 A typical mammalian eukaryotic cell structure (adapted from Alberts, 1988)

Table 2-1 Summary of the functions of cellular components (from Alberts, 1988)

Component	Function
Cytoskeleton	Provides scaffolding that determines the overall cellular shape and the organisation of the cellular contents
Ribosomes	Contains ribonucleic acid (RNA) for protein synthesis to be used in the plasma membrane and cytosol
Endoplastic reticulum	Synthesises glycoproteins and phospholipids (rough ER); synthesises fatty

(ER)	acids and steroids, inactivates or detoxifies drugs and other harmful substances, removes the phosphate group from glucose-6-phosphate and stores and releases calcium ions that trigger contraction in muscle cells (smooth ER)
Golgi complex	Processes and delivers proteins and lipids to the membrane
Lysosomes	Contain enzymes and thus are involved in digestion of foreign substances, and transportation of digestion products to cytosol. Also involved in autophagy, autolysis and extracellular digestion
Peroxisomes	Contain oxidases and thus are involved in the oxidation of organic substances
Mitochondria	Generates most of the cellular energy in the form of adenine triphosphate (ATP) via aerobic cellular respiration

The plasma membrane is of particular importance since on one hand, it acts as the barrier between the intracellular components and the external environment; but on the other, it also acts as gateway between the two environments, thus allowing interaction between the two environments and fulfilling its role within the more complex organism.

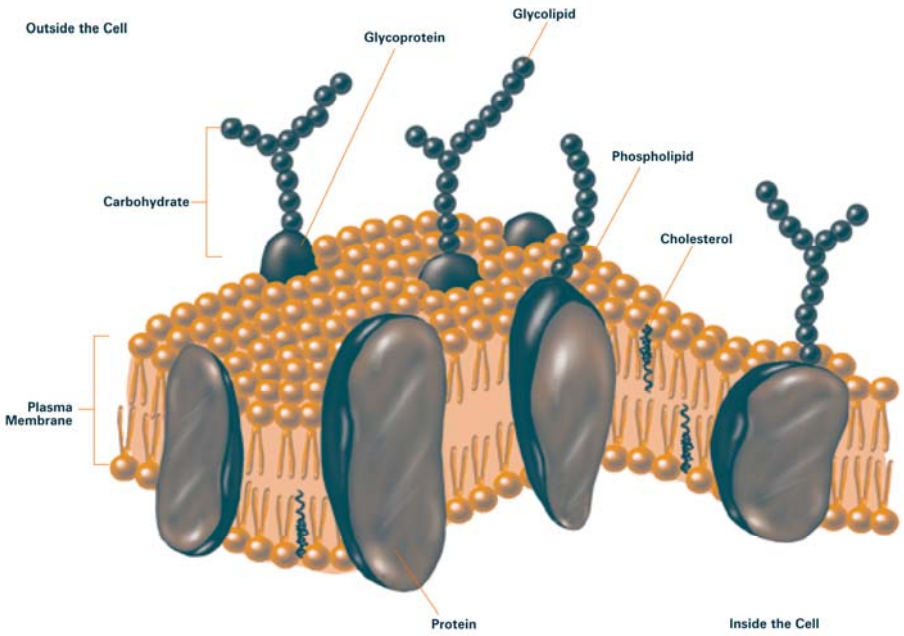

Figure 2-6 A schematic diagram of plasma membrane, showing the lipid bilayer and membrane proteins (adapted from Alberts, 1988)

The plasma membrane is made up of lipid molecules (diverse combinations of phospholipids, cholesterol and glycolipids) arranged in a bilayer structure (Figure 2-6). Due to its hydrophobic nature, the membrane naturally restricts the permeability of substances into and out of the cytoplasm, except for water, oxygen and carbon dioxide molecules. Nevertheless, there are numerous ion channels scattered all over the lipid bilayer that allows selective transport of ions across the barrier that directly affect the overall functioning of the cell. In a typical plasma membrane there will be K^+ (potassium), Cl^- (chloride), Na^+ (sodium), and Ca^{2+} (calcium) ion channels; of which K^+ and Cl^- ion channels are more abundant.

These ion channels are more effective at transferring the ions across the plasma membrane, compared to passive diffusion. Therefore if the mechanism of this active transport is known and controlled, it is possible to control the transfer of certain molecules across the lipid bilayer and effectively controlling the activity of the whole cell. And this is one of the mechanisms in which anti-cancer treatment works, i.e. by actively transporting specific molecules that were able to render the cancerous cells harmless and prevents it from metastasising.

2.4.1 Cancer

By definition, cancer cells are simply cells with an abnormal growth rate and/or pattern; but it nevertheless conjures up a sense of dread and despair. This is naturally understandable, given that the cause for any given type of cancer is yet to be ascertained, and for most malignant cases the prognosis is death. Although with the latest scientific and medical advances this may not be entirely true for all types of cancer (Jemal *et al.*, 2004), particularly with an early diagnosis; this gruesome reality is the preconception of the general public about cancer (Doll and Peto, 1981).

Although technically cancer may develop in any organ or tissue, there are a number of tissue types that are more prevalent than others, namely the lung, colon, breast, skin, bones, and nerve tissues. To compound the problem even further, given that the cause of cancers is largely unknown, which may include chemicals, the environment and/or individual lifestyles, different type of cancers are more prevalent in certain population than others (Baquet and Commiskey, 2000). In the United States for example, the three most common cancer types in men are prostate, lung, and colon cancers; while breast, colon, and lung cancers are more common in women (Jemal *et al.*, 2004; 2008). In Japan, on the other hand, gastric cancers are more dominant, which may (or may not) point to the effect of dietary differences between the two populations.

The current view with regards to the cause of cancer is multifactorial, even though a range of causes have been closely linked to cancer and these include benzene and other chemicals, certain poisonous mushrooms, certain viruses, radiation, sunlight, and tobacco. Of particular importance, apart from the concerted effort in documenting the myriad of causes and its consequent treatment options, is the general consensus that having an early diagnosis in any type of cancer increases the survival rate (Jemal *et al.*, 2004). This is why a great number of research efforts are focused on screening programmes and scientific techniques/methods that allow positive diagnosis to be made as accurately and as early as possible. And due to the advancement of medical interventions at these early stages of cancer development, a decrease in the rate of cancer morbidity has been seen in certain types of cancer (Jemal *et al.*, 2008).

2.4.2 K562 cells

The K562 cell line was originally derived from a 53 year old female patient with chronic myeloid leukemia (Lozzio and Lozzio, 1975). The cells were found to be non-adherent and round with few short microvilli on the surface. It was widely researched when it was first discovered because of its similarities to T-cell leukaemia; but due to its low level of differentiation, its exact nature cannot be stated with certainty. Klein *et al.* (1976) concluded that the cells belong to the granulocytic series of cells.

Nowadays, the cell line is used in many DEP-based studies, focusing on its apoptosis mechanisms and reaction to anti-cancer treatments (e.g. Gascoyne *et al.*, 1993; Wang *et al.*, 1994; Patel and Markx, 2008). The Centre for Biomedical Engineering at University of Surrey has also used K562 cell line extensively in its research (e.g. Labeed *et al.*, 2003; Broche *et al.*, 2005; Chin *et al.*, 2006; Labeed *et al.*, 2006; Duncan *et al.*, 2008).

2.4.3 Jurkat cells

Jurkat cells are an immortalised line of T lymphocyte cells and were first established in the late 1970s from the blood of a 14-year-old boy with T-cell leukaemia (Schneider, 1977). It is widely used in scientific research to determine the different mechanism of susceptibility of cancer cells to anti-cancer treatments and cell death (Gottlieb *et al.*, 1996; Faris *et al.*, 1998; Samali *et al.*, 1999; Scarlett *et al.*, 2000). The Centre for Biomedical Engineering at the University of Surrey has also successfully used Jurkat cells previously in its DEP research (Hoettges *et al.*, 2008).

2.4.4 Apoptosis

Apoptosis, or programmed cell death, is a natural cellular phenomenon that comprised of a series of biochemical events that preceded specific morphological changes and cell death. These changes may include the loss of cell membrane integrity, reduction of cell size, and fragmentation of the nuclear contents (Kerr *et al.*, 1972). The outcome of apoptosis is the production of apoptotic bodies, which will be engulfed by surrounding cells before the lysing contents of the dying cells are capable of causing damage to the surrounding cells and environment.

Apoptosis plays an important role in the life cycle of cells, particularly in ensuring that cell differentiation is occurring in a highly-controlled manner. Many embryonic developments, for example, rely on apoptosis to occur at the right time in order for the different parts of the organism to develop correctly. The loss of the said control may lead to either increased cell proliferation (as in hyperplasia or cancer) or increased cell death (as in atrophy). In addition, the control may be conducted by a number of cellular signals and/or factors, either originating extrinsically (e.g. hormones, growth factors, and toxins) or intrinsically (e.g. binding of specific molecules to nuclear receptors, or changing concentrations of specific cytoplasmic contents).

The apoptosis pathway consisted of a series of cellular enzymatic events that is initiated by specific regulatory proteins. Possible modes for the regulation include (Alberts *et al.*, 2008):

a) **Mitochondrial**: Apoptotic proteins act in several ways with the general aim to affect the provision of aerobic respiration by mitochondria. This is achieved primarily by decreasing mitochondrial membrane permeability, and the subsequent release of mitochondrial protein into the cytoplasm. These mitochondrial proteins commonly bind to inhibitors of apoptotic proteins, thus allowing apoptosis to occur.

b) **Direct transduction**: There are currently two suggested theories regarding the mechanism of direct apoptotic initiation, namely the tumour necrosis factor (TNF) model, and the Fas-Fas ligand-mediated model. Both models involve the binding of TNF receptor to various extrinsic signals, resulting in the initiation of apoptosis pathway.

3 System design and development

3.1 Introduction

The system to be developed for the project must comprise a number of essential components, namely the multiple output waveform generator, the microelectrode device (i.e. microelectrode attached to a specialised gasket to create a chamber for the DEP experiments to take place), the image capturing device (i.e. digital video camera with at least one frame per second capture rate), and the computer program to analyse the captured images prior to the production of DEP spectra and the conducting of subsequent electrophysiological analyses (Figure 3-1).

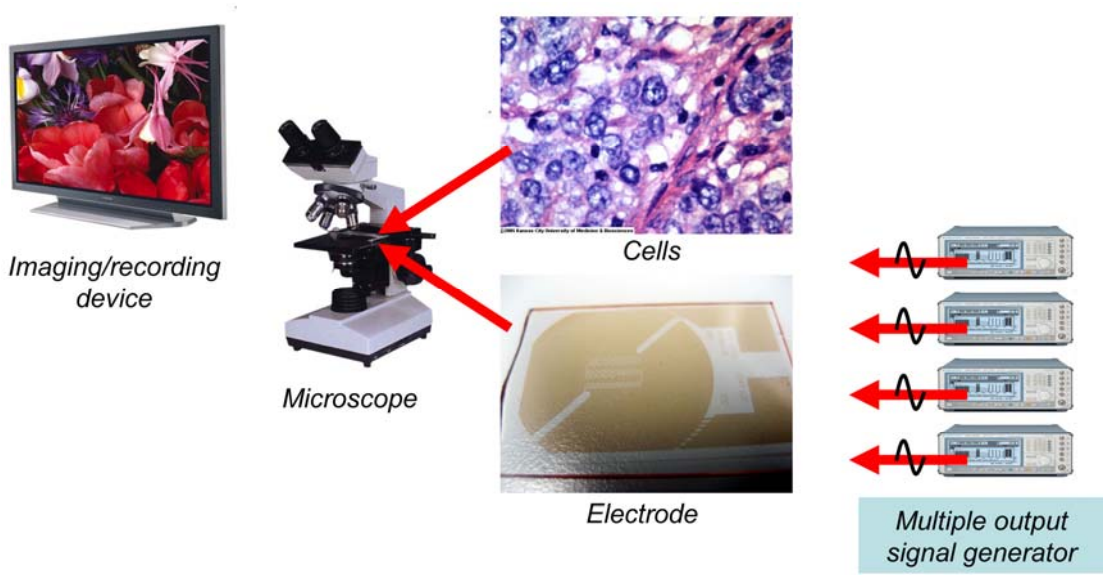

Figure 3-1 A schematic diagram of the system design

The actual course of the said development however, does not chronologically follow in order. The project set out with the design of a prototype four-channel waveform generator, along with a small MATLAB program to control the frequency of the output signals. This was successful when tested on a prototype board, and the output signals were verified using an oscillator. Nevertheless, the fabrication of a PCB board having the same circuit design failed to produce the intended output signals. This was most probably due to errors in transferring the circuit design to PCB layout, compounded by several unforeseen electronics considerations in PCB fabrication, namely the addition

of ground planes, and shielding of the generated input signals, among others. This led to the development of a second-generation multiple output waveform generator. This generator was subsequently adopted for the current project, along with the software intended to control the output frequency of the waveform generator and the subsequent analysis of the captured images. The finally developed system was comprised of:

1. Multiple output waveform generator, which is currently limited to 8-channel, but is extensible for up to 16 channels. The number of output channels depends on the type of multiplexer used, while the fidelity of the output signal depends on the filtering and shielding of the fabricated PCB board;

2. Microelectrode device, which consists of a gasket layer sandwiched between an ITO and gold-coated glass slides to create a chamber for the DEP experiments to take place. The electrode is fabricated using photolithography method and the design was based on the microdot array planar electrode used by Fatoyinbo *et al.* (2008); and

3. PC-based control and analysis program, to allow various parameters and variables (e.g. frequency range, and input signal voltage) to be entered prior to the conducting of DEP experiments, and to control the analysis of the captured images. The program allows the analysis to be conducted using a selection of analysis algorithms, and for different types of resulting plots to be displayed.

This chapter documents the processes involved in completing each of the above components. Section 3.2 describes the design and development stages of the first version of the waveform generator, while Section 3.3 briefly covers the second version of the generator. This chapter then continues with the documentation on the development of the microelectrode device (Section 3.4), and the techniques used in analysing the captured images in order to produce corresponding DEP spectra from which the electrophysiological properties will be extracted (Section 3.5). The outcomes from a number of improvements made to the hardware and software of the currently developed system are explained in Section 3.6.

3.2 Multiple output waveform generator (Version 1)

There is a need for developing an in-house programmable, multiple output waveform generator unit because there is none currently available general purpose signal generator on the market. This is reflected to a certain extent by at least two patents that involved the generation of electrical signals for multiple outputs, namely Patent Numbers 6,038,477 and 6,293,941; and most probably due to the lack

of demand for such devices. Since the current project requires the AC signal to be supplied independently at different frequencies for each of the individual electrodes, it is therefore of utmost importance that such waveform generator be designed and developed.

A waveform generator is essentially a device capable of producing repetitive waveform (i.e. sinusoidal, in the case of AC), and therefore requires an electronic oscillator. Nowadays however, the same outcome may be achieved by first creating the waveforms digitally using digital signal processing techniques, and followed by a digital to analog converter (DAC) to produce the required analog output. Due in part to the advancement of microfabrication, and another to its wide usage in the electronics, direct digital synthesis (DDS) integrated chips are now widely available to produce both of the aforementioned functions. The added advantage of using DDS chips as opposed to analogue oscillators, is the ability to finely tune the output using computer programming methods.

These DDS chips primarily differ in terms of the number of output channels, frequency range, input and output power, and output accuracy. For the purpose of this project it was decided that the DDS of choice must be able to produce stable sinusoidal signals up to a minimum of 20 MHz, with as low power consumption as possible. The chip must be programmable (either through computer or microcontroller interface), and the output be of sufficient voltage to be amplified accurately. The outline in designing the multiple output waveform generator for the project therefore can be summarised in Figure 3-2. The desirable output frequency values will be entered by the user through a computer user interface, which will then be converted to machine readable commands to be executed by the microprocessor, prior to it being sent to the DDS chips. These commands will be sent in series to each of the DDS chips in use via a multiplexer, which will assign the order of the receiving DDS chips based on their addresses. Although this might not technically fulfil the objective of producing concurrent output signals, this is still practically achievable since the lag between the sending of the commands in between these DDS chips is in the region of microseconds. Once the DDS chips have received the required command, each of the chips will then synthesise the corresponding signal digitally that will subsequently be converted to an analog signal. The output signal normally will not have the required voltage to be used directly, and therefore will need to be amplified using a series of amplifier circuitry.

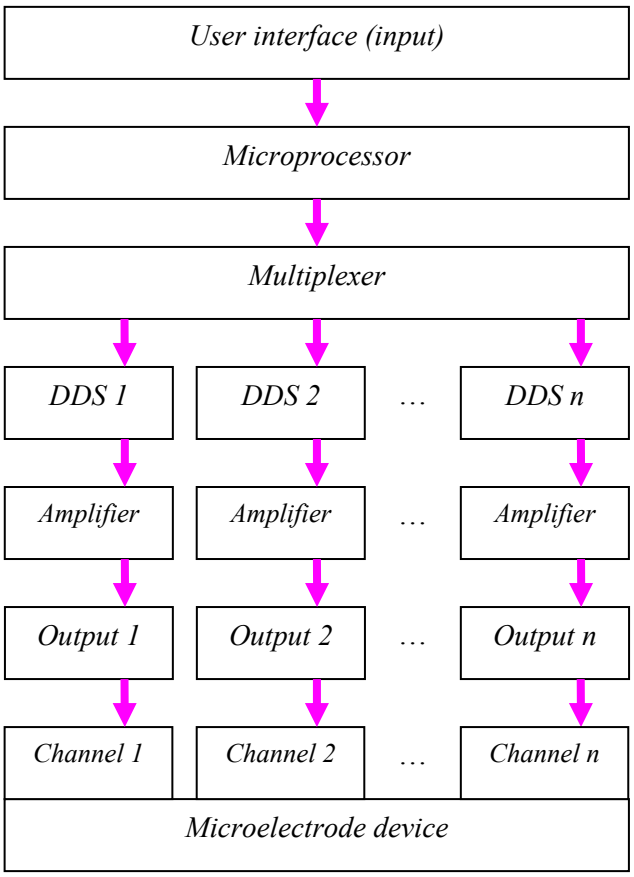

Figure 3-2 A flowchart of the overall waveform generator circuit design

3.2.1 Waveform generator chip

The choice of the DDS chips directly affects the overall scheme of the circuit design, as it affects the programming of the input/output control and the subsequent amplification of the output. The AD9833 (Analog Devices, Norwood, MA, USA) waveform generator is chosen because it generally fulfils the criteria mentioned in the previous section, and primarily due to its low power (2.3 to 5.5 V) and easily programmable interface (i.e. compatible with digital signal processing and microcontroller standards). Since the frequency registers are 28 bits, an output signal having a resolution of 0.1 Hz may be achieved with a 25 MHz clock rate (Analog Devices, 2003).

3.2.2 Microcontroller

The microcontroller chip chosen for the project is PIC16F877 (Microchip Technology Inc., Chandler, AZ, USA), a 40-pin, programmable CMOS FLASH-based 8-bit microcontroller. It is one of the widely used microcontrollers in the market catering to the needs of analog-to-digital applications in

automotive, industrial, and consumer applications (Microchip, 1999). The primary consideration in using it in the hardware development of this project is due to its uncomplicated assembler language programming, and also the availability of five programmable input/output ports.

A complete assembler language code used in the hardware development of the project is available in the CD-ROM supplied in Appendix B.

3.2.3 Circuit and PCB design

Prior to the circuitry being assembled onto a prototype board, it was first tested *in silico* in a simulation program to ensure the design was electronically sound. The circuit was modelled and tested using Multisim 10.1 (National Instruments, Austin, TX, USA). By using the information gathered from the manufacturer datasheet of each of the main components (RS-232 receiver, DDS chip, microcontroller, and the amplifier chip), the complete circuitry was designed, with particular attention towards the power and grounding needs of each of the components. Once the simulation of the circuitry was proven to be satisfactory, the schematic circuit design was prepared using an open-source software, ExpressSCH v6.1.4 (ExpressPCB, Santa Barbara, CA, USA). Figure 3-3 shows the final schematic design of the 4-channel output waveform generator circuitry (showing only two of the output channels) using AD9833 DDS chip. The final high-resolution version of the schematic diagram is available in the CD-ROM supplied in Appendix B.

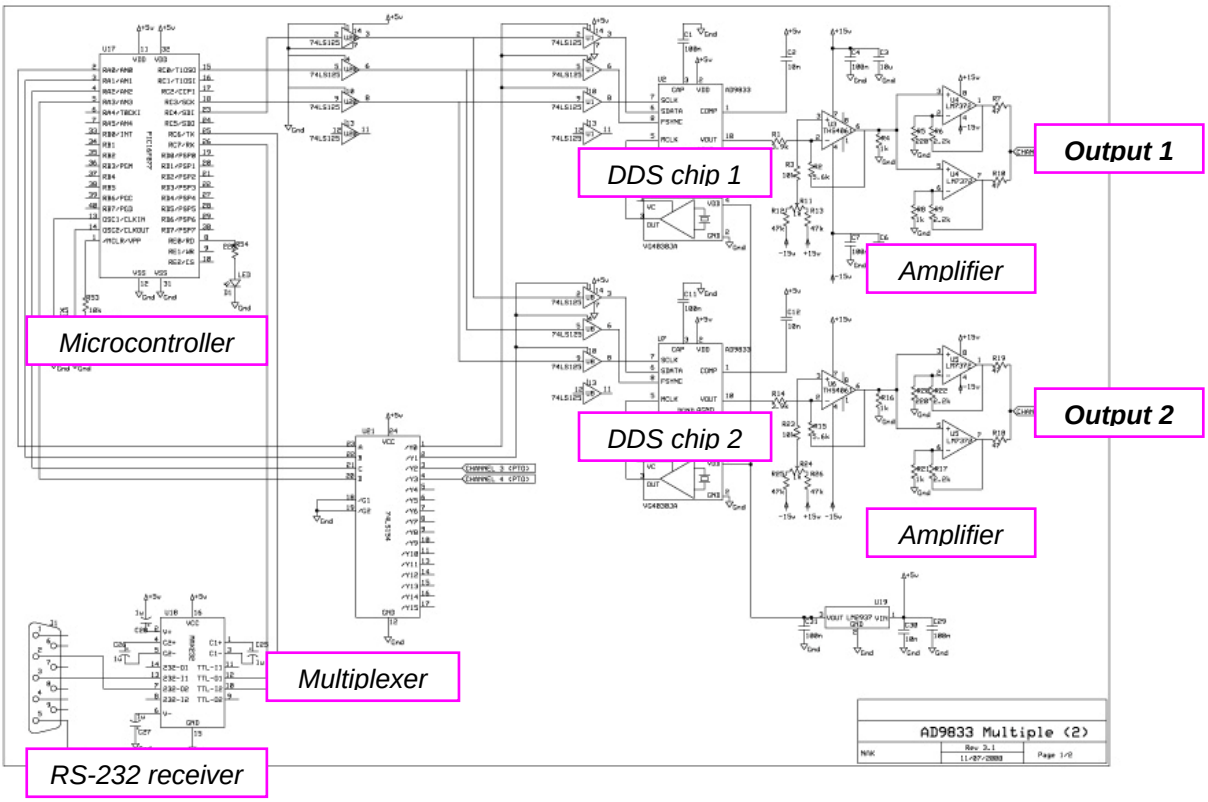

Figure 3-3 The final schematic circuit design for the 4-channel output using AD9833

The PCB design was produced using another open-source software, Pad2Pad v1.8.8 (Pad2Pad, Mahwah, NJ, USA). The primary reason of choosing this software over the bundled PCB design software that comes with ExpressSCH is that Pad2Pad provides an auto-router feature, thus making it easy to verify all of the connections. The graphical user interface of the software is also intuitive and easy to learn.

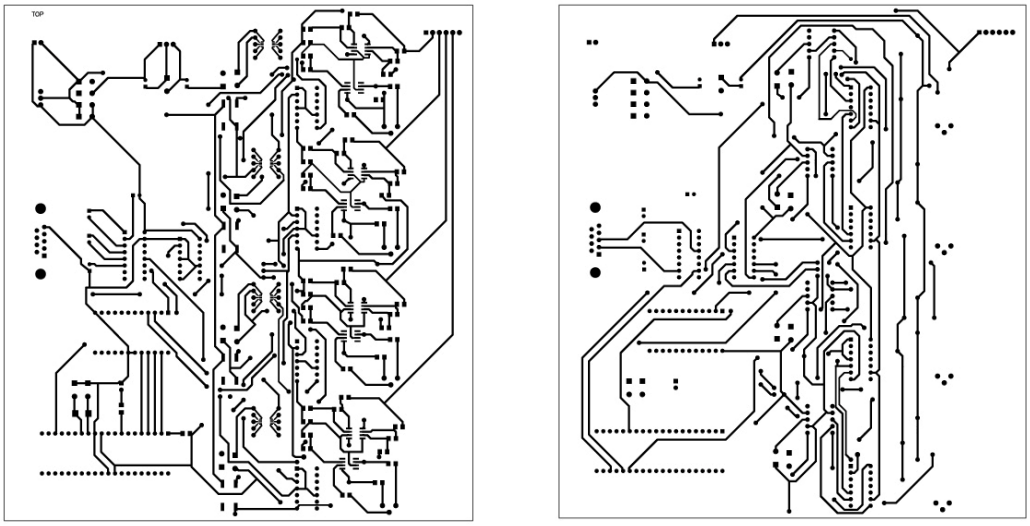

(a) (b)

Figure 3-4 The final 2-layer PCB design for the 4-channel output using AD9833; a) the top layer, and b) the bottom layer

The PCB design for a 4-channel output using AD9833 is shown in Figure 3-4 (the final high-resolution version of the PCB design is available in the CD-ROM supplied in Appendix B). Table 3-1 summarises the protocol used in fabricating the PCB board in this project. Figure 3-5 shows the fabricated PCB that was intended to supply four individually programmed output signals. As mentioned in the Introduction section of this chapter, the PCB was not functioning, and thus the development of this version of the waveform generator was terminated at this point.

Table 3-1 Summary of PCB board fabrication

Steps	Actions
Step 1	Print the final PCB layout design for both top and bottom layers onto a transparent or semi-transparent film, e.g. transparency acetate film for overhead projectors (3M, Austin, USA). Ensure that the top layer is mirror-imaged.
Step 2	Staple these printed films together (printed sides together).
Step 3	Prepare the developer (add 25 g of Universal Developer (RS Components, Northamptonshire, UK) into 1 L of warm water) and etchant (heat about 4 L at 50°C) solutions. The etchant solution was prepared earlier using ferric-chloride hexahydrate granules (Mega Electronics, Cambridge, UK).
Step 4	Cut the PCB board according to size. Place it in between the stapled films.
Step 5	Place the arranged layers in the UV lightbox, and expose for 120 seconds. Ensure that the UV lightbox is warmed up prior to actual exposure.
Step 6	Place the exposed board into developer solution. Wash with warm water once the

	exposed photoresistant layer has washed off. Dry the board.
Step 7	Place the board into the etching solution. Warm for about 5 minutes on each side. Repeat until all exposed copper layer has washed off.
Step 8	Wash with water and dry.

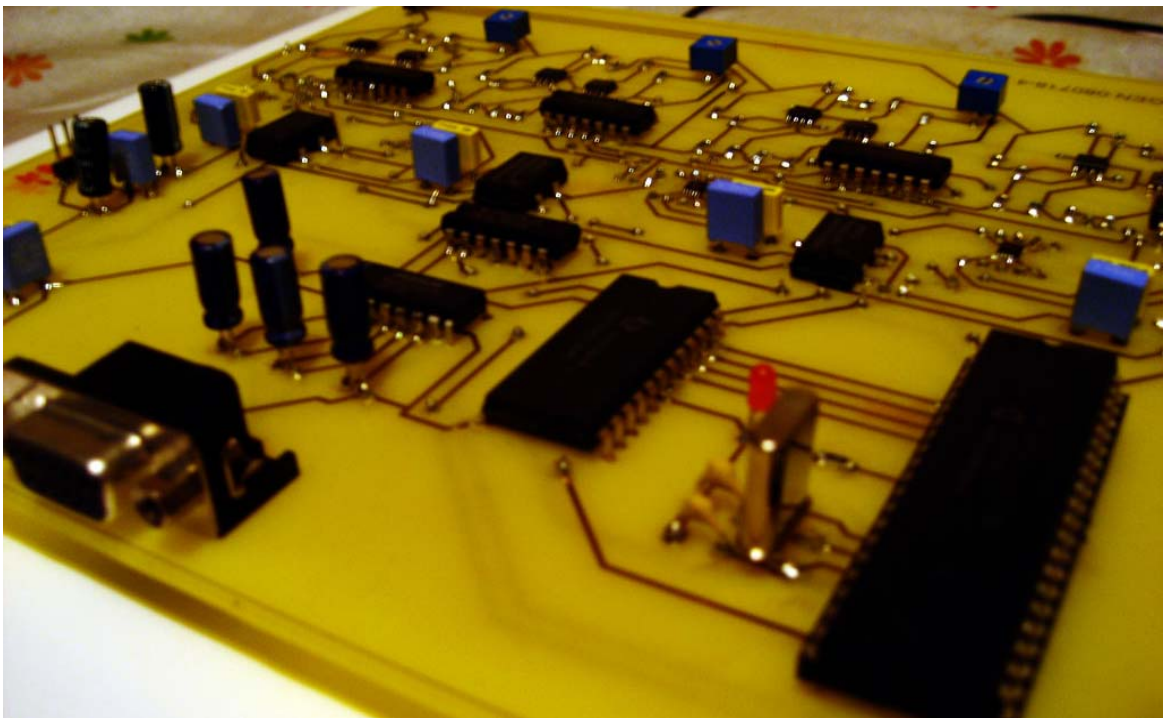

Figure 3-5 The fabricated PCB board of the multiple output waveform generator (Version 1)

3.2.4 Graphical user interface and software

MATLAB (The Mathworks, Natick, MA, USA) is the high level programming language of choice in developing the graphical user interface to send input data to the microcontroller (Figure 3-6). The data consists of the different frequency values (in Hz) for each of the channel outputs and the period (in seconds) for the signal to be sent. The data were sent using RS-232 serial connection to the microcontroller, which subsequently is responsible for sending the equivalent commands to the waveform generator chip. The output from the waveform generator has been verified using an oscillator. Although there was a plan to expand this simple program to include the analysis algorithm for the produced DEP spectra, this was also terminated due to the non-functioning of the fabricated waveform generator.

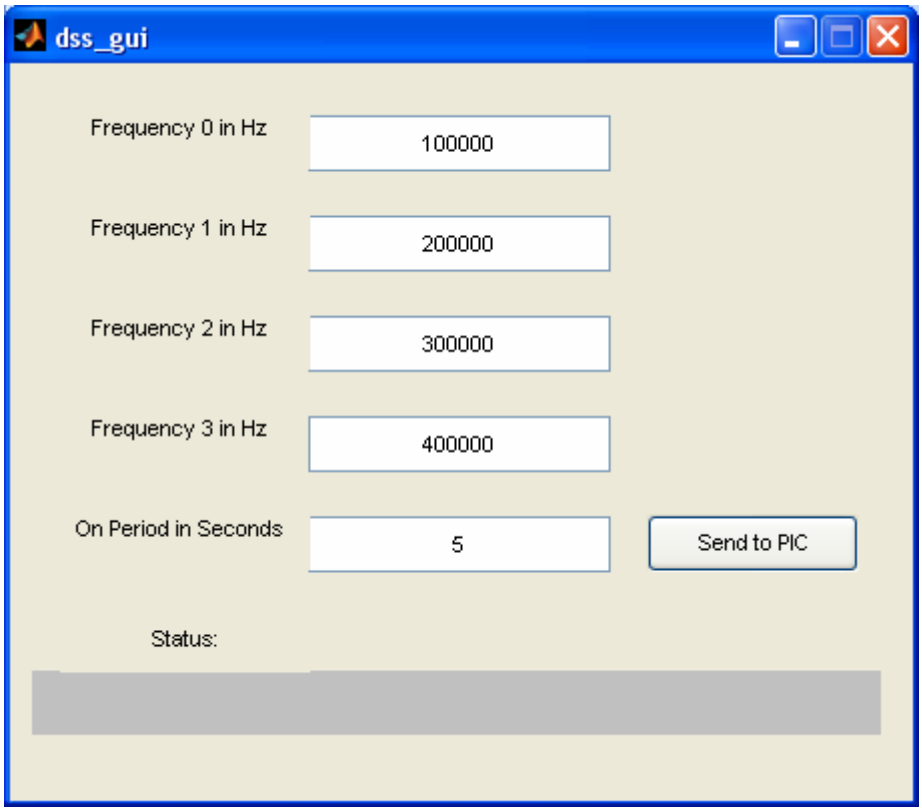

Figure 3-6 Graphical user interface developed for the system

Table 3-2 shows the output of the prototype waveform generator from a selected range of frequencies between 1 kHz to 1 MHz, verified using a digital oscilloscope (Isotech IDS710, RS Components, Northants, UK). The output frequencies seemed to closely match the setting frequency entered via the graphical user interface with small error margins. This error may be further corrected by the implementation of offset-reducing or filtering circuitry. The error could even be simply down to the quality of the printed circuit board production, which was fabricated in-house.

Table 3-2 Stability of system output

Setting Frequency (kHz)	**V_{P-P} (V)**	**V_{RMS} (V)**	**Output Frequency (kHz)**	**Error (%)**
1	8.8	3.0	1.0	0.0
5	9.0	3.0	4.9	2.0
10	8.9	3.0	9.8	2.0
20	8.8	3.0	19.5	2.5
50	8.8	3.1	48.7	2.6

100	8.9	3.1	97.8	2.2
200	9.0	3.1	196.8	1.6
500	9.2	3.2	490.6	1.9
1000	9.2	3.4	983.6	1.6

3.3 Multiple output waveform generator (Version 2)

A modular system was developed, using a PC, to interface with a master microcontroller block. This was in turn capable of interfacing with up to five signal generator modules, each capable of producing four signals with independently controllable amplitude, frequency and phase signals. The timing of channel switching (on/off) is also applied centrally, allowing multiple electrodes to be connected to signals of different frequencies for a preset time and analyzed in parallel.

3.3.1 Waveform generator chip

A four channel direct digital synthesizer (DDS AD9959, Analog Devices, USA) was used to provide independent frequency, phase and amplitude control on each channel, while reducing PCB component numbers. The AD9959 can attain a maximum reference clock input of 500 mega samples per second; the four channels are synchronized by sharing a common clock. Each channel has 15 registers which allow a 32-bit frequency tuning word, giving a frequency resolution of 0.12Hz, and 10-bit resolution DAC output with maximum full scale current steering output of 10mA.

3.3.2 Microcontroller

An 8-bit CMOS microcontroller (PIC16F887, MicroChip Technology, USA) was embedded with firmware developed in-house on MPLAB IDE v8.36 software (MicroChip Technology, USA). The microcontroller was used to control the AD9959 and other peripheral devices on the PCB. Data transfer between the PIC16F887 and AD9959 took place via a serial peripheral interface (SPI) single bit 3-wire mode, enabling both register writing to and reading from the AD9959 on separate lines. Serial communication between PC and microcontroller was achieved using a standard 9-pin RS-232 serial port via an IC surface mount transceiver (MAX232, Maxim Integrated Products, USA). Figure 3-7 shows the developed PCB of the waveform generator.

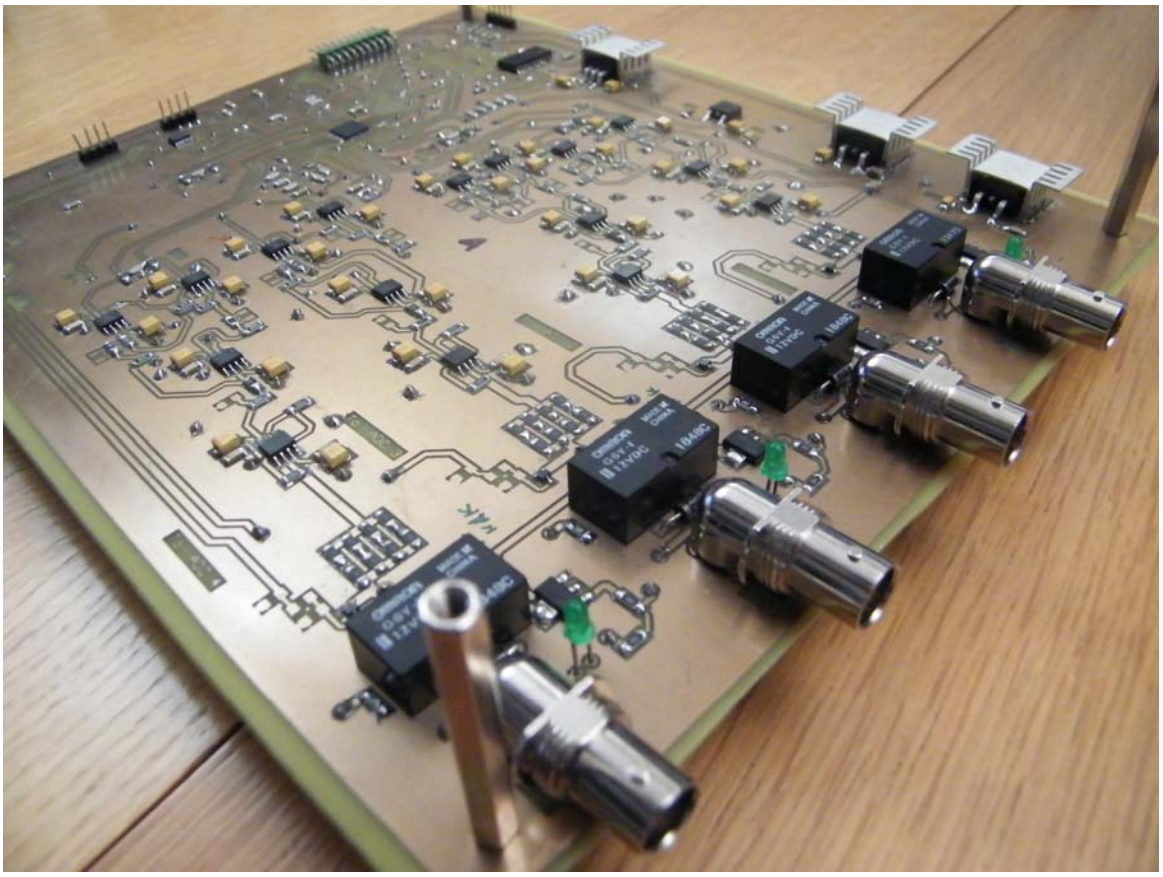

Figure 3-7 The fabricated PCB board of the multiple output waveform generator (Version 2)

3.3.3 Graphical user interface and software

Control of the DDS took place at the PC level, via menu options embedded on the microcontroller. To facilitate a quick and easy programmable system a master graphical user interface with five main panel sections was designed (Figure 3-8). Sections A and B are used primarily to control the input signal and image acquisition, respectively, when conducting a DEP experiment. Variables such as number of input channels, frequency range, and peak voltage of the input signals may be entered in Section A, while camera selection and file naming parameters may be entered in Section B. The bottom row of panels are involved in the analysis of the captured images, which may be done either in real-time (i.e. following an actual experiment), or off-line (i.e. for previously saved captured images). Sections C and E are display panels for captured image frames and plots for analysed data, respectively; while Section D controls the analysis process. A number of analysis algorithm is available, and the user may quickly view the difference in the generated plot displayed in Section E. A detailed explanation on the processes involved in the image analysis of the captured images will be presented in Section 3.5.

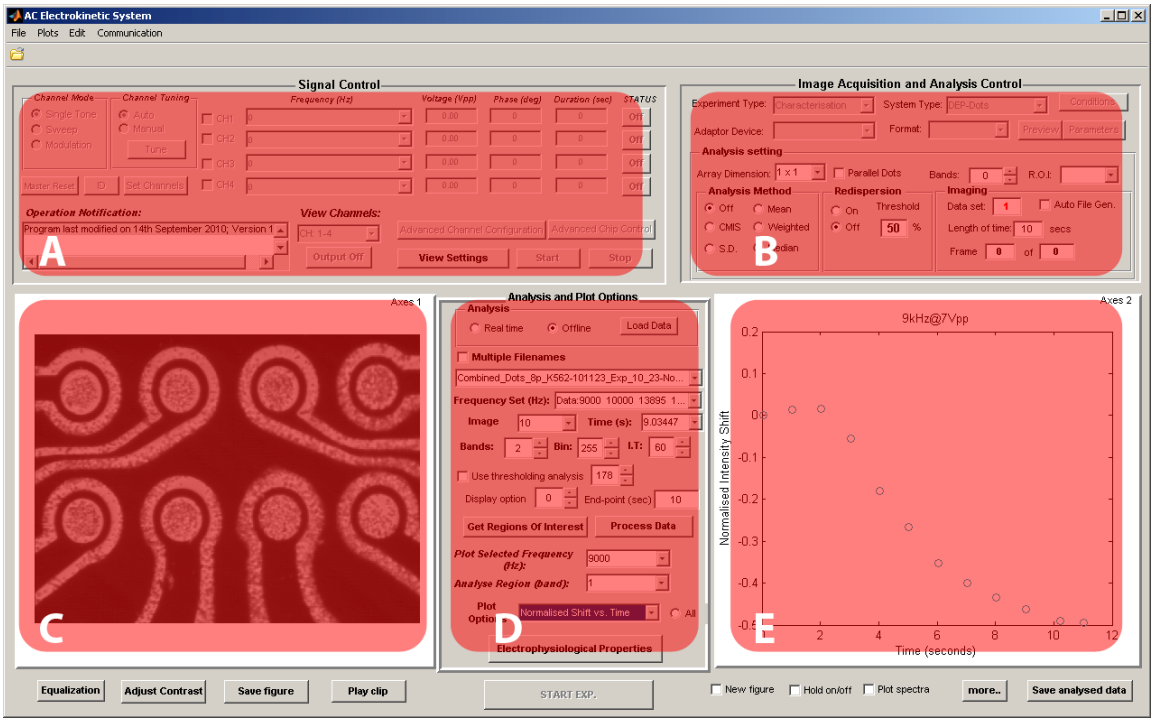

Figure 3-8 The graphical user interface to control the developed system, shown with the different panel sections highlighted

3.4 Microelectrode device

Another important component to the hardware is the microelectrode device, where the cell suspension will be placed and the actual DEP effect will be observed under the microscope and captured using the attached digital camera. The device consists of a gasket sandwiched in between the electrode and the ITO layer. The input signal will be connected to the electrode, and the ITO will be connected to the circuit ground. Both electrical connections will be made using flexible wires, and connected with silver-loaded epoxy. The gasket will act as a spacer in creating a chamber for the cell suspension to be placed and DEP experiments to be conducted in and recorded from. Figure 3-9 shows a schematic of the arrangement, and Figure 3-10 shows an actual microelectrode device used in the experiments. The subsequent subsections will detail the processes involved in fabricating each of the component layers for the microelectrode device.

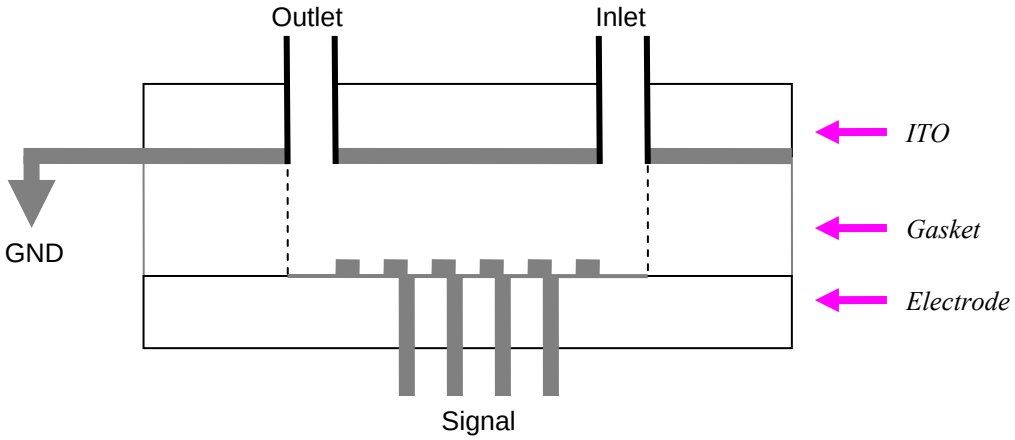

Figure 3-9 A schematic diagram of the microelectrode device; where Inlet and Outlet indicates the flow path of the cell suspension, Signal is output from the waveform generator, and GND is circuit ground

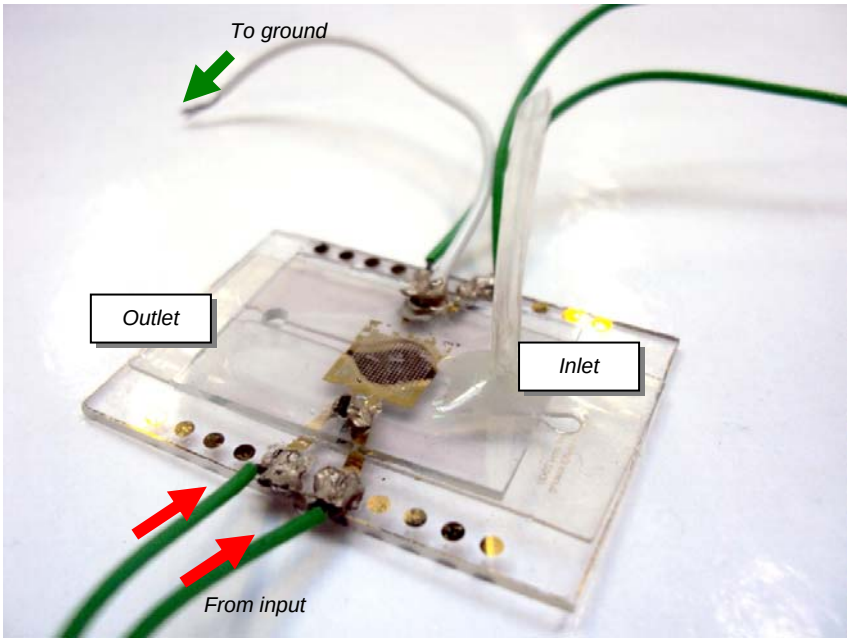

Figure 3-10 An example of the prepared microelectrode device for serial set-up

3.4.1 Microelectrode

As briefly mentioned in Chapter 2, the electrode geometry of choice for the current project is planar in nature; and the design is a modification of that used in the single dot system proposed by Fatoyinbo *et al*. (2008), which has been shown to be capable in conducting DEP-based cell characterisation experiments in a short period of time. The electrode used in the previous study by Fatoyinbo *et al*.

(2008) employed a 4-by-4 dot array design, but did not allow individual dots to be energised separately. For the current project, a 4-by-4 array of individually connected dots was designed to allow individually-programmed input signals with different frequencies to be supplied (Figure 3-11). Ground planes were added in between the electrodes (Figure 3-11(c)) to ensure the generated electrical field over each of the individual dots does not affect any of the adjacent ones.

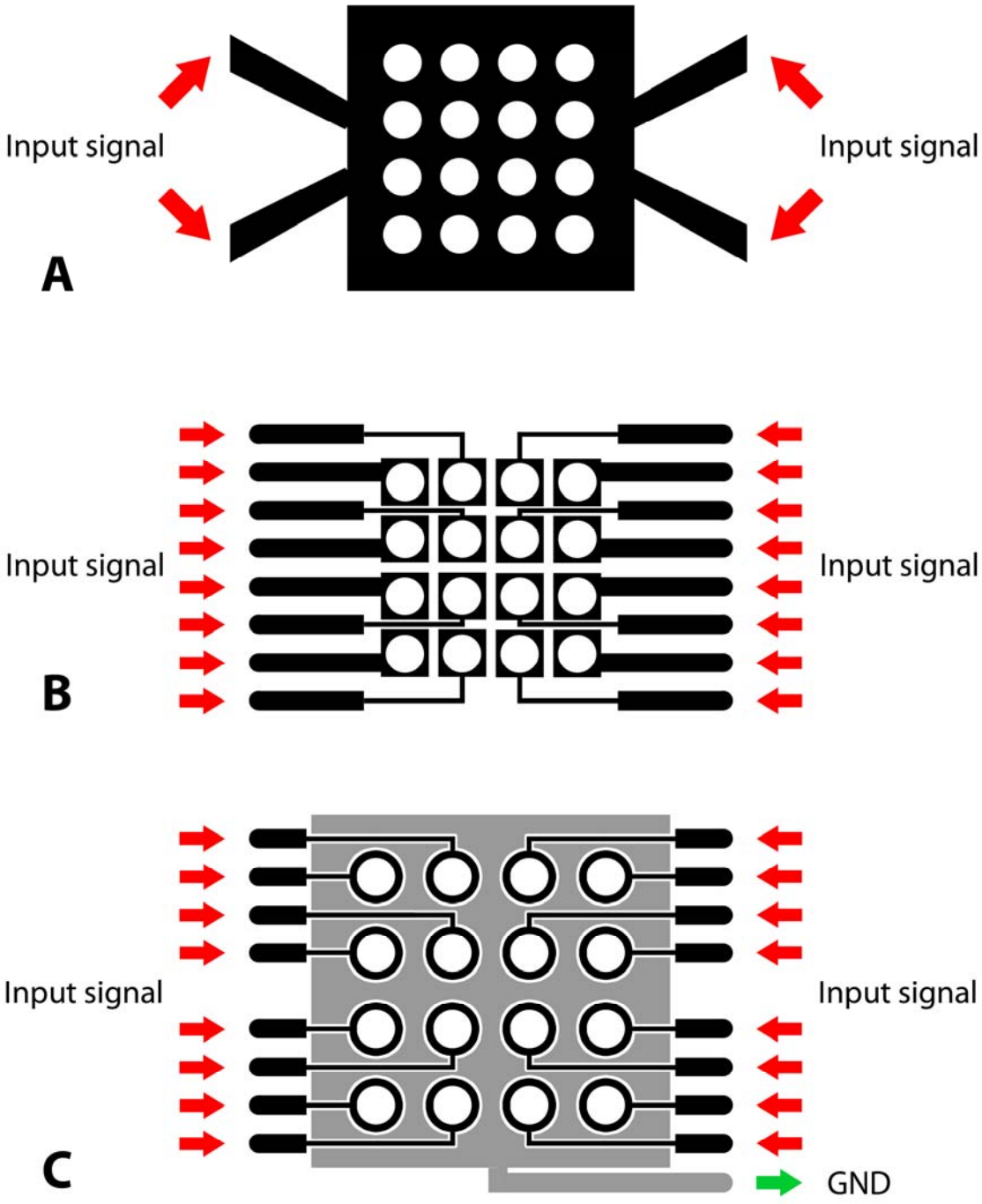

Figure 3-11 A schematic diagram of the electrode design used for a) the serial set-up, b) the parallel set-up (without ground planes), and c) the parallel set-up (with ground planes)

The reason the dot array design was chosen compared to the other available designs for planar electrodes was due to the capability of generating electrical fields with axisymmetrical gradient over each of the dot aperture. In the single dot system, the field gradient of the dot was observed to have a hemispherical geometry at the centre of the dot aperture, thus indicating that the DEP force was also axisymmetrical within the dot volume (Fatoyinbo *et al*., 2008). The force should be greater at the electrode edge, and decreasing in magnitude towards the centre of the dot, and should therefore provides a correlation between the particle motion and the relative polarisability. By having multiple dots with similar diameters receiving individualised signals in parallel, the DEP effects for a very small population of cells (i.e. smaller than cell samples used in the DEP-well system) should be able to be observed and recorded, as opposed to limiting the observation and recording to single cells in previous DEP studies employing planar electrodes (e.g. Müller *et al.*, 1996, Wang *et al.*, 1997, Prasad *et al.*, 2005).

The microelectrode fabrication process starts with the design of the masks required to be used in exposing the gold-coated glass slides (10 nm Ti, 100 nm Au). The design may be made with any vector-based drawing software or applications that allow precise dimensions to be produced at very high resolution (more than 1200 dpi). The Centre for Biomedical Engineering at the University of Surrey is currently using Solid Edge V19 (Siemens PLM Software Inc., Munich), but other drawing or computer-aided design (CAD) tools, including a wide range of application suites from Adobe (Adobe Systems Inc., San Jose, USA), Autodesk (Autodesk Inc., San Rafael, USA), or Corel (Corel Corp., Ottawa, Canada) should be technically compatible as well. The high resolution requirement in printing the masks is due to the nature of the electrode design that may include openings that are separated by a distance in the region of microns.

The fabrication process is based on the photolithography method, using UV exposure and subsequent developing and etching processes. Table 3-2 summarises the protocols used in fabricating the microelectrode for this project. Figure 3-13 shows an example of the completed microelectrode. Originally the microelectrode was designed without ground planes in between the individual dots, but this was later improved to include the additional ground planes, which helped in the generation of electric fields with stronger gradients.

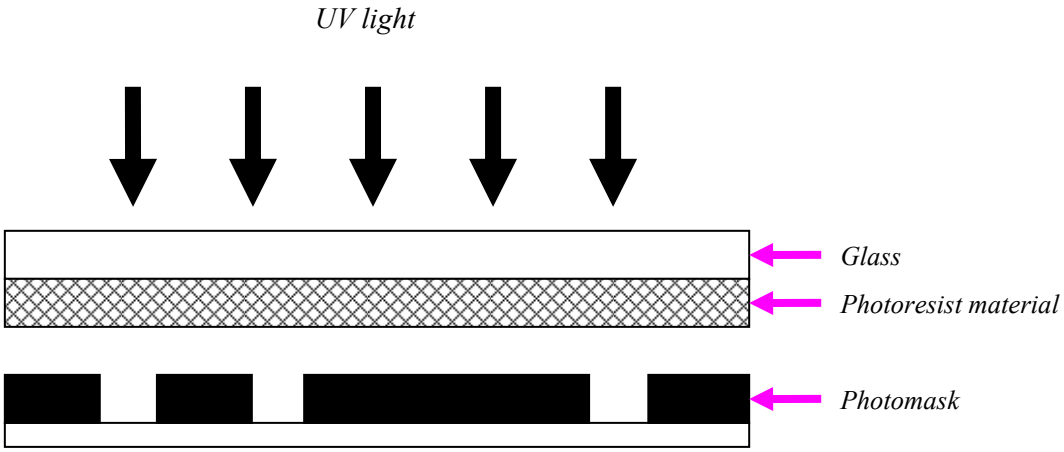

Figure 3-12 Arrangement of glass slide and mask in the UV lightbox

Table 3-2 Summary of microelectrode fabrication

Steps	Actions
Step 1	Cut the gold glass slides according to the mask dimensions, i.e. about 26 mm × 38 mm. Leave overnight in 70% ethanol solution.
Step 2	Clean and dry the glass slide; then attach the glass slide on top of the photoresist spinner (Headway Research Inc., Garland, USA) set at 4000 rpm and 50 seconds. Mark the centre of gravity for the glass to ensure it will not fly off when spinned.
Step 3	Apply several drops of the photoresist solution (Microposit S1813 SP15 Photoresist, Rohm and Haas (UK) Ltd., Staffordshire, UK) onto the glass slide. Avoid producing bubbles to ensure uniform covering of the surface.
Step 4	Remove glass slide from spinner and leave it on top of magnetic stirrer hotplate (Heidolph Instruments GmbH + Co. KG, Germany) set at 100°C for 60 seconds ('soft' baking).
Step 5	Once completed, put it away from possible light sources.
Step 6	Repeat Steps 2 to 5 for any remaining glass slides.
Step 7	Arrange the glass slides and mask accordingly on top of the glass platform of the UV lightbox (manufacturer location). Figure 3-12 shows a schematic of the arrangement. Expose for 50 seconds.
Step 8	Develop the exposed glass slide with Microposit 351 (Rohm and Haas (UK) Ltd., Staffordshire, UK) solution, previously prepared at 4:1 dilution, for about 5-10 seconds. Leaving the glass slide longer in the developing solution will adversely affect the unexposed gold layer.
Step 9	Put the glass slides into the oven set at 90°Cfor 45 minutes ('hard' baking).
Step 10	Prepare three solutions: gold etchant, 18% HCl, sodium carbonate (Na_2CO_3), and

	sodium thiosulfate ($Na_2S_2O_3$)
Step 11	Place the glass slide into the gold etching solution, and remove once the exposed gold has washed off. Clean with sodium thiosulfate solution and deionised water.
Step 12	Heat the HCl solution on the hotplate until it reaches boiling point. Place the glass slide in the solution.
Step 13	Remove glass slide once the seed layer has bubbled away. Clean with deionised water.
Step 14	Place the etched glass slides into a positive photoresist stripper (SVC^{TM}-175, Rohm and Haas (UK) Ltd., Staffordshire, UK) solution for 5-10 seconds to remove excess photoresist. Clean with deionised water, and dry.
Step 15	Dispose all solutions safely.

The gold etchant solution used in Table 3-2 was prepared earlier and made up of 10% potassium iodide (KI) and 2.5% iodine (I_2) solutions, with the remaining made up of deionised water.

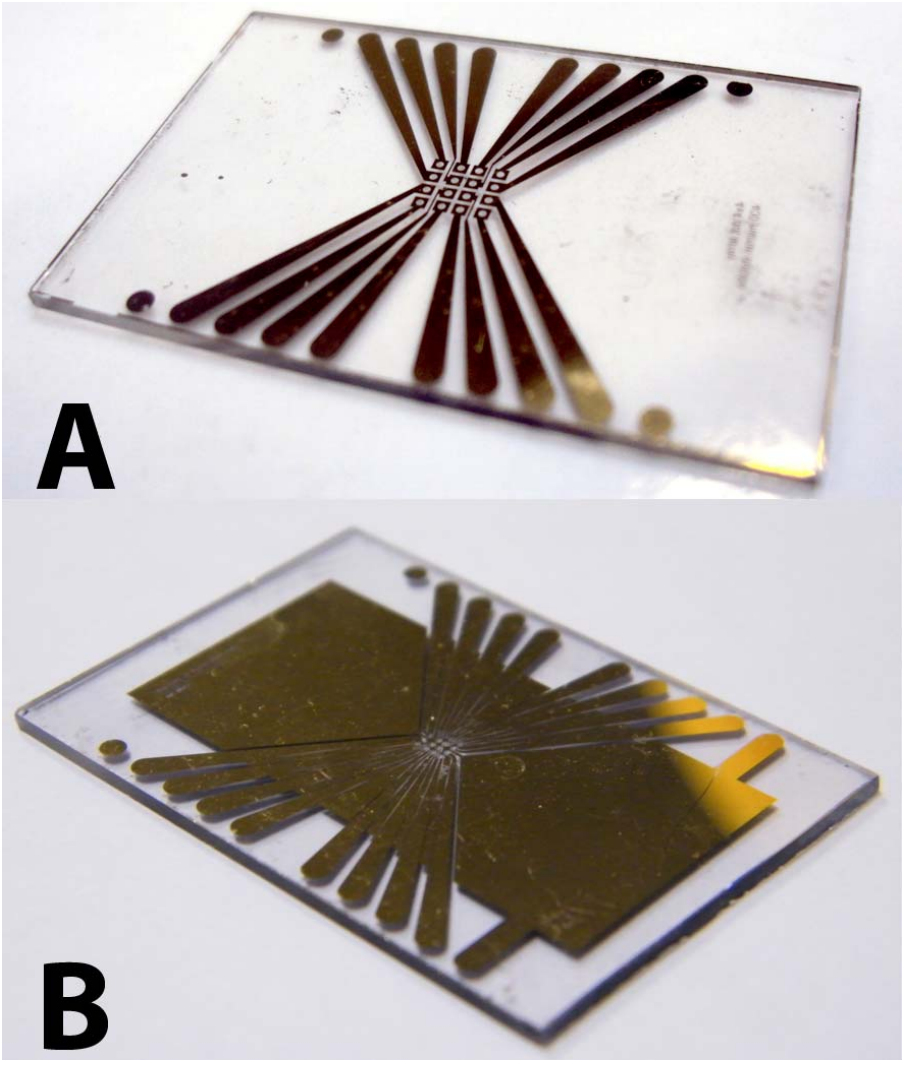

Figure 3-13 A completed microelectrode a) without ground plane in between the dots; b) with ground planes

3.4.2 Gasket

Over the course of the project two materials have been considered and used for the gasket construction, namely the double-sided sticky tape and polyresin (Polydiam Industries Ltd., London, UK) (Figure 3-14). The design invariably revolves around a rectangular gasket with a circular shape cut at the centre (Figure 3-13), creating a chamber for the cell suspension to be placed. As part of the improvement for the device, the current gasket design does away with the circular centre, as it was thought that the smooth flow of the solution will be considerably impeded as it travels from the inlet towards the outlet. This is particularly troublesome for the microelectrode setup, as a uniformly spread layer of cells is a prerequisite prior to conducting the experiments.

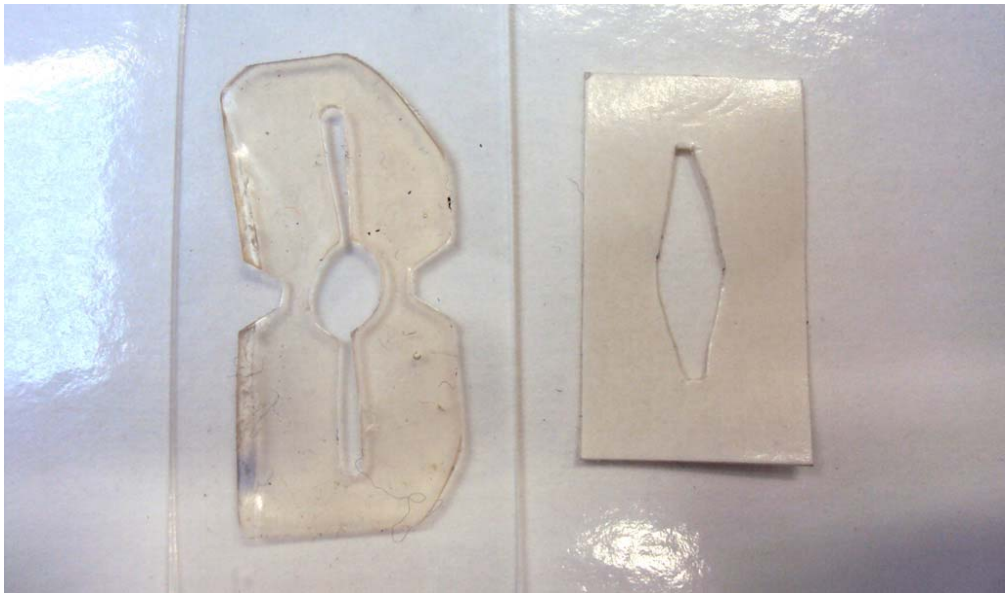

Figure 3-14 Gaskets for the microelectrode prepared from and polyresin (left), and double-sided sticky tape (right)

The advantage of using the tape is that it may be fabricated easily using a pair of scissors and/or scalpel, and the shape may easily be changed according to the geometry requirements of the electrode and experimental needs. However, this may also become a disadvantage in itself because the final shape of the chamber may not be perfectly symmetrical, and thus will not ensure a smooth flow of the cell suspension moving from the inlet towards the outlet. It has been found that an uneven flow will create a localised collection of cells around the edges of the chamber, and also make the uniform re-suspension of cells at the end of each experimental set more difficult. Due to the presence of adhesive material on the surface of the tape, it is also considerably much harder to remove from the device, compared to when using the polyresin gasket. The adhesion of a polyresin gasket only relied on the

electrostatic effect between the gasket and the glass slides, and this may easily be compromised by the seepage of the suspending solution via capillary action.

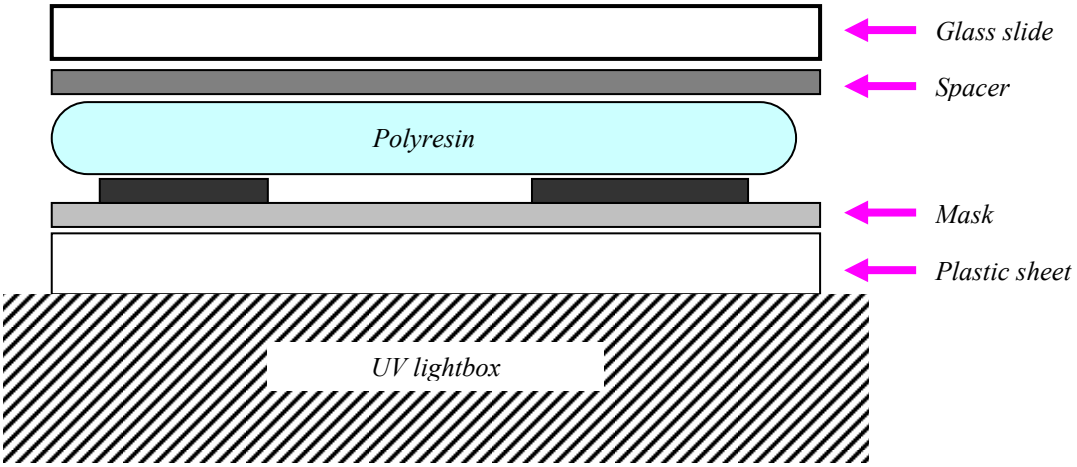

Figure 3-15 Arrangement of materials and gasket mask in the UV lightbox

Although a gasket made from the polyresin will be perfectly symmetrical, and thus removes the problem of an uneven flow of the cell suspension, the processes involved in fabricating a polyresin gasket is slightly longer, as it involved the design and printing of the appropriate mask, the UV exposure, and finally the washing of the unexposed polyresin. Depending on the complexity of the mask design, the whole fabrication process will take anything between 30-60 minutes. Nevertheless, this may be completed up to a few days before conducting an experiment, and will remain useable for up to 2 to 3 weeks. Table 3-3 summarises the steps taken in fabricating a polyresin gasket.

Table 3-3 Summary of gasket fabrication using polyresin

Steps	Actions
Step 1	Design a high resolution (300dpi minimum) mask in any graphic editing software.
Step 2	Print the design onto a transparent or semi-transparent film, e.g. transparency film for overhead projectors (3M, Austin, USA). Any types of film commonly used in transferring PCB circuit designs onto PCB boards may also be used.
Step 3	Arrange the materials and mask accordingly on top of the glass platform of the UV lightbox (manufacturer location). Figure 3-15 shows a schematic of the arrangement.
Step 4	Expose for 40 seconds.
Step 5	Remove the plastic sheet and wash away the unexposed polyresin using a washing detergent solution mixed in warm water. Alternatively use an ultrasonic bath (Branson 1510, Branson Ultrasonics Corp., Danbury, CT, USA) to remove excess polyresin, to

	avoid scrubbing of the gasket surface.
Step 6	Leave the gasket to dry, or blow it dry using the air pump.
Step 7	Carefully remove the gasket from the glass slide and affix it to the microelectrode surface.

Note that the spacer thickness will determine the height of the chamber of microelectrode. The thickness may be adjusted by using small cuttings of sticky tape, and measured using a digital micrometer prior to conducting the experiments. Thicker gasket sizes will require a larger volume of cell suspension to be used. In this project, a layer of sticky tape was routinely used and gave rise to a gasket thickness of about 180 μm.

3.4.3 ITO layer

The ITO (R_s = 4-8Ω, Delta Technologies, Stillwater, MN, USA) needed to be cut to cover the entire chamber created by the gasket (Section 3.4.2). Each of the pieces then required drilling to create the inlet and outlet paths for the delivery of the cell suspension. Another set of holes were also drilled to create a connection between the conductive layer and the electrical ground. Table 3-4 summarises the steps taken in preparing the ITO layer to be used in the device.

Table 3-4 Summary of ITO layer preparation

Steps	Actions
Step 1	Cut the ITO piece into rectangles of about 15 mm by 25 mm.
Step 2	Drill a set of holes for the inlet and outlet. Distance between them must match the design of the gasket in Section 3.4.2. A small tube may be affixed to the inlet.
Step 3	Drill another set of holes for the ground connection. Affix a wire to be connected with the conductive layer using conductive epoxy. Remove excess conductive epoxy to ensure a smooth conductive layer (Figure 3-16).
Step 4	Conductive layer must be dry before it may be affixed to the gasket.

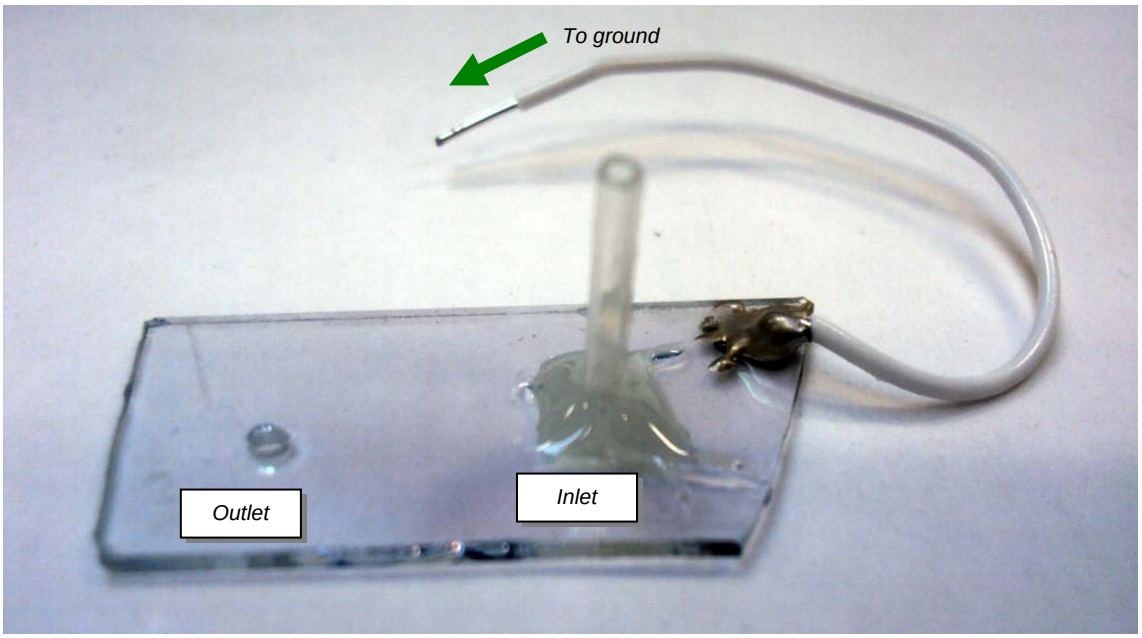

Figure 3-16 An ITO layer used in the project, with the inlet and outlet paths, and the electrical ground connection (wire)

3.5 Image analysis

For the system to be able to extract useful DEP information from the captured images, an image analysis program was developed in-house at the Centre for Biomedical Engineering, University of Surrey, to measure the extent of cellular movement under the DEP influence in order to quantify the relative polarisability of the cell populations in use. The measured values will be normalised and employed in the construction of the corresponding DEP spectrum. The algorithm for the relative polarisability measurement was based on the Cumulative Modal Intensity Shift (CMIS) image analysis technique that was developed for use with single dot planar microelectrode systems (Fatoyinbo *et al.*, 2008). As the name suggests, this method relied on the modal value of the histogram of the captured images. Generally, the algorithm will first detect the modal value by finding the peak of the histogram, and subsequently will sum the total number of pixels starting from this point onwards to the maximum light intensity value of the histogram.

3.5.1 Image segmentation

Before the captured images can be analysed and the corresponding DEP spectrum be plotted, segmentation of the actual dots within the image must be completed. The process will 'segment' out the regions of interest (ROI) from the captured images, which in this case are the images of cell

movements within each of the dots. The algorithm that was used in the current program was based on the microwell DEP system developed at the Centre for Biomedical Engineering, University of Surrey, and used in a number of previous studies (e.g. Broche, 2005; Chin *et al.*, 2006; Labeed *et al.*, 2006; Hoettges *et al.*, 2008).

The segmentation algorithm will generally conduct two main processes, namely the production of a layer mask to distinguish between the electrodes and the dots based on a chosen intensity threshold value, and the detection of bona fide dots based on the similarities of the area sizes. Figure 3-17 shows a summary of the outcome from the segmentation process, prior to the analysis stage.

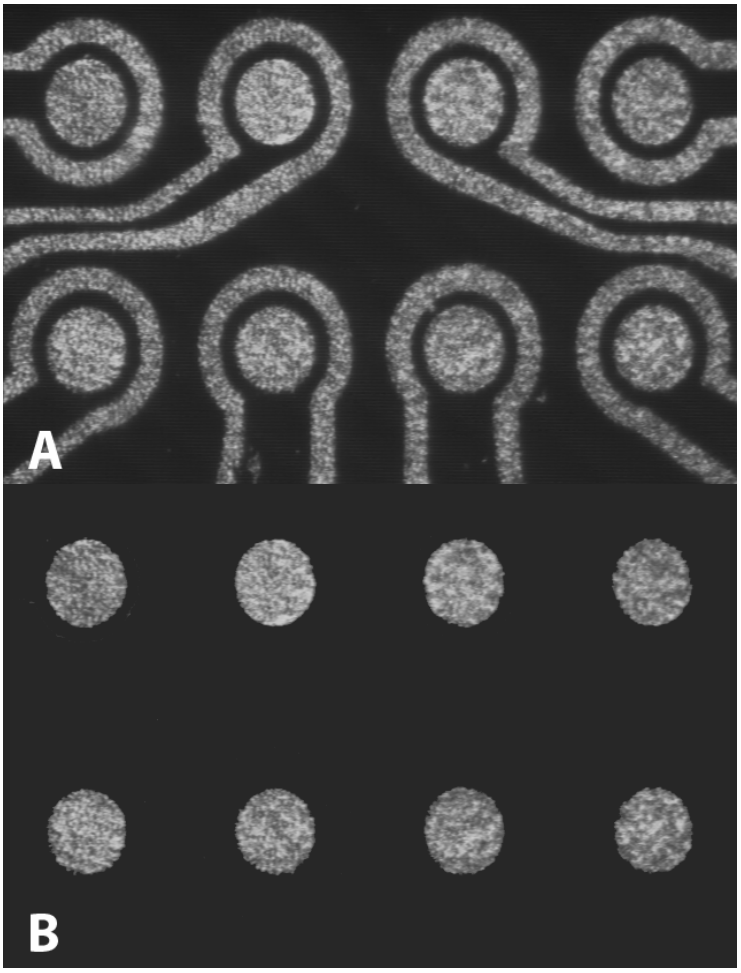

Figure 3-17 A typical captured image of the electrode during a DEP experiment, showing a) before, and b) after the completion of the segmentation process that leaves out the detected ROIs to be analysed later

3.5.2 CMIS method

The fundamental idea behind the method is the relationship that may be found between the Clausius–Mossotti factor and the shift in cellular concentration for a population under microscopic observation, based on the quantification of the latter using the Beer-Lambert's law of light absorption. If a selected central area of the dot is chosen to be the Beer-Lambert region, attraction and repulsion of cells from the dot perimeter by the DEP force will change the light intensity going through the said region. Negative DEP for example, will create an accumulation of cells at the centre of the dot due to the repulsion experienced at the dot perimeter, and thus will limit the light intensity coming through that particular region. Positive DEP on the other hand, will have the opposite effect and will allow a greater amount of light intensity to come through, since the cells will be attracted towards the dot perimeter (Figure 3-18). Quantification of the Clausius–Mossotti factor is made by comparing the changes in the light intensity values between the captured images at a certain time frame with a reference image.

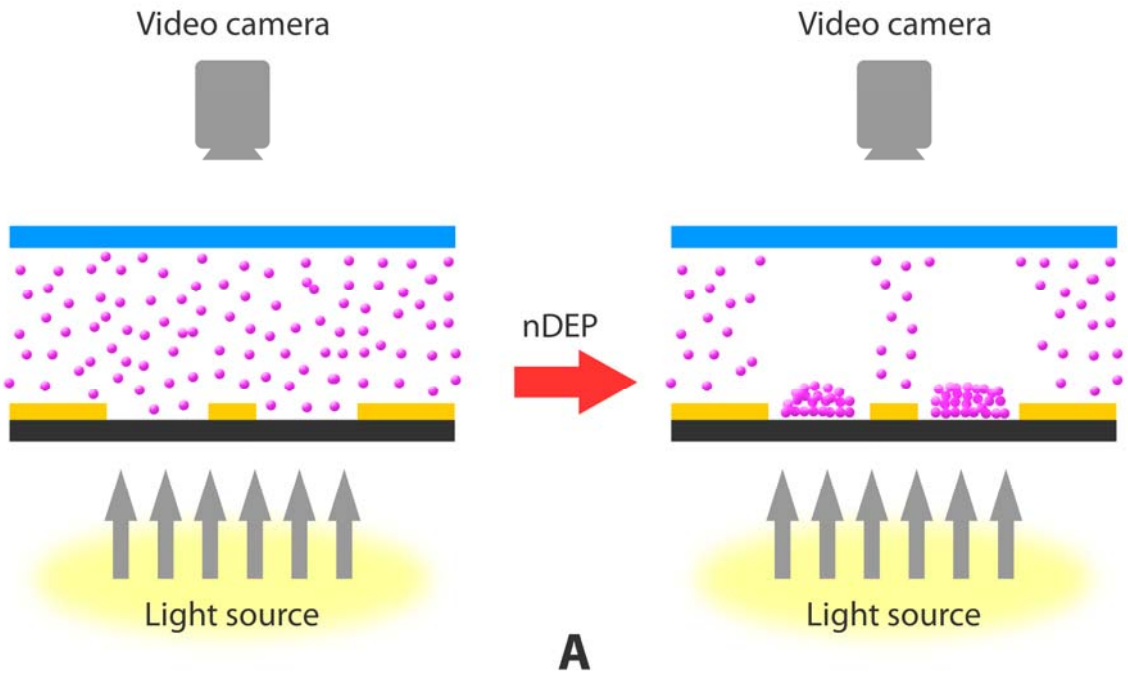

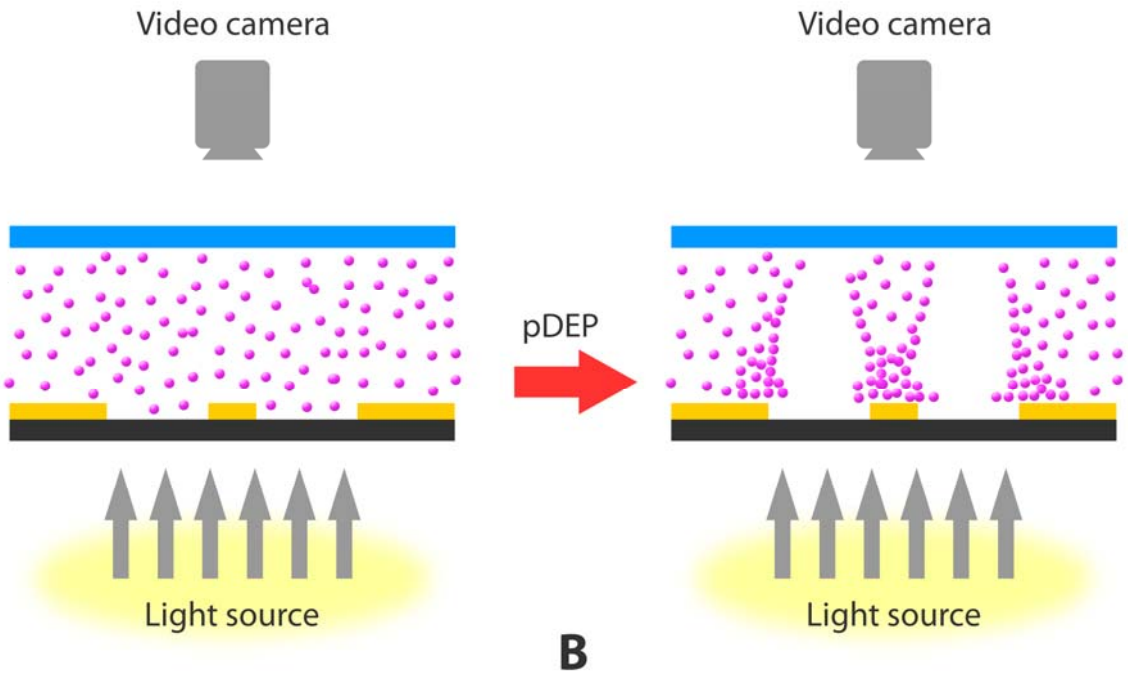

Figure 3-18 A schematic diagram of the movement of cells within the microelectrode device when experiencing a) negative DEP, b) positive DEP, viewed from the side

By assuming that a uniformly dispersed collection of cells as having an initial light intensity of I_0, the final light intensity value of the said region may be defined as:

$$\ln\left(\frac{I}{I_0}\right) = -CA\Delta z \tag{3.1}$$

where C is the concentration of the cells, A is the area of the region and Δz is the total length of the light path. It was found that the cellular concentration is proportional to the average velocity of the cell population movement, and therefore is proportional to the Clausius–Mossotti factor and the applied DEP force. Empirical studies by Fatoyinbo *et al.* (2008) found that the best area to be defined as the Beer-Lambert region for the CMIS method is the central dot area but limited to one-half of the dot radius.

The aforementioned quantification process is based on the sum of the cumulative pixel intensity values of a chosen image, since the value of each pixel in a digital image is represented by a discrete value representing the quantised intensity (Gonzalez *et al.*, 2004). The images were captured using the 8-bit greyscale spectrum, and therefore will have values ranging from 0 (black) to 255 (white). The histogram of each of the captured images will count and sort all pixels with common intensity values.

Figure 3-19 shows the typical histogram plots for the dots before and after signal application, showing the differences depending on whether negative or positive DEP were experienced.

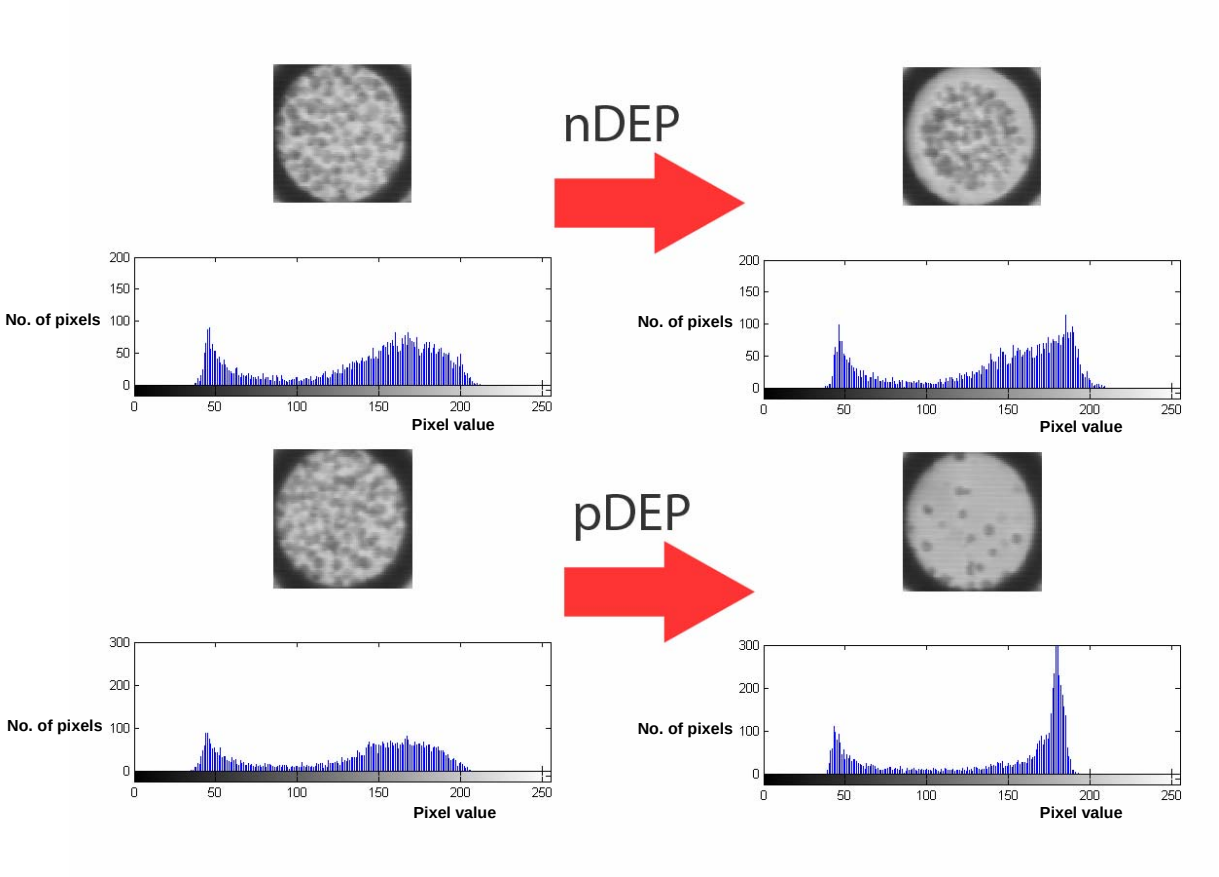

Figure 3-19 The captured images and the corresponding histogram plots for dots experiencing negative DEP (top) and positive DEP (bottom)

The histogram showed a slightly larger proportion of pixels having lesser pixel values (i.e. darker) when negative DEP was experienced (Figure 3-19(a)), while a larger proportion of brighter pixels (i.e. larger pixel values) was seen in dots experiencing positive DEP (Figure 3-19(b)). The cumulative value of pixels, counted from the modal value (i.e. the histogram peak) upwards towards the spectral maximum, should shift to negative and positive values for negative and positive DEP, respectively; when compared and normalised against the values of a reference image.

3.5.3 DEP spectrum

The magnitude of the shifts in the cumulative pixel values, when plotted against the corresponding frequency at which the images were taken from, will be used to construct the corresponding DEP spectrum for the chosen cell population (Figure 3-20). For the purpose of this project, the single shell

model was used for the construction of a model plot that will be fitted onto the experimental DEP in order for the frequency-dependent electrophysiological parameters to be extracted.

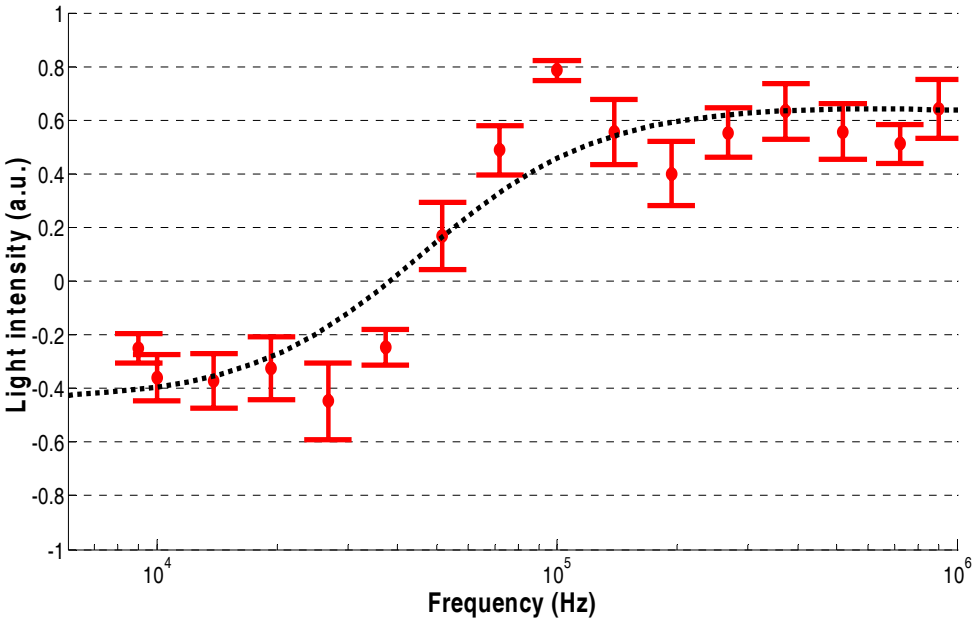

Figure 3-20 A typical DEP spectrum constructed using the values of the cumulative pixel value shifts from several sets of experiments. The dotted line represents the closest fit from the model data

3.6 Results and discussion

Over the course of conducting the preliminary experiments, a number of hardware and software improvements have been proposed and incorporated for the device. These improvements include the PCB platform for mounting the electrode, the design and fabrication of the gasket, the design of additional modules for the software, and the design of alternative algorithms to be used in the analysis of the captured images.

3.6.1 Design and fabrication of PCB platform

Another improvement was the fabrication of a specific PCB 'platform' for the electrode to be attached prior to its placement on top of the microscope viewing platform. This is particularly pertinent since the incoming signal must be electronically shielded from each other, as much as possible, to avoid an overlapping of frequencies in the selected dots of the electrode. This is not so much of a problem in the serial setup, since all of the dots will be receiving the same frequency value. Figure 3-21 shows an example of the PCB platform for the 4-channel system; complete with an affixed microelectrode

device, and equipped with four grounded SMB connectors to ensure input signals with accurate frequencies were delivered to each of the selected dots via coaxial cables.

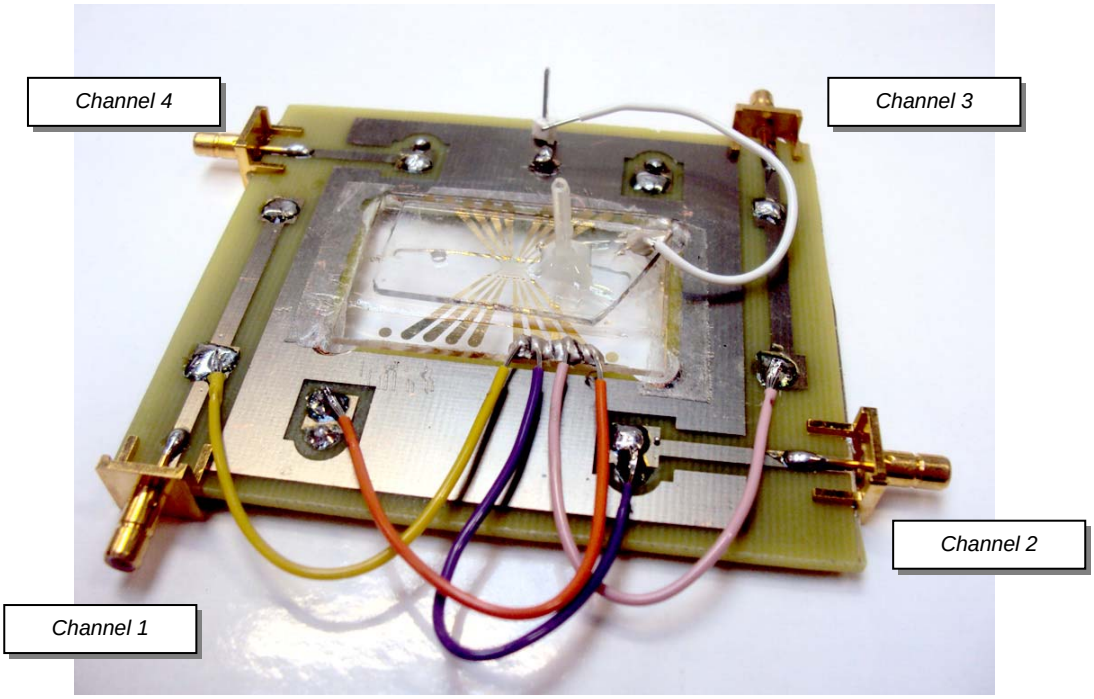

Figure 3-21 PCB platform for the 4-channel parallel microelectrode

3.6.2 Design and analysis of gasket design

One of the main practical problems in conducting the experiments were the non-uniformity of fluid flow across the chamber when the cell suspension is being pushed through the inlet. Although the cells may still occupy the individual dots uniformly, localised collections of cells will start to appear around the central region of the chamber, as the cell suspension is pushed repeatedly as the experiment progresses. These cell collections directly affect the accuracy of produced DEP spectrum, since it provides an inaccurate light intensity analysis over the affected dots.

Figure 3-22 shows the fluid flow analysis results using COMSOL Multiphysics (COMSOL Inc., Palo Alto, USA) for the original gasket design, and two proposed new designs. The right columns present a snapshot of the velocity profile of the fluid flow at the central vertical cross-section of each of the designs. From the first velocity profile (Figure 3-22(a)) it is clear that the reason for the localised cell collections around the circular region is caused by the very low velocity of the fluid around that particular region compared to the central horizontal area (reaching a maximum velocity of 0.32 m/s), thus causing a localised build-up of cells over time. Although the velocity profiles of the new designs

may not be perfectly uniform, but the difference in the fluid velocities between the different regions have been vastly improved. The velocity difference between regions of the lowest and the highest velocities of the new designs were only 3.0 and 1.6 times for Figures 3-22(b) and 3-22(c), respectively; while the original design recorded a difference of 16.0 times. Because of the improvement in velocity difference shown by the third design, it was adopted as the new gasket design to be used with the developed system.

Figure 3-23 shows the final mask design to be used in fabricating the gasket, with three different widths to accommodate different microelectrode dot array sizes.

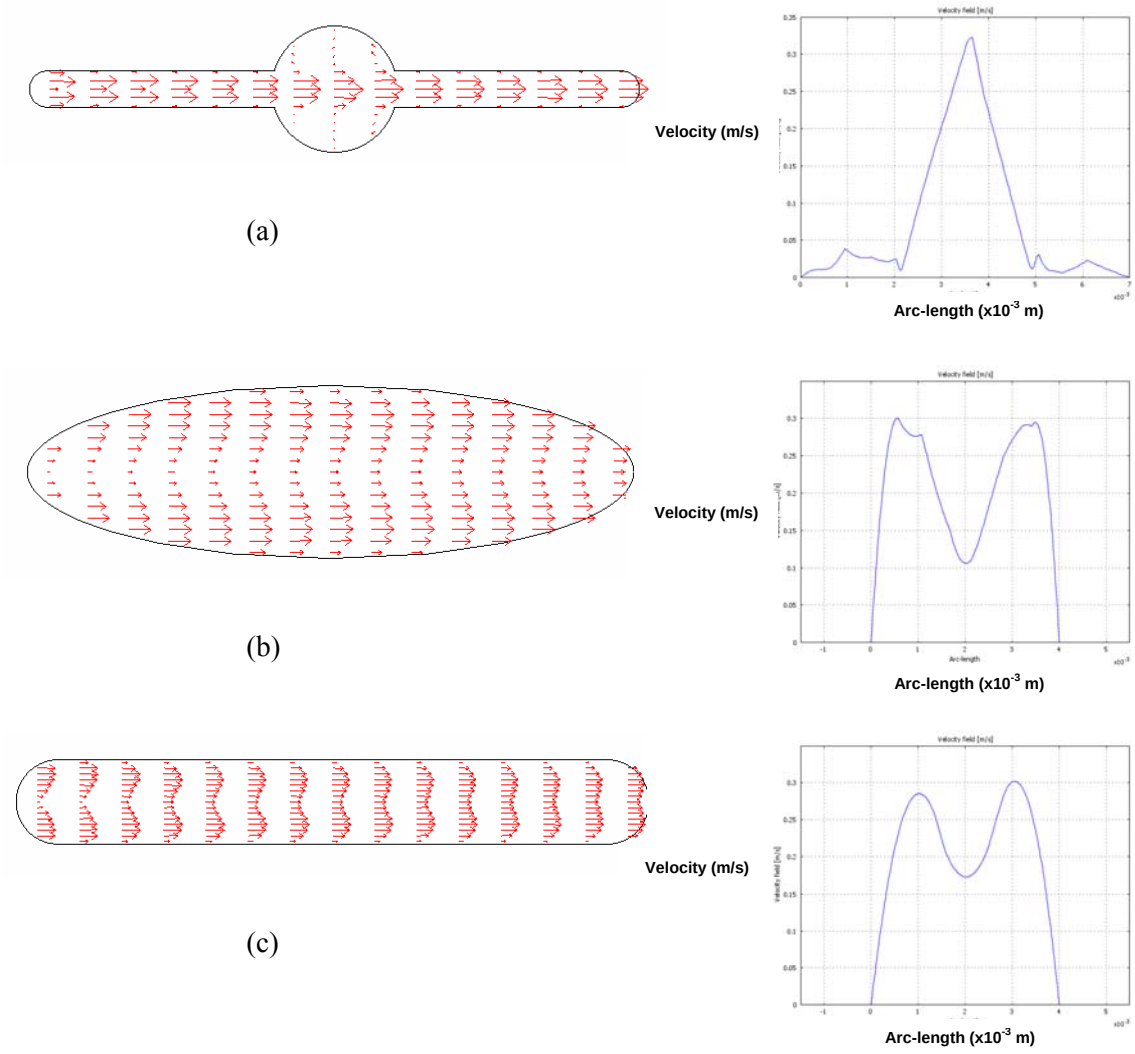

Figure 3-22 Fluid flow analysis of three gasket designs. The left column shows the average velocities across the length of the design. The length of the arrows is representative of the average flow velocity. The right column shows the velocity profile at the central cross section of the design.

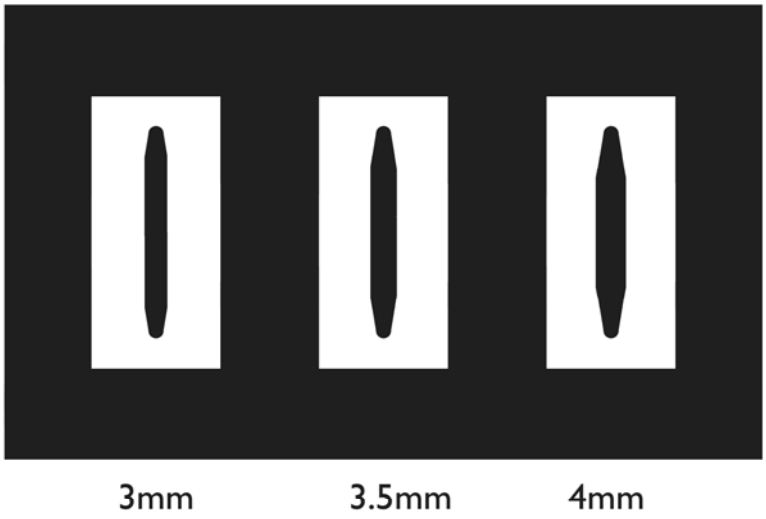

Figure 3-23 Final mask designs for the gasket to be used in the microelectrode device

3.6.3 Design of initial intensity indicator

Since the algorithm in the current analysis relies upon the histogram of light intensity in the captured images, it is of utmost importance therefore that the quality of the images is at the required optimal level. The contrast and brightness of the image, prior to conducting the experiment, must be set accordingly for the subsequent analysis to be completed. The analysis particularly requires that the image must not be too dark or too bright, in order for it to correctly detect the dots and later to complete the analysis of the histogram within each of the dots.

In the current program however, there is not a facility to quantify the level of contrast and/or brightness of the captured image; thus leaving it entirely to the judgement of the user to decide if the light intensity and the focusing of the microscope lenses were optimum. An ideal additional feature to the program would be a facility to automatically capture the contrast and brightness levels of the captured image, and use those values to automatically adjust the camera settings that allow it to capture the best images for the purpose of analysis. This approach however, requires additional programming that must interface with the digital camera, which is both time-consuming and demands high computing resources. In addition, any adjustment on the camera settings relies on the light intensity level coming from the microscope anyway, thus still requiring the subjective input of the user to a certain extent. An additional difficulty is in determining the uniformity of cell distribution

over the dots, since the analysis algorithm relies on the light intensity coming through each of the individual dots.

A simpler approach is therefore proposed to address both of the said problems in the current program, whereby it allows a user to quickly determine if the captured images are within the optimal range of contrast and brightness, and if the cells are distributed uniformly over each of the dots, prior to starting an experiment. If the captured images were not at its optimal starting conditions, the user simply have to adjust the light intensity of the microscope and/or re-suspend the cells within the chamber, and restart this additional feature of the program. Figure 3-24 shows the flowchart of the algorithm for this feature.

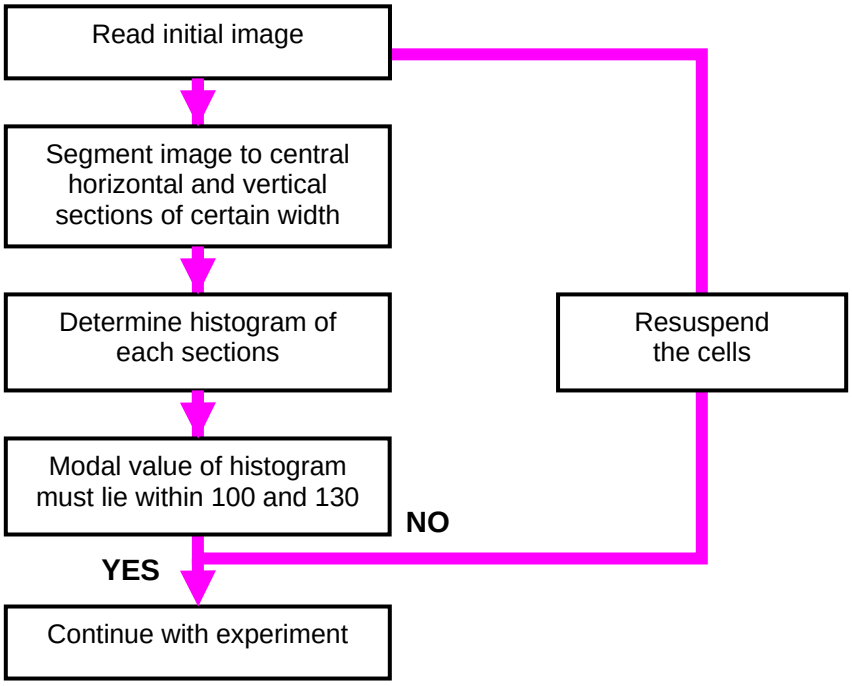

Figure 3-24 Flowchart of algorithm for detecting the initial intensity level of the captured images

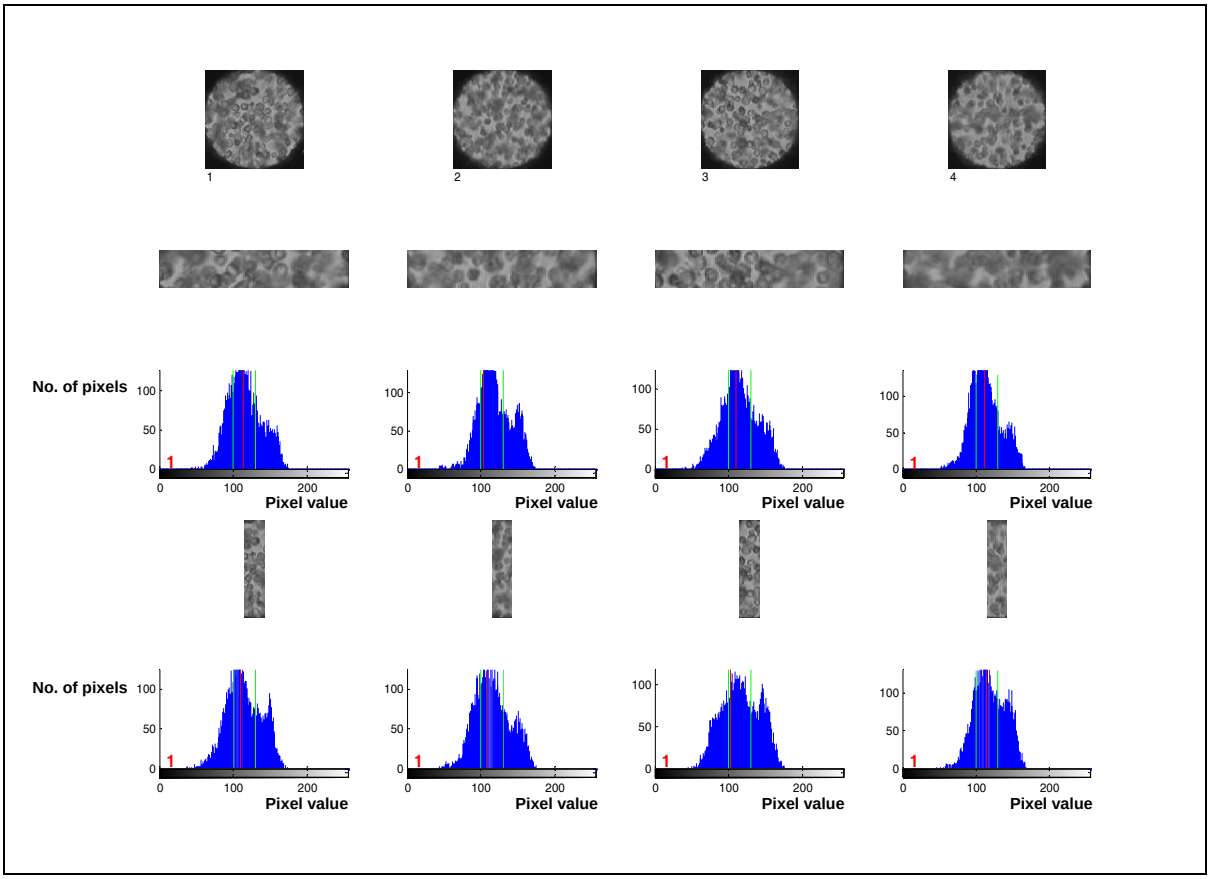

Figure 3-25 Results of an example of the proposed analysis of the initial captured image.

As mentioned in the flowchart, the chosen indicator for the additional feature is the modal value of the histogram of each of the dots. This is primarily due to the finding that the majority of dots that provide satisfactory cell distribution and subsequently good DEP spectra has its modal histogram value within the same region of intensity. Following an examination of 112 dots that fulfils the said criteria, it was found that the modal intensity level is 127.76 (±15.45). Therefore, it is proposed that the rounded intensity values of between 100 and 130 be used as an indicator to determine that the captured images have the optimal contrast and brightness required for the subsequent analysis. It was also found that a uniformly distributed cells within a given dot gave similar histogram plots, particularly values for maximum and minimum intensity levels, and the height (corresponding to total number of pixels at a particular intensity level) of the plot.

Figure 3-25 shows the results window that is generated by this additional module that analyses the captured initial image of a four-dot system. Note that in this example, each of the dots scored a '1' for both the horizontal and vertical central 'strips', meaning that the distribution of cells within each of the dots was uniform; and the modal value of the histogram level (red) lies within the suggested

optimum boundary levels (green), which indicates that the images had optimum contrast and brightness for it to be efficiently analysed.

3.6.4 Design of automated intensity threshold level

As part of the image segmentation process, one of the required parameters is the intensity threshold value. This value will be used as the starting point, where anything less will be detected as the electrode and the rest will be considered the dots. This parameter was assigned '60' as the default value, and worked for the majority of captured images. However, in cases where the contrast of the captured images was not optimal, the system could not proceed to the subsequent part of the program, and simply produced an error message. Although this value may be changed manually by altering the value of the 'I.T.' value (Figure 3-26), this requires the analysis to be restarted from the beginning.

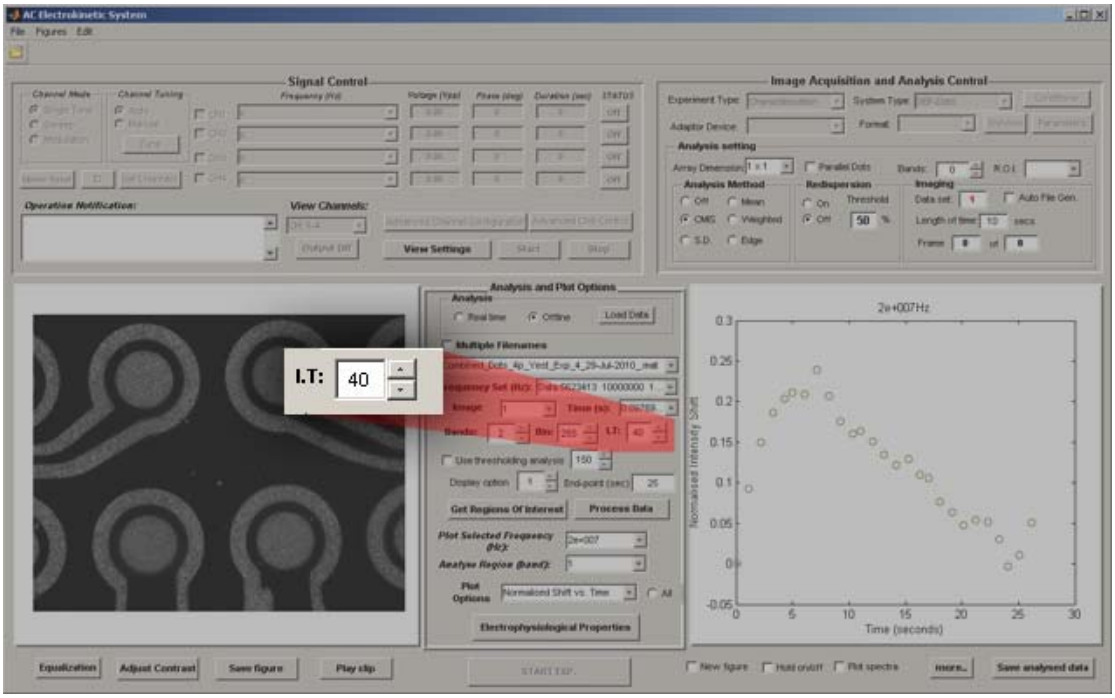

Figure 3-26 Screenshot of the program showing the intensity threshold value that may be changed during analysis

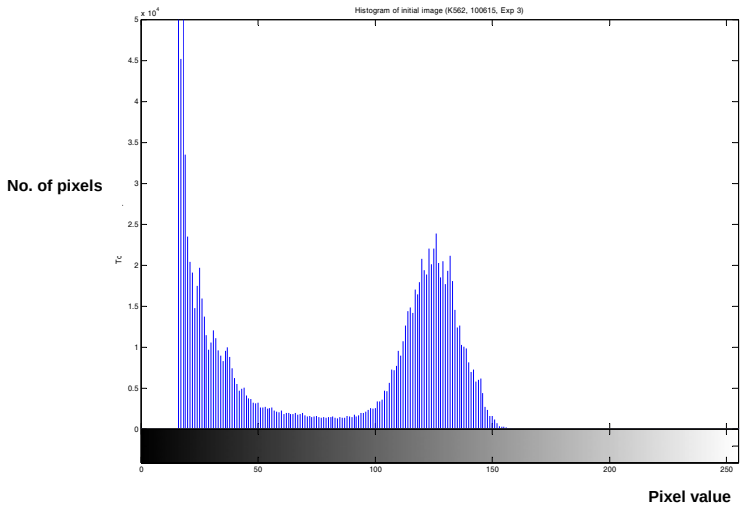

Figure 3-27 Histogram of the captured initial image with optimal contrast, where the minimum value of the histogram dip is around 80

The reason why '60' worked for most of the experiments was that there is a unique shape to the histogram plot of the initial image. An example of the histogram of the initial image (Figure 3-27) shows that there is a dip between histogram values of 50 to 100; and thus by having '60' as the default threshold value, the program can safely determine anything less than that as the electrode, and discard those areas within the image as not part of the dots that needs to be segmented out. This shape is typical of an image whereby there are only two prominent areas of interest, namely the foreground and the background (Gonzalez and Woods, 1992).

Although this value may be automatically determined using a number of iterative programming techniques; a much more elegant method would be to use a classic technique that has been employed in digital image processing for at least three decades, namely the Otsu's method. The technique was proposed by Nobuyuki Otsu in 1979 to calculate the optimum threshold value to separate the foreground from the background with minimal intra-class variance. Figure 3-28 shows the flowchart for the algorithm in automatically detecting the suitable threshold value. In MATLAB, the technique may be implemented by calling the `graythresh` function.

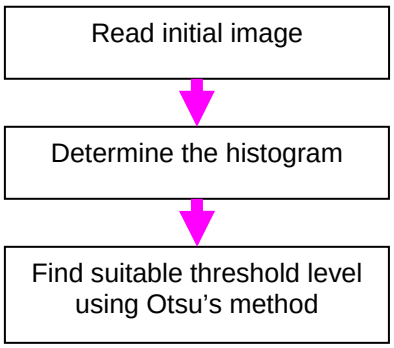

Figure 3-28 Flowchart of algorithm for automatic detection of threshold level

3.6.5 Design of module for displaying the saved analysis data

One of the drawbacks of the current system is the inability to display the saved data, once the selected sets of experiments have been processed and analysed. Therefore a desirable additional module for the system would be the ability to display these saved data, and conduct a simple model fitting onto the displayed DEP spectrum to determine the electrophysiological parameters, namely the membrane conductance and capacitance. Figure 3-29 shows an example of the implementation, with the Results section displaying all of the entered parameter variables (cell radius; cell membrane thickness; conductivity and permittivity values for cytoplasm, membrane and medium), along with the calculated specific membrane conductance (G_{spec}) and capacitance (C_{spec}), and the crossover frequency. Both the G_{spec} and C_{spec} values were determined using the single-shell model. This may be changed according to the types of cell populations used in the experiments.

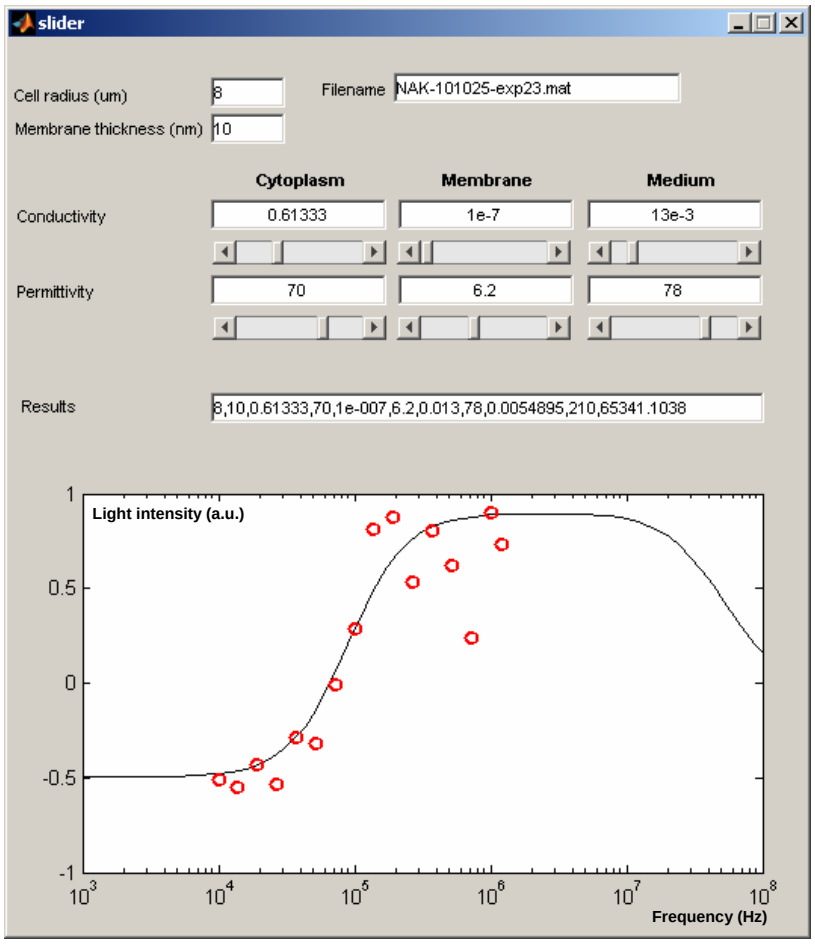

Figure 3-29 An example implementation of the additional module to display saved results data

3.6.6 Improvement on the area selection for analysis

Following the segmentation of dots from the captured images, the current analysis program may be set to select certain areas within each of the dot to conduct the analysis on (Figure 3-30). These areas are called 'bands'; and each of these bands have the same centre as the dot, and the radii are multiples of the radius of the segmented dot (Figure 3-31). The reason for having these bands is that it allows the program to focus its analysis within specific areas of the circle, since the DEP force created by the dots are axisymmetrical, if viewed vertically (Fatoyinbo *et al.*, 2008). This is obviously advantageous, since the difference in dot and cell sizes will undoubtedly affect the overall movement of the cells within a given dot. By having these different bands, a user may focus the analysis on a specific band that gives out the best dataset to be used in the DEP spectrum plot. In the current system, Band '2' refers to the whole dot; Band '3' to a circular area having half the original dot radius; Band '4' with a third of the radius; and so on.

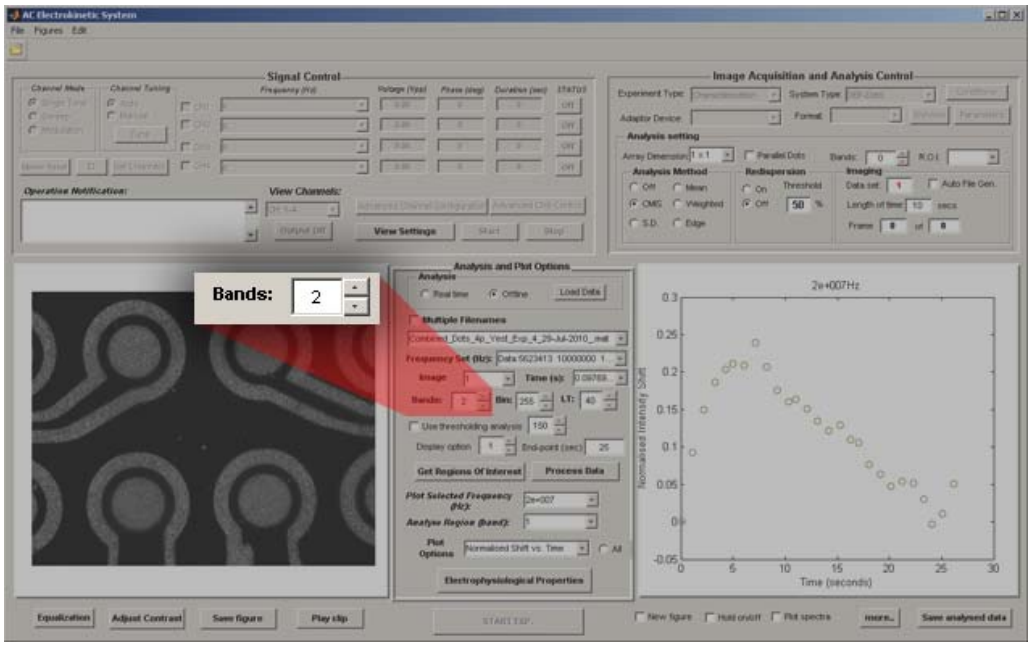

Figure 3-30 Screenshot of the program showing the different bands available for analysis

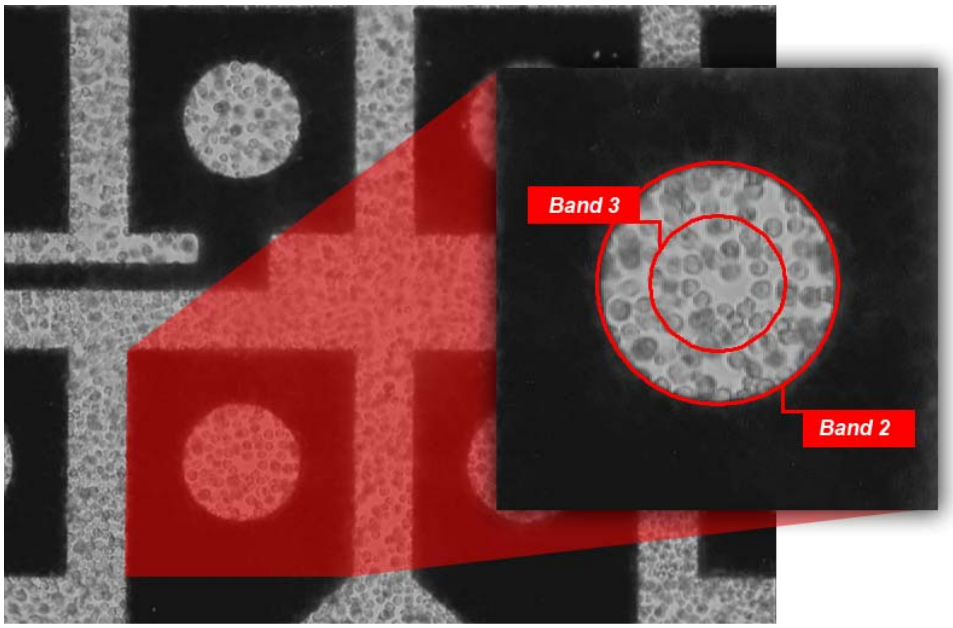

Figure 3-31 A segmented dot from the captured image with superimposed 'bands'

In the course of validating the system, it was found that there is no discernible difference when using different bands to analyse the data (data not shown). More often than not, the analysis was left with the default setting (Band '2') that focuses the analysis on the whole dot. Although this is not a

problem in itself, and the setting does produce a reasonably good DEP spectrum; there is no way of setting somewhere in between Band '2' and Band '3', and thus may prove to be a problem in correctly analysing a negative DEP in certain situations. For example, Figure 3-32 shows a K562 cell population experiencing negative DEP. If Band '2' was selected, the analysis will take into consideration the background area that appears around the collection of cells, while Band '3' will ignore the said area and instead focus on the circular area with half of the radius. The problem with selecting Band '2' in this particular case is that it may shift the modal value towards the right, thus affecting the analysis; while selecting Band '3' may not yield such a strong negative DEP value since there is not much difference between the intensity levels of the two images (Figure 3-32(c)). A better setting would be something in between the two bands, but this is not allowed in the current system.

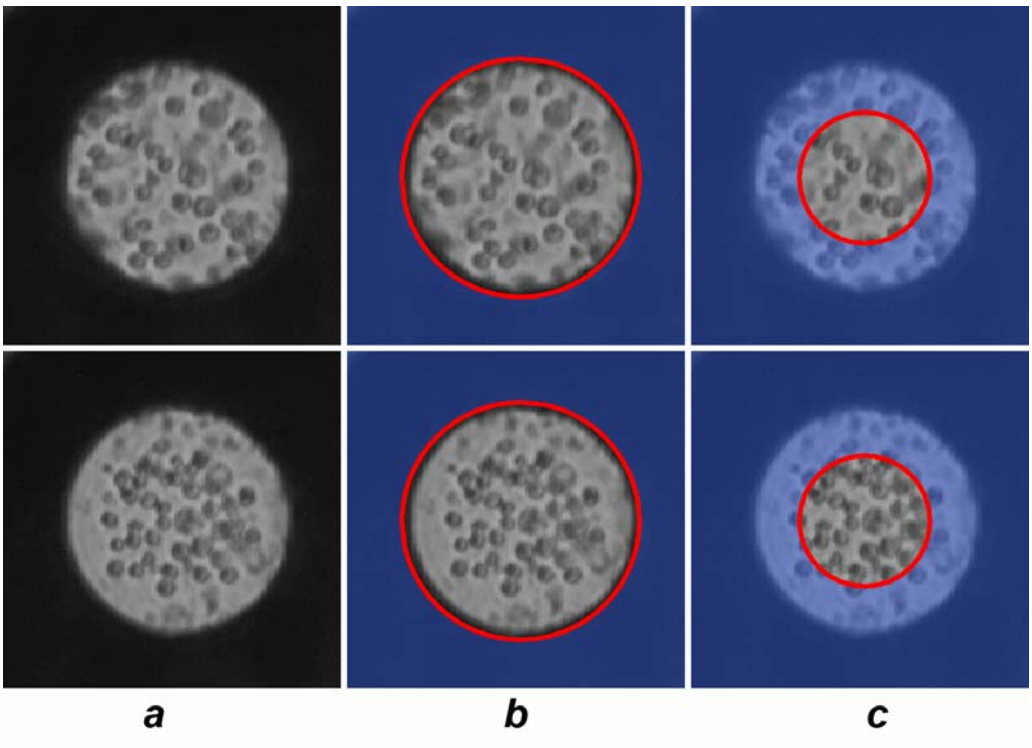

Figure 3-32 K562 cells experiencing a negative DEP at 10 kHz on a 200 µm dot; before (top row) and after (bottom row) an experiment. The original images are shown in a), while b) and c) shows the superimposed lines and areas demarcated by Band '2' and Band '3', respectively

This project therefore would like to propose an alternative selection method that may be used in analysing the dots. Instead of using circular bands, the proposed method uses a square with a width of half the radius of the dot, thus selecting an area with a quarter the size of the original segmented dot (Figure 3-33). Over the course of conducting the experiments, this alternative technique has been proven to be consistently helping to produce good DEP spectra (Figure 3-34).

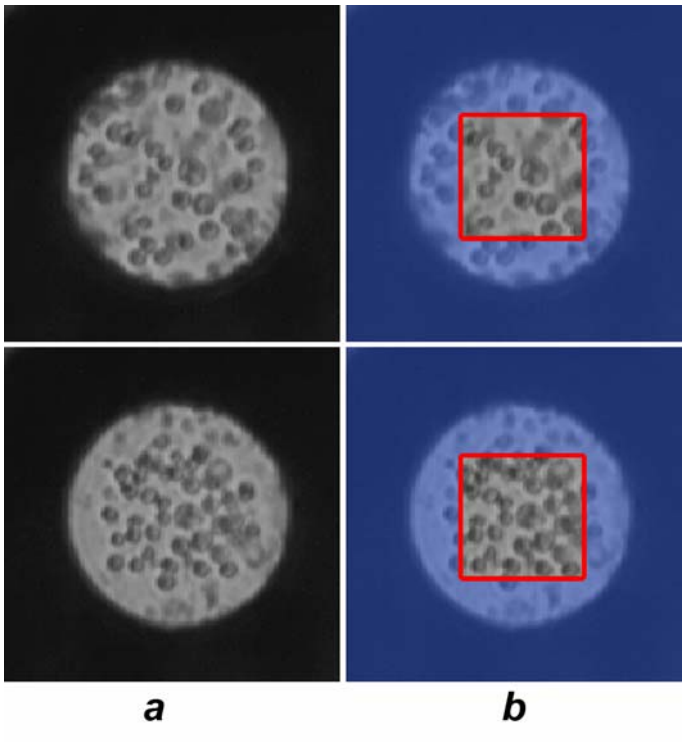

Figure 3-33 K562 cells experiencing a negative DEP at 10 kHz on a 200 µm dot; before (top row) and after (bottom row) an experiment. The original images are shown in a), while b) shows the superimposed lines and areas demarcated by the proposed square selection method

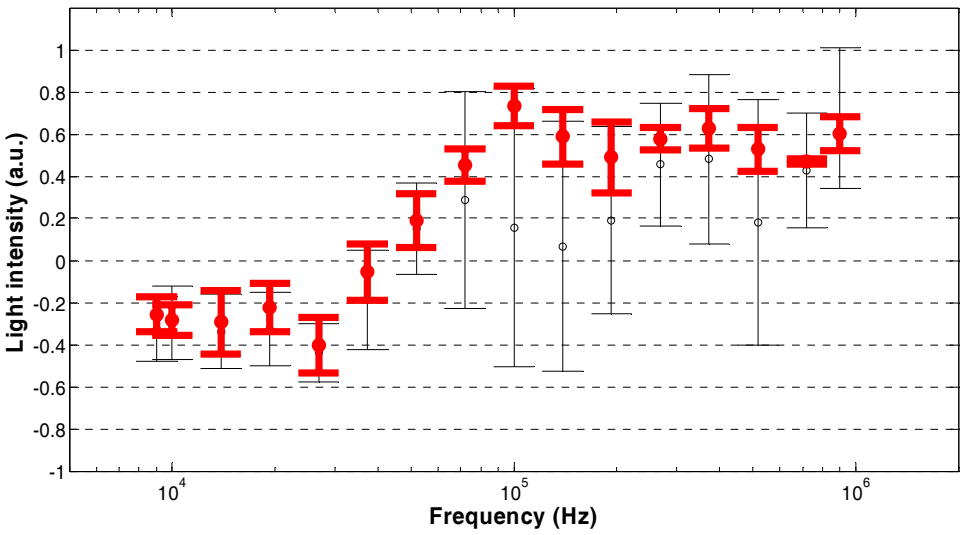

Figure 3-34 DEP spectra from the same set of experiments, analysed using current ROI detection method (top) and the proposed alternative method (red)

3.6.7 Design of median histogram width analysis algorithm

The analysis algorithm currently used in the system, also known as Cumulative Modal Intensity Shift (CMIS) method, was primarily based on the work done by Fatoyinbo *et al.* (2008), which was satisfactorily employed in the production of DEP spectra for yeast and the subsequent analysis of the electrophysiological properties of the membrane. This algorithm, in turn, was based on a previous algorithm that was successfully used on DEP microwell system (e.g. Broche *et al.*, 2005; Chin *et al.*, 2006; Labeed *et al.*, 2006; Duncan *et al.*, 2008). The general premise of the algorithm was to determine any changes to the histogram of the captured images. The change (primarily the shift of the histogram peak) is then measured, and the normalised and scaled data is plotted. A plot based on the real values of the Clausius-Mossotti will then be fitted onto the produced DEP spectrum so that the electrophysiological properties of the cell sample may be determined.

Over the course of conducting the experiments for the project, it was found that the program gives the most desirable DEP spectrum, if the thresholding value (Figure 3-35) were to be changed to a value closest to the median of the width of the histogram. However, in the current program, this is not quite possible at all times, since the intensity levels of the images may differ in between the different experimental sweeps.

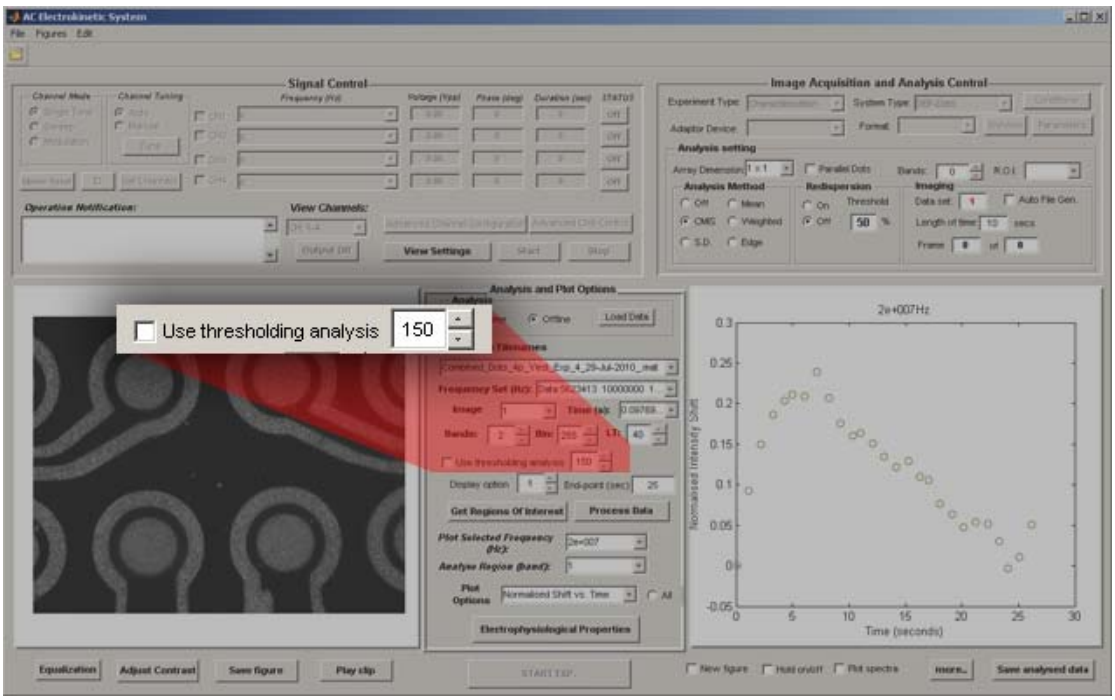

Figure 3-35 Screenshot of the program showing the thresholding value that may be changed during analysis

An alternative analysis method is therefore to automatically detect the width of the histogram of the initial image in each sweep separately, and use the median value as the thresholding value (Figure 3-36). Figure 3-37 shows the MATLAB code to complete the said algorithm.

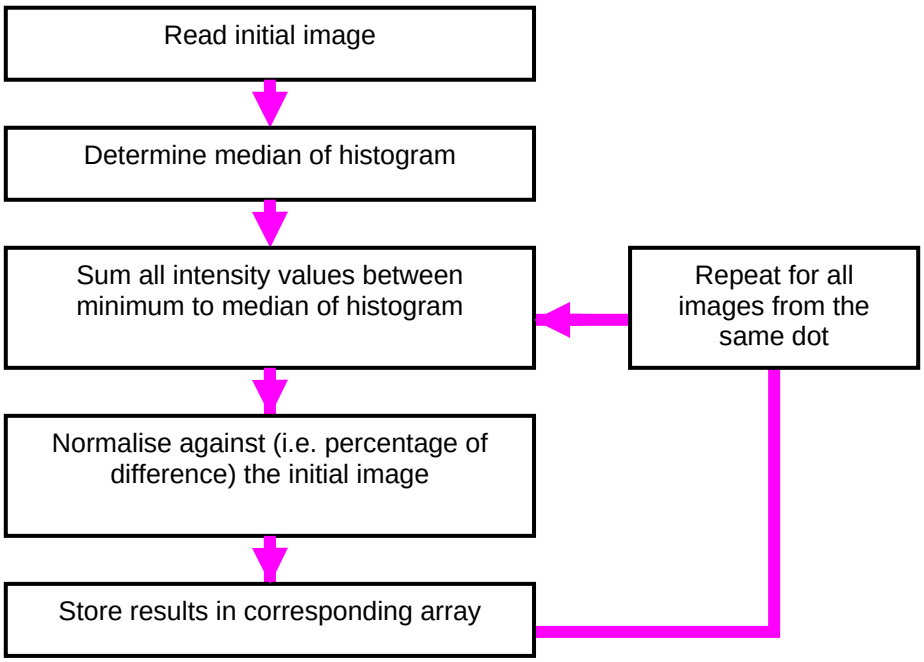

Figure 3-36 Flowchart of the median histogram analysis algorithm

```
for p=1:DDS_control.Timer
   for m = 1:DDS_control.ElectrodeTotalNum*counter_set
     [counts_h,x_h] = imhist(uint8(para.NAKhistopotong{p,m}));
     nonzero = find(counts_h); % find non-zero ones
     tempNAK = 0;
     for ii = min(nonzero)+round(length(nonzero)*0.2):median(nonzero)
         tempNAK = tempNAK + counts_h(ii,1);
     end
     para.NAKhistoTOP(p,m) = tempNAK;
   end
end
```

Figure 3-37 MATLAB code snippet for the median histogram analysis algorithm

Although both method provided the same crossover frequency value, the median histogram analysis technique provided a much more consistent DEP spectrum (Figure 3-38), thus enabling an easier fitting of the produced spectrum to the expected DEP model, and the subsequent determination of the biophysical properties. Figure 3-39 compares the produced DEP spectra from a set of eight experiments, using K562 cells at about 1×10^7 cells per ml, medium conductivity of 10 mS/m, dot size

of 200 μm, and the supplied voltage was set for 20 seconds. The plots showed that the median histogram analysis techniques produced a smaller standard deviation value over the course of the experiments, particularly when positive DEP was experienced, which took a total of 45 minutes. In addition, several dots that experienced positive DEP were incorrectly analysed as having negative DEP by the CMIS method, thus producing a very wide standard deviation to the results. The inconsistencies were attributed to the inherent problem of incorrect detection of modal histogram values in the affected dots by the CMIS method. The proposed median histogram method eliminated this problem by ignoring the modal histogram value, but taking into consideration the median histogram value instead. The incorrect detection of modal values was commonly due to occasions whereby non-uniform cellular distribution over the dots and/or poor lighting conditions caused a localised increase in certain pixel value.

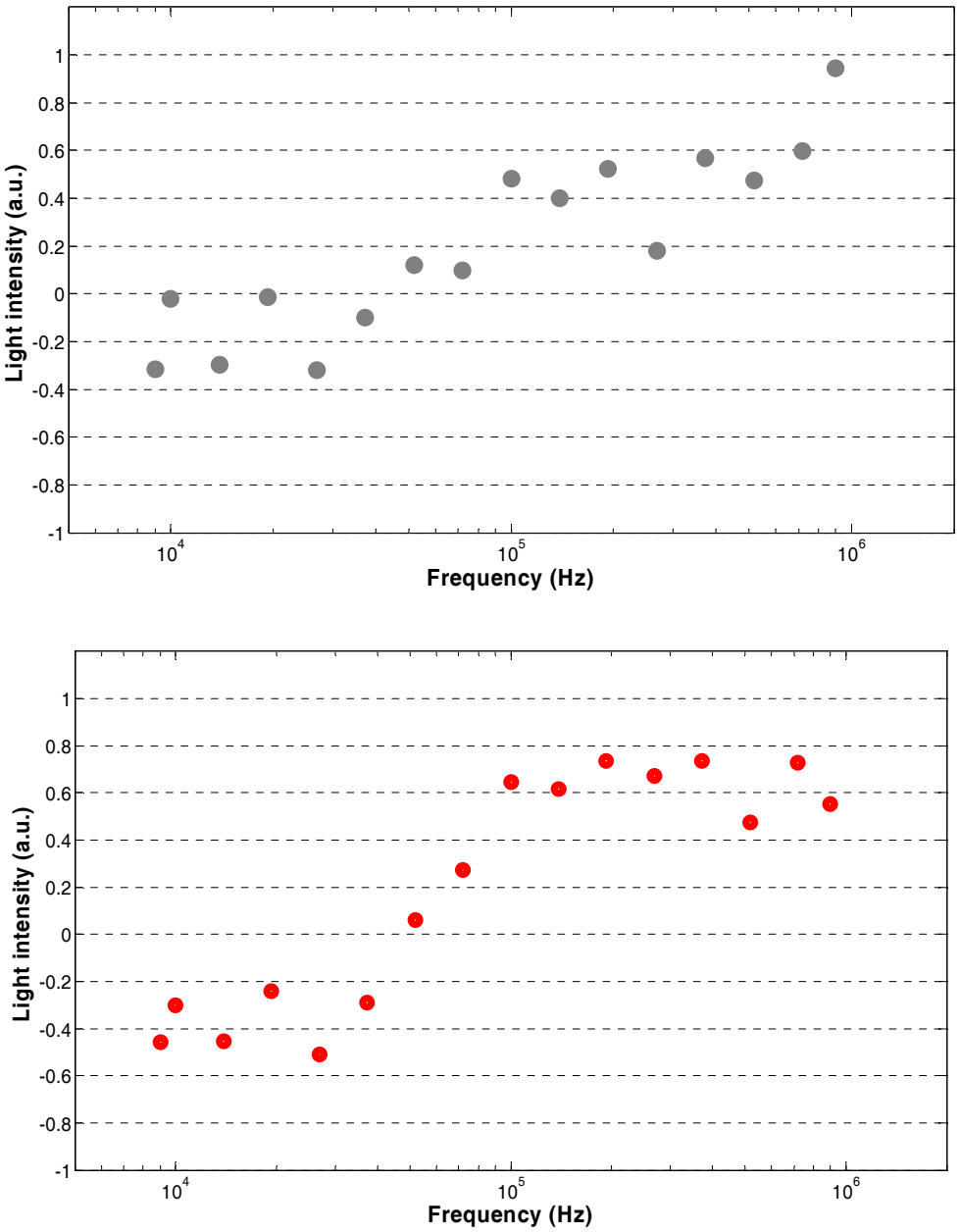

Figure 3-38 DEP spectra from the same single experiment, analysed using CMIS technique (with default settings, top), median histogram analysis technique (bottom)

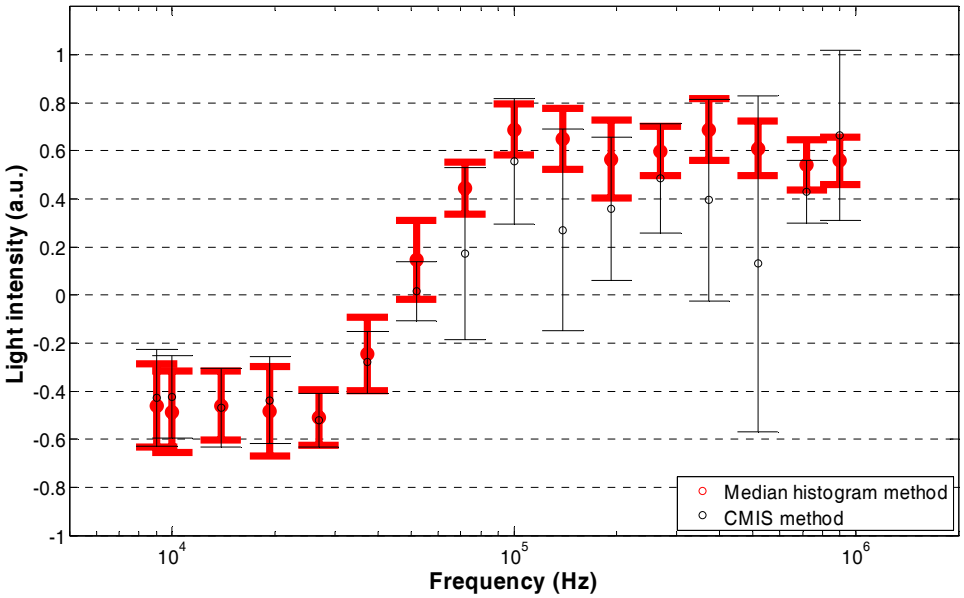

Figure 3-39 DEP spectra from the same set of experiments, analysed using the CMIS method (black) and the proposed median histogram method (red)

3.6.8 Design of bitmapped image analysis algorithm

Although the analysis stage of the previous system involved the use of images, there is no actual image processing involved. This study found that the CMIS technique proposed by Fatoyinbo *et al.* (2008), may not work very well for a microarray dot setup, where each of the dot receives a different input frequency. One of the major difficulties in employing the CMIS technique, is in the inconsistency of the light transmission through each of the dots. Although the analysis may still be completed satisfactorily by changing a multitude of parameters, as shown in Figure 3-34, this obviously is not an ideal solution. Although the median histogram analysis has been shown to be capable of producing a much more consistent DEP spectra (Figures 3-37 and 3-38), the technique still suffers if there was a noticeable difference in light intensity in between the different sets of experiments. The said intensity change is sometimes practically inevitable, since it was caused by the movement of the microscope platform due to the required re-suspension process. In addition, both the CMIS and the median histogram techniques do not work well with less than optimal cell concentrations, and/or off-focus images.

Nevertheless, the author is of the opinion that the addition of image processing techniques could very much improve the algorithm of the analysis, and produces quicker results and thus consumes less computing resources. One of the simplest image techniques is the binarisation of an image, also

known as 'thresholding'. The technique basically involved the conversion of each of the pixels in a given image to a value of either 0 or 1, depending on the threshold level determined by the application. And in most of these applications the objective of thresholding an image is to separate foreground (i.e. those pixels with intensity level less than the threshold) from background data (i.e. those pixels with intensity level more than the threshold) (Gonzalez and Woods, 1992). The important factor in determining the success of a thresholding process is selecting the correct threshold value from the histogram. The easiest image to threshold would be one that display distinct grey scale clustering in its histogram, since the suitable threshold value would then be the grey scale value corresponding to the valley in between the peaks within the histogram. Figure 3-40(b) shows the histogram of an image taken from one of the datasets of the project. By using a threshold value of 80, which roughly corresponds to the valley in the histogram, the outcome of the thresholding process (Figure 2-7(c)) have satisfactorily segmented the cells captured within the dots from the image. The employment of this technique for the analysis part of the project will be discussed in detail in the 'System design and development' section.

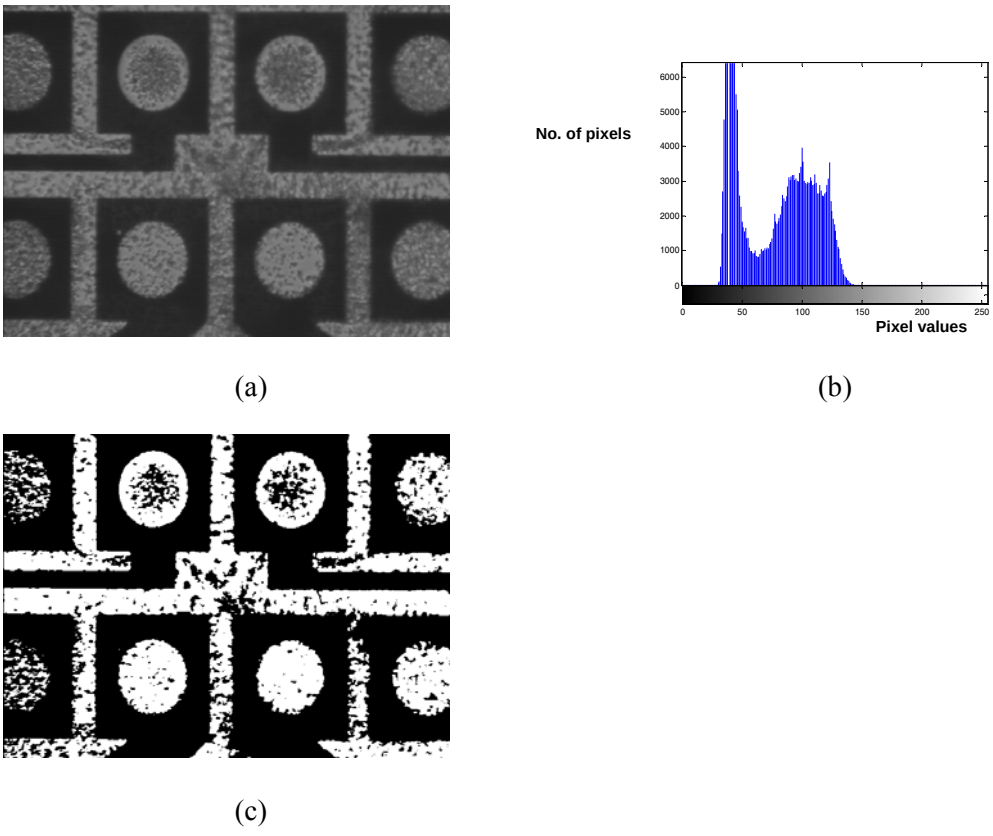

Figure 3-40 a) The original image taken from one of the conducted experiments, where the central four dots were being supplied with input signals at four different frequencies; b) the histogram of the original image; c) the outcome from the thresholding process, when using '80' as the threshold value

Faster processing time may be achieved by employing this technique, since the program will only have to count the number of either black or white pixels, and does not have to analyse the histogram of each of the captured image. Figure 3-41 shows the flowchart of the proposed algorithm.

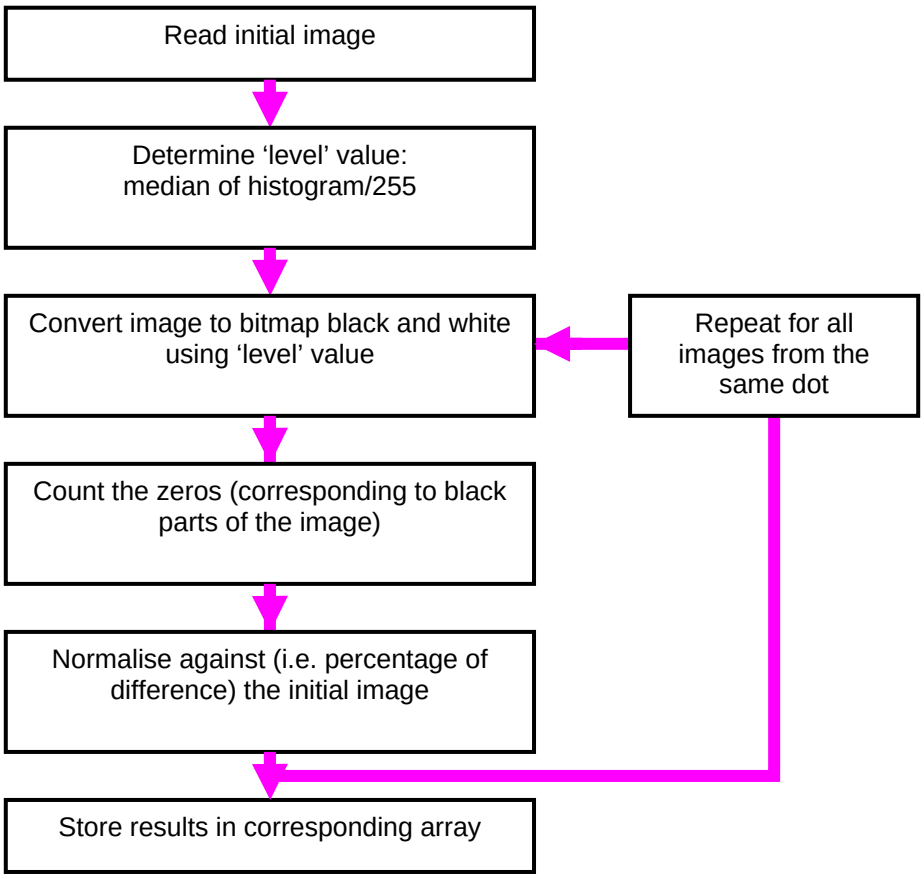

Figure 3-41 Flowchart of the analysis algorithm using a bitmapped version of the captured image. The steps will be repeated for each of the different dots

In MATLAB, there is a built-in `im2bw` function that converts an image to its black-and-white counterpart. The function accepts two parameters, namely the image itself (formatted as unsigned integer) and a 'level' value. The 'level' is a value between 0 and 1, and determines the intensity level boundary at which anything more than the value will be converted to a '1' (white) and anything less is a '0' (black). Figure 3-42 shows the outcome of the thresholding process when using the Otsu's method to determine the most suitable threshold value. Figure 3-43 shows the MATLAB code snippet to implement the algorithm. Figures 3-44 and 3-45 show the marked improvement in the produced DEP spectra when the proposed bitmapped image analysis technique was implemented.

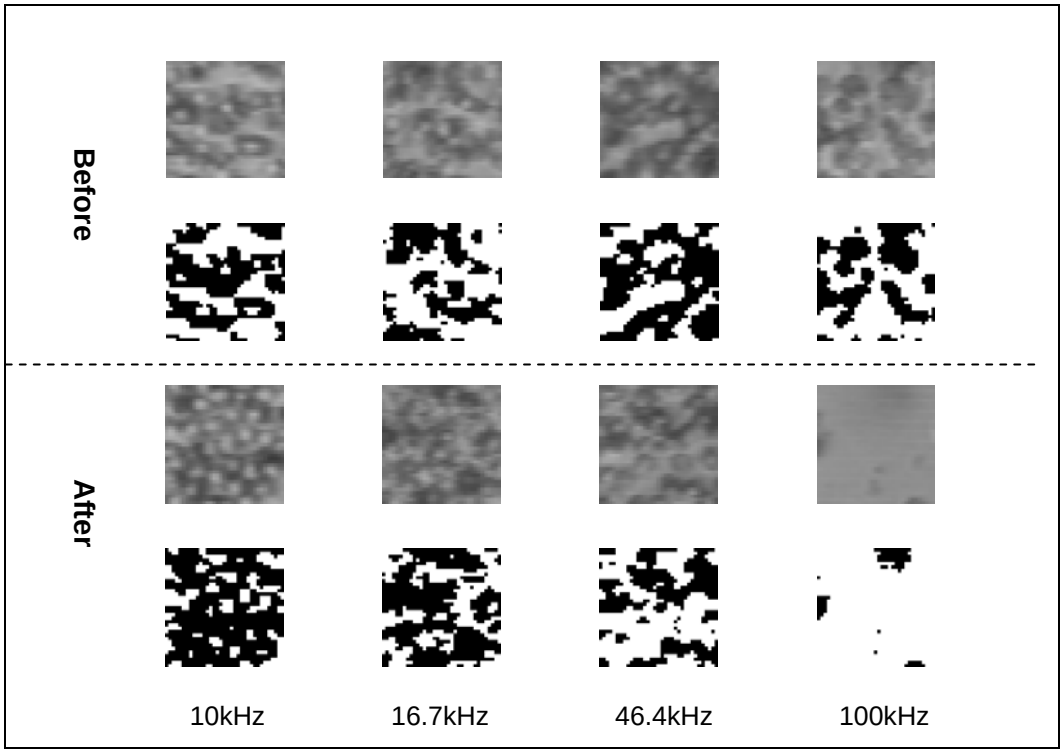

Figure 3-42 Results from the thresholding process using Otsu's method. The first and third rows show the captured dot images, before and after signal application, respectively; while the second and fourth rows show the corresponding thresholded outcome of the images. The frequencies used were (L-R) 10 kHz, 16.7 kHz, 46.4 kHz, 100 kHz

```
for p=1:DDS_control.Timer
    for m = 1:DDS_control.ElectrodeTotalNum*counter_set
        NAKthresh = graythresh(uint8(para.NAKhistopotong{1,m}));
        % threshold the image
        NAKhistotemp = im2bw(uint8(para.NAKhistopotong{p,m}),NAKthresh);
        % count zeros
        templagik = size(NAKhistotemp);
        tempNAK = (templagik(1,1)*templagik(1,2)) -
length(find(NAKhistotemp));
        para.NAKhistoTOPT(p,m) = tempNAK;
    end
end
```

Figure 3-43 MATLAB code snippet for the bitmapped image analysis algorithm

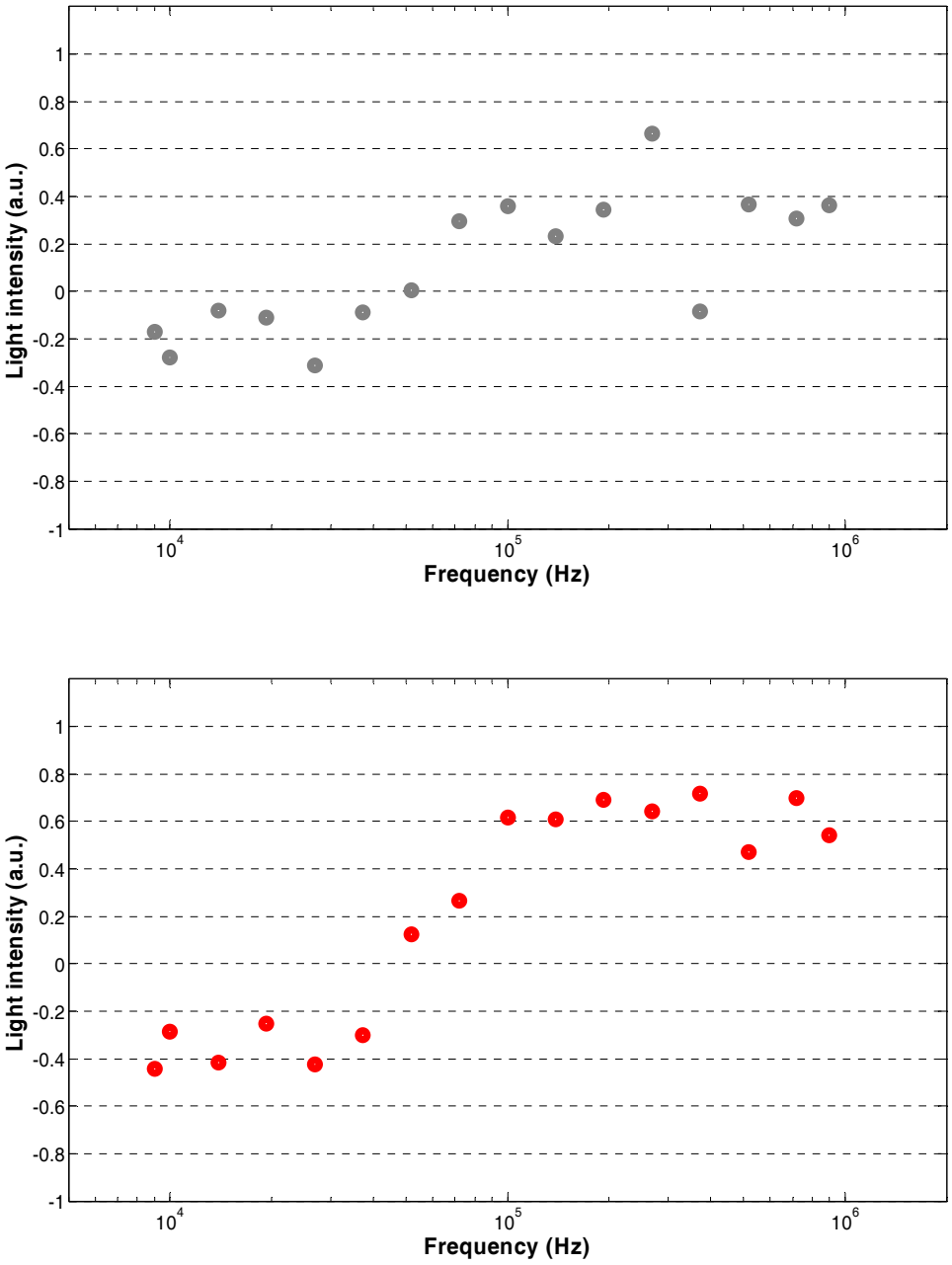

Figure 3-44 DEP spectra from the same set of experiments, analysed using a) current technique (with default settings, top), and the proposed bitmapped image analysis technique (bottom)

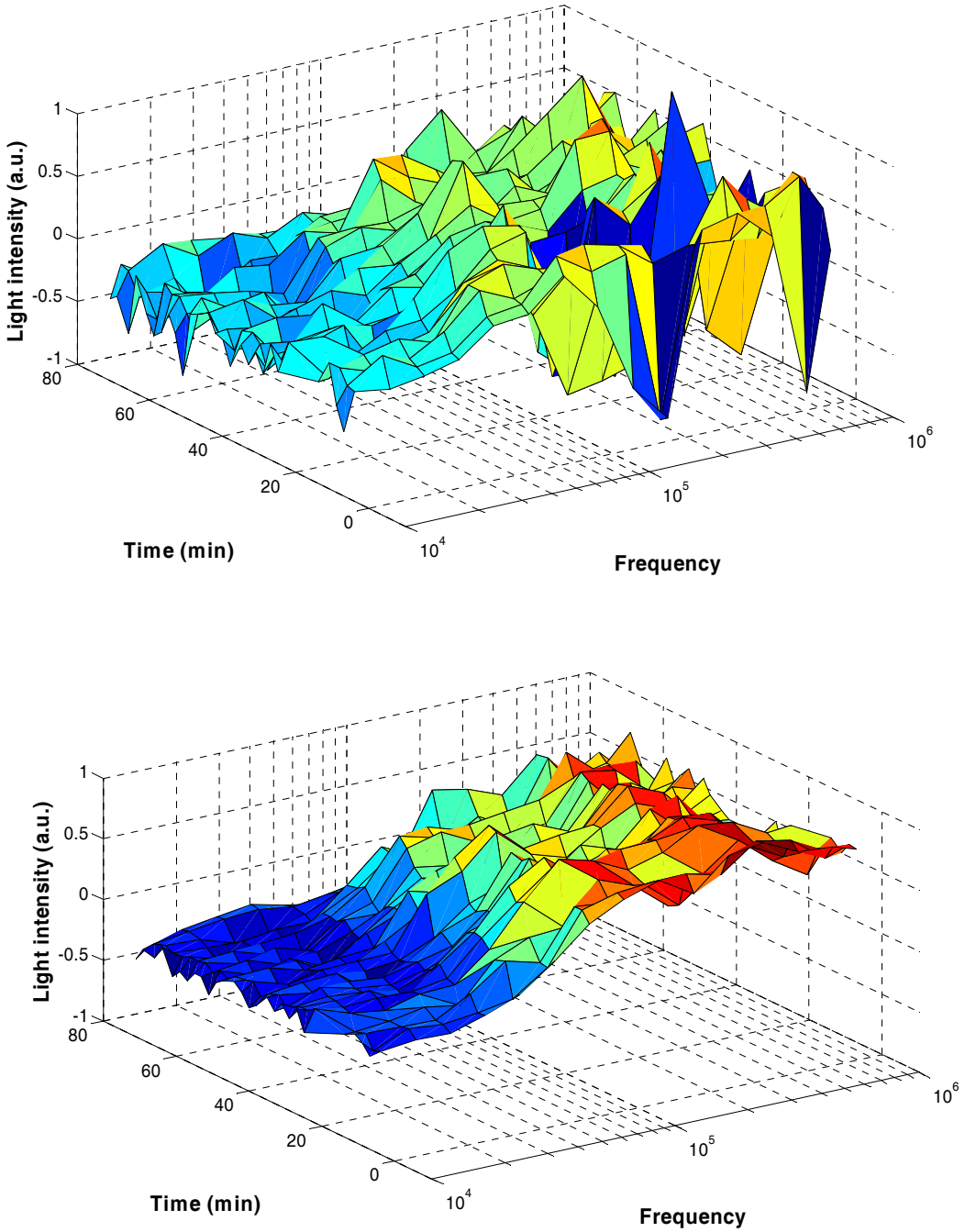

Figure 3-45 DEP spectra from the same set of experiments displayed in 3D, analysed using CMIS method (top), and the proposed bitmapped image analysis method (bottom)

3.7 Conclusion

A number of improvements proposed for the current system, either to help in conducting the DEP experiments or as an alternative in the subsequent analysis, has been discussed and found to be of

benefit to the overall functioning of the developed system. The alternative algorithms for example, has been proven to be more efficient in producing consistent DEP spectra, and its robustness has been tested by using datasets with less than optimal cell concentrations and light intensity.

4 System validation and optimisation

4.1 Introduction

The following subsections document the series of experiments that will help to determine the efficacy of the system, and validate the initial outcomes prior to its deployment in actual DEP experiments. The 'Materials and Methods' section covers all of the aspects relating to cell preparation and the experimental protocols; while the 'Results and Discussion' section documents the outcome from the initial experiments to determine the robustness of the system with changing parameter values, namely input supply voltage and frequency, conductive medium type and concentration, cell concentration, and microelectrode design and geometry. Results of the feasibility studies cover all of the developed microelectrode geometries over the course of the project, starting with the original 4-dot serial system to the current 8-dot parallel system. The validation results, on the other hand, are based on the latest 8-dot parallel set up.

4.2 Materials and methods

The cell lines used in the project were leukemic K562 and Jurkat cells, sourced from Sigma Aldrich Co., (St. Louis, USA), unless otherwise noted. Upon purchase, the cells were divided into 1 ml aliquots containing the culture medium in 5% DMSO, and cryogenically frozen.

4.2.1 Cell culture

These mammalian cells require a specific culture medium, consisting primarily of RPMI solution (GIBCO® RPMI Media 1640, Invitrogen Ltd., Paisley, UK), along with other supplements. The cells were cultured in the incubator (CO-150, New Brunswick Scientific, Edison, NJ, USA) set at 37 degrees Celsius and 5.0% CO_2. Although the cells may be kept alive indefinitely, but the best practice would be to renew the cell culture from the frozen stock once the suspension reached 30 to 40 cell passages (Konopka *et al.*, 1984; Gascoyne *et al.*, 1993).

4.2.2 Suspension medium preparation

The suspension medium needs to be prepared prior to the cell culturing process, since a number of specific supplements need to be added to the RPMI solution. The following are the steps taken in the said process, as used previously in various studies at the Centre for Biomedical Engineering at the University of Surrey (e.g. Labeed *et al.*, 2003; Hoettges *et al.*, 2008; Fatoyinbo *et al.*, 2008). For each 500 ml of RPMI-1640 flask, the following supplements were used:

- 50 ml of heat-inactivated fetal bovine serum (FBS) (PAA, Pasching, Austria)
- 15 ml of L-glutamine (Sigma-Aldrich Co., St. Louis, USA)
- 15 ml of penicillin-streptomycin solution (Sigma-Aldrich Co., St. Louis, USA)

Since all of the supplements are normally prepared earlier and stored in the freezer; each of the solutions need to be thawed in the water bath until 37 degrees Celsius prior to its mixing with the RPMI solution. FBS was routinely added first, followed by the L-glutamine and the antibacterial solutions.

To ensure satisfactory living conditions for the cells, and thus the viability of the cells to be used in the experiments; the suspension needed to be passaged (change of culture medium) regularly. The RPMI also contained a pH indicator, such that it will progressively turn yellow from its original red colour, indicating a rise in waste products and non-viable cells. This may be used as a convenient indicator in determining the need for cell passaging. Table 4-1 summarises the steps required in passaging the cell suspension.

Apart from passaging, the cell suspension occasionally required splitting (dividing of cell suspension into smaller volumes), again to ensure satisfactory living conditions for the cells.

Table 4-1 Summary of protocol in cell passaging

Step 1	Take the culture medium from the fridge, and warm to 37°C in water bath. Place 20 ml of medium into a new T75 flask.
Step 2	Take 15 ml of cell suspension from culture flask, and put into 50 ml centrifuge tube.
Step 3	Centrifuge at 180 g for five minutes. Remove supernatant when completed.
Step 4	Add 5 ml of the medium and mix thoroughly.
Step 5	Add cell suspension into the new T75 flask prepared in Step 1.

4.2.3 Conductive medium

All DEP experiments require the preparation of a conductive medium in which the cells will be suspended. For the purpose of this project, the chosen medium is potassium chloride (KCl) solution with 8.5% sucrose (Sigma-Aldrich Co., St. Louis, USA) and 0.3% dextrose (Sigma-Aldrich Co., St. Louis, USA).

The conductivity was set at 10 mS/m using a previously prepared 100 mM KCl solution, and verified by a conductivity meter (Jenway 470, Bibby Scientific Ltd., Staffordshire, UK). The conductivity value was arbitrarily chosen to provide a crossover frequency in the regions between 10-100 kHz of the applied input signal (Altomare *et al.*, 2003; Labeed *et al.*, 2003).

Table 4-2 summarises the protocol in preparing the conductive medium for this project.

Table 4-2 Summary of protocol in preparing the conductive medium

Step 1	Measure 8.5 g of sucrose and 0.3 g of dextrose using a clean and dry weighing boat.
Step 2	Put the sugars in a suitable beaker, and make a 100 ml solution using deionised water. Mix the solution thoroughly using the magnetic stirrer.
Step 3	Pipette about 100 µl of the 100 mM KCl solution, and slowly add droplets of the solution into the sugar solution while simultaneously measuring the conductivity. Stop adding once the required conductivity level is reached.
Step 4	Bring the solution under the fume hood, and filter the solution into two 50 ml centrifuge tubes to avoid contamination, using a syringe-driven filter unit (Millipore Corp., Billerica, MA, USA).

4.2.4 Cell concentration estimation

Prior to conducting the DEP experiments, an estimate of the cell count was required in order for the sample concentration to be determined. This is imperative as it is one of the determining factors in achieving an optimal condition in which to conduct the experiments. The other factors are cell size (closely related to cell count), medium conductivity, dot microarray diameter, and the amplitude of the AC signal input.

The total number of cells, and thus the concentration of the cell suspension, was calculated using a Neubauer type hemocytometer (Paul Marienfeld GmbH & Co. KG, Lauda-Königshofen, Germany) (Figure 4-1), which has a graduated counting chamber that can be viewed under a microscope (Nikon Eclipse TS100, Nikon Instruments Inc., Melville, NY, USA). The chamber is defined by glass ridges

such that when a cover slip is put on top of the chamber, its distance is exactly 0.1 mm. Since the volume of cell suspension is fixed, the total number of cells counted in the chamber is taken as the concentration of the cell suspension (after the factoring in of dilution).

In this project, about 50 µl of cell suspension was loaded into the chambers. Five diagonal squares at the centre of the chamber were routinely selected as the location for cell counting. The approximate cell suspension concentration is made as follows:

$$\frac{C_{total} \times d}{\frac{0.1 \times n}{25}} \times 10^3 \ \textit{cells per ml} \tag{4.1}$$

where C_{total} is the total cell count, d is the dilution factor, and n is the number of squares used in the counting process. For the purpose of conducting the subsequent experiments, the concentration of the cell suspension preferably is about 1.0×10^6 cells per millilitre.

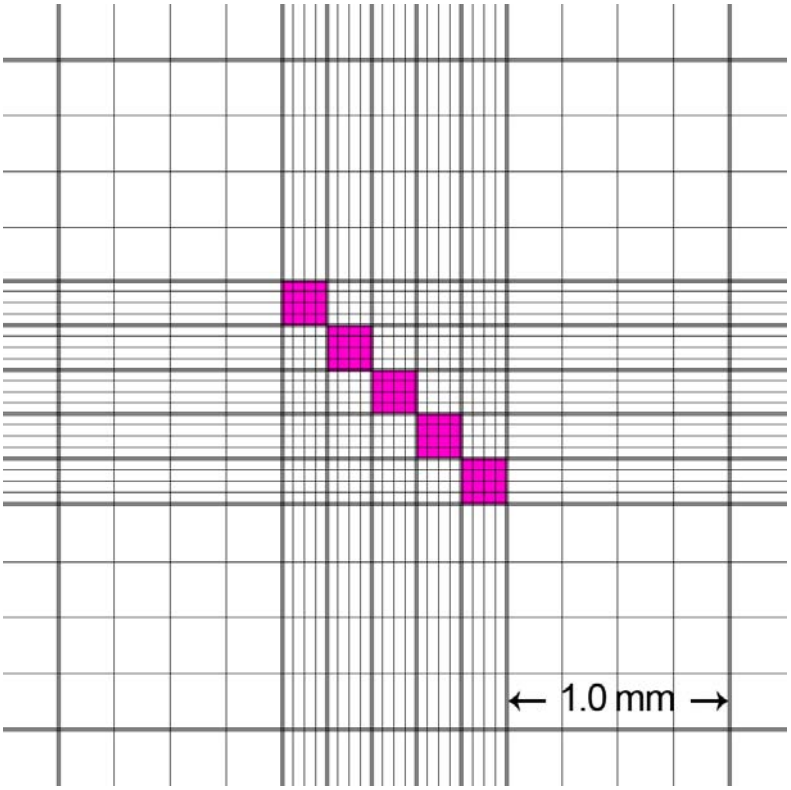

Figure 4-1 The shaded squares at the central part of the hemocytometer indicate the selected squares used in cell counting

If the concentration was found to be higher than required for the experiment, then the sample needed to be re-centrifuged and re-suspended with an additional conductive medium, prior to another round of cell count. On the other hand, if the concentration needed to be increased, less conductive medium was used during the re-centrifugation and re-suspension processes. Table 4-3 summarises the protocol used in the estimating the cell concentration.

Table 4-3 Summary of protocol in estimating cell concentration

Step 1	Mix the cell suspension thoroughly. Take 100 µl and place it in an Eppendorf tube.
Step 2	Add 100 µl of Trypan blue to the Eppendorf tube.
Step 3	Add 300 µl of the conductive medium to the mixture, and mix thoroughly.
Step 4	Take about 50 µl of the mixture and load it into both chambers of the hemocytometer.
Step 5	View the hemocytometer under the microscope at 10x magnification.
Step 6	Count the cells in 5 squares from each side of the chambers.
Step 7	Estimate the concentration using Eqn. 4.1; with a dilution factor of 5, and 10 squares.

Note that the volumes of the cell suspension, Trypan blue, and the conductive medium used in Table 4-3 will determine the dilution factor, and may be adjusted accordingly depending on the requirements of the experimental protocol.

4.2.5 Cell viability estimation

Subsequent to the cell counting process, a cell viability estimation was also made using the Trypan blue (Sigma-Aldrich Co., St. Louis, USA) dye exclusion method. This is a widely used technique in estimating cell viability (Altman *et al.*, 1993) and has been used in previous DEP-based studies (e.g. Labeed *et al.*, 2003; Hoettges *et al.*, 2008; Fatoyinbo *et al.*, 2008). In this technique, non-viable cells can be clearly seen as blue-coloured cells under low-powered (10× is routinely used) microscope (Figure 4-2), since its membrane is permeable to the Trypan blue dye. Viable cells will not allow the Trypan blue molecules to traverse through the membrane, and thus remain unstained and appear transparent under the microscope (Jones and Senft, 1985; Altman *et al.*, 1993).

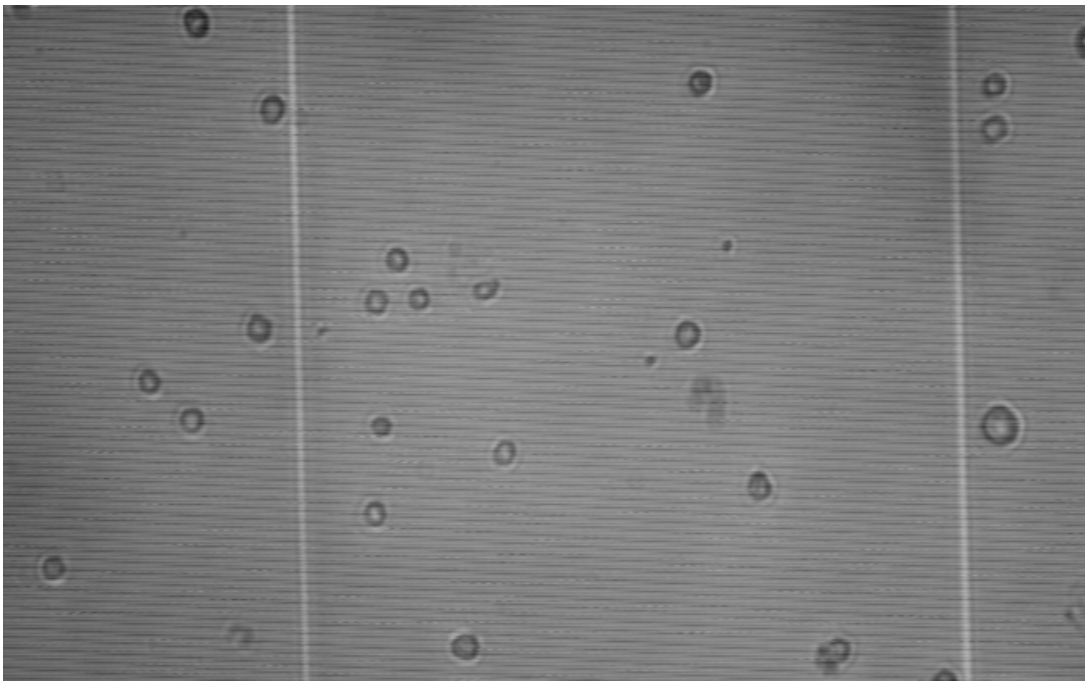

Figure 4-2 Non-viable cells appear blue, and commonly without a consistent circular shape, when viewed under the microscope following Trypan blue staining

The approximate viability percentage was calculated as follows:

$$\left(1-\frac{C_{dead}}{C_{total}}\right)\times 100\% \tag{4.2}$$

where C_{dead} is the total count of non-viable cells, and C_{total} is the total cell count (both viable and non-viable). For the purpose of conducting the subsequent experiments, the viability of the cell suspension should preferably be more than 90%, to ensure that the non-viable cells do not significantly affect or contribute towards the outcome of the DEP experiment. More importantly, the viability should also not significantly change over the course of an experiment; and as such a second cell count and viability estimate should be performed following the completion of an experiment.

4.2.6 Experimental protocol

The experimental protocol developed for the project was based on a typical DEP-based study, which have also been employed in previous studies at the Centre for Biomedical Engineering at the University of Surrey (e.g. Labeed *et al.*, 2003; Hoettges *et al.*, 2008; Fatoyinbo *et al.*, 2008). Table 4-4 summarises the steps involved in the said protocol.

Table 4-4 Summary of experimental protocol for K562 and Jurkat cells

Step 1	Take 20 ml each of cultured cells from two T75 flasks (commonly the day after cell passaging to maximise cell viability)
Step 2	Place cell suspension in 50 ml tubes, and centrifuge each at 180 g for five minutes. Remove supernatant when completed.
Step 3	Add 10 ml of conductive medium (10 mS/m) to each tube, and gently mix the suspension using a pipettor.
Step 4	Centrifuge each tube at 115 g for five minutes. Remove supernatant when completed.
Step 5	Repeat Steps 3 and 4.
Step 6	Depending on the cell concentration required, appropriate amount of conductive medium is added. Typically, add 1 ml of medium to achieve 1×10^7 cells per ml.
Step 7	Pipette the solution into an Eppendorf tube.
Step 8	Conduct cell counting (Section 4.2.4) and cell viability estimations (Section 4.2.5).
Step 9	Set up the microelectrode device (preferably completed prior to conducting an experiment): fabricate the gasket (Section 3.4.2) and attach it to the electrode (Section 3.4.1).
Step 10	Set up the microscope: 4x magnification, and ensure uniform amount of light shining through the dots of the electrode.
Step 11	Set up the program: number of electrodes to be used (multiples of 4), start and end frequency, duration of signal and image capture, peak-to-peak voltage, dot diameter, and other information. The typical steps and values used for conducting an experiment are detailed below.
Step 12	Using a syringe, push a small amount of cell suspension through the inlet to completely cover the chamber created by the gasket. Avoid bubbles and/or over spilling of cell suspension out of the outlet.
Step 13	Start applying the signal.
Step 14	Re-suspend the cell suspension at the end of an experimental run, either by lightly tapping the electrode or pushing another small amount of cell suspension through the inlet.
Step 15	Repeat Steps 13 and 14 as necessary.

The typical settings used in a DEP experiment currently were as follows:

a) Using the 8-electrode setting, the frequency was set from 10 kHz to 1 MHz, at 8 points per decade. This produced sixteen data points that were used in constructing the DEP spectrum (NB. Higher resolution DEP spectra may be achieved by increasing the amount of data points to be recorded per decade).

b) The duration of the signal application was 20 seconds, and the image capture duration was 22 seconds (NB. Longer capture duration may be required to observe redispersion of the cells within a microelectrode dot, if any).

c) Peak-to-peak voltage was set at 8 V_{pp} (NB. Shorter periods of signal application may be used for higher voltages).

d) The diameter of the microelectrode dots used was 200 μm and the experiments were repeated 10 to 15 times (NB. Smaller diameter dots may be used for smaller cells, e.g. yeasts).

A complete step-by-step guide in setting up and running a typical DEP experiment using the developed system, along with a screenshot of the program at each of these steps, is attached in Appendix A.

4.3 Results and discussion

The first five subsections will cover the outcome from the preliminary feasibility studies involving the different microelectrode set up, while the rest of the section will contain the outcome of the various validation studies involving the effects of input signal frequencies and strength, medium conductivities, and microelectrode dot sizes.

4.3.1 Impedance analysis

Prior to the device being used in experimental conditions, an impedance analysis was conducted for the electrode setup using a variety of conductive media, namely KCl, PBS, and RPMI solutions. The impedance values were recorded using a phase sensitive multimeter (NumetriQ PSM 1735, Newtons4th Ltd., Leicestershire, UK) with the following parameters: 10 kHz to 20 MHz sweep, 32 data points, and connected serially. Calibrations for both short and open circuits were performed immediately prior to each experimental session.

Figure 4-3 shows a plot of impedance (in ohms) against conductivity (in mS/m) for the solutions taken at 10 kHz. The plot displays the expected reduction in impedance of the system as the medium conductivity increases (caused by increased amounts of K^+ and Cl^- ions). The recorded impedance also seemed to be stable across the range of frequencies typically used in a DEP experiment (Figure 4-4), apart from a sudden drop at around 10 MHz. This drop was much higher than 50 Hz, thus ensuring that the output impedance of the waveform generator is matched.

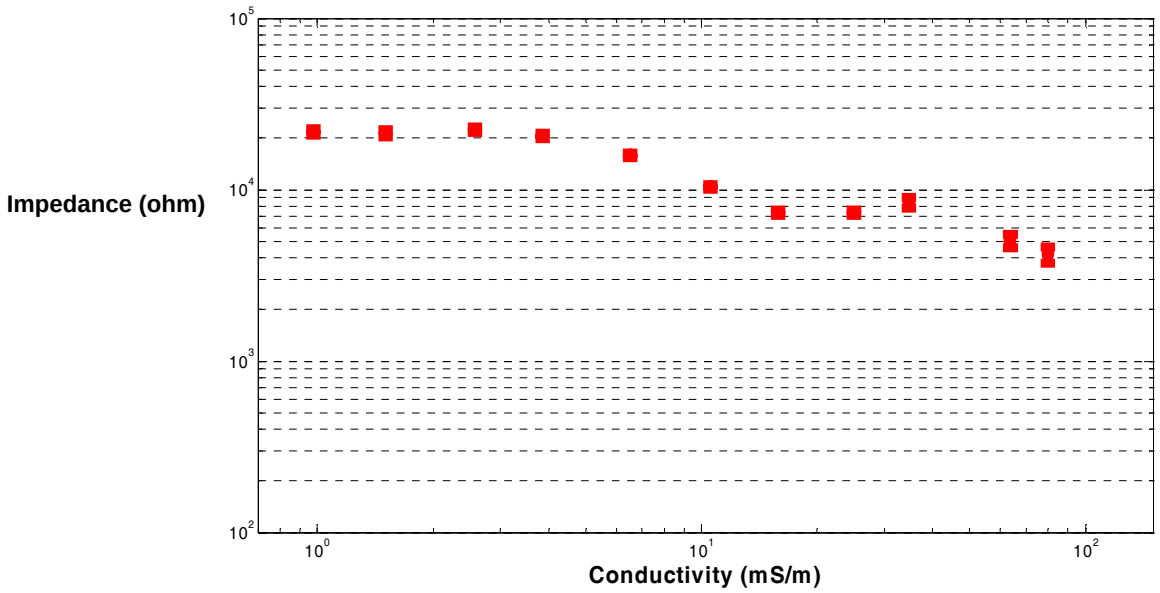

Figure 4-3 Plot of impedance against conductivity for the system, recorded at 10-20 kHz

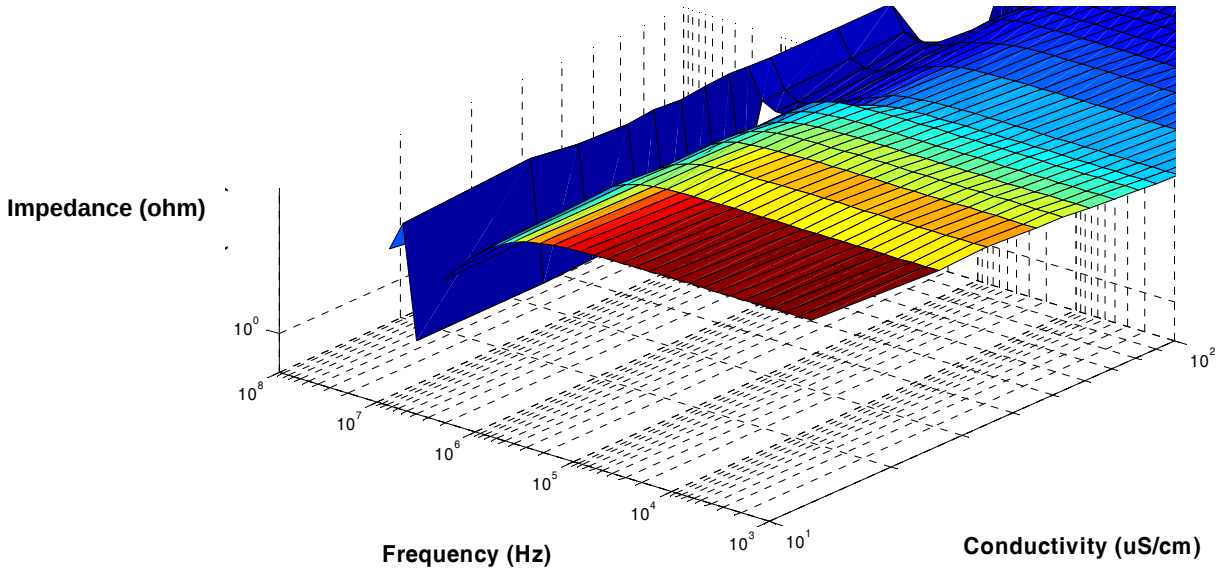

Figure 4-4 Plot of impedance against conductivity and frequency of applied signal for the system

4.3.2 Cell size analysis

One of the required parameters in determining the electrophysiological properties of the cells in a given sample is the approximate cell size. ImageJ (1.37v by Rasband W, 2004, public domain) was used to determine the approximate size of the cells used in the experiments. The program allows a number of methods to estimate the cell size in a given image, including the Straight Lines tool, Elliptical Selection tool (using Feret's diameter), and the Analyze Particles command. Both Straight Lines (Figure 4-5) and Elliptical Selection (Figure 4-6) required manual selection of areas on the image considered to be cells; while the Analyze Particles command (Figure 4-7) allowed automated cell detection, based on the boundaries created in the image following a thresholding process. The actual averaged radii of the cells were determined by comparing the lengths with known distances in the images, namely the width of the smallest haemocytometer square which measures at 0.05 mm. It was found that the average radii of Jurkat and K562 cells were 6.80 (± 0.70) µm and 8.18 (± 0.74) µm, respectively.

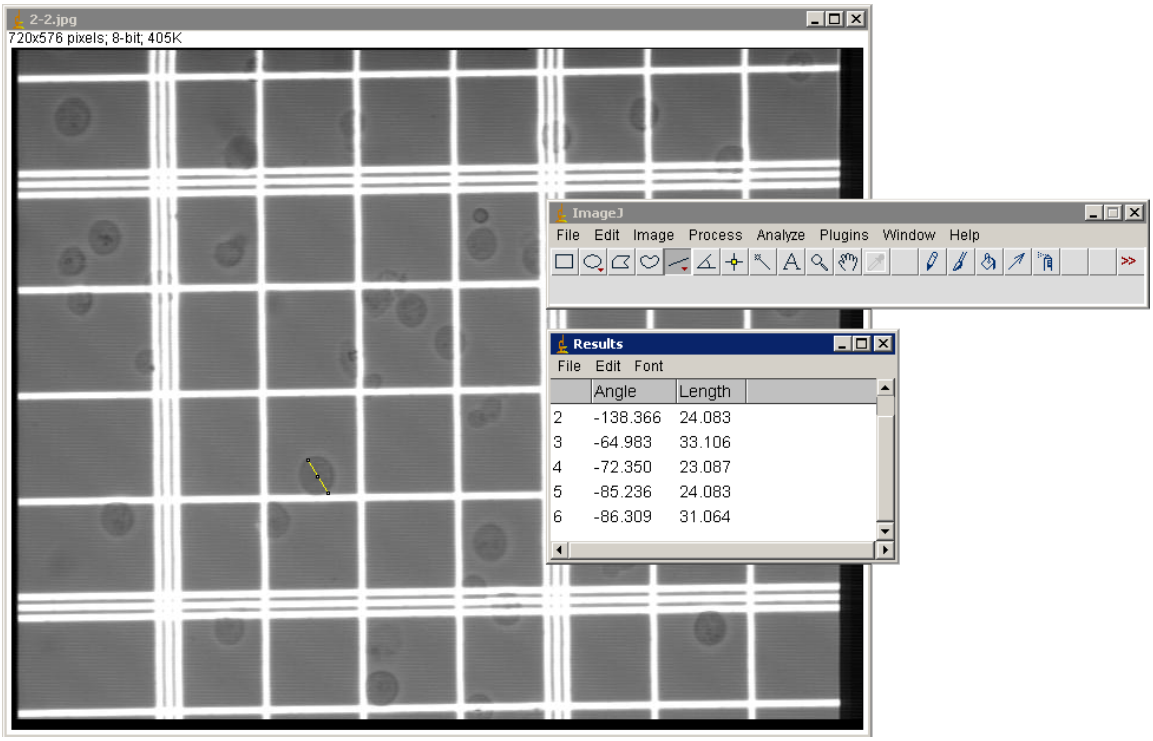

Figure 4-5 Determining the diameter of a cell using 'Straight Lines' tool in ImageJ

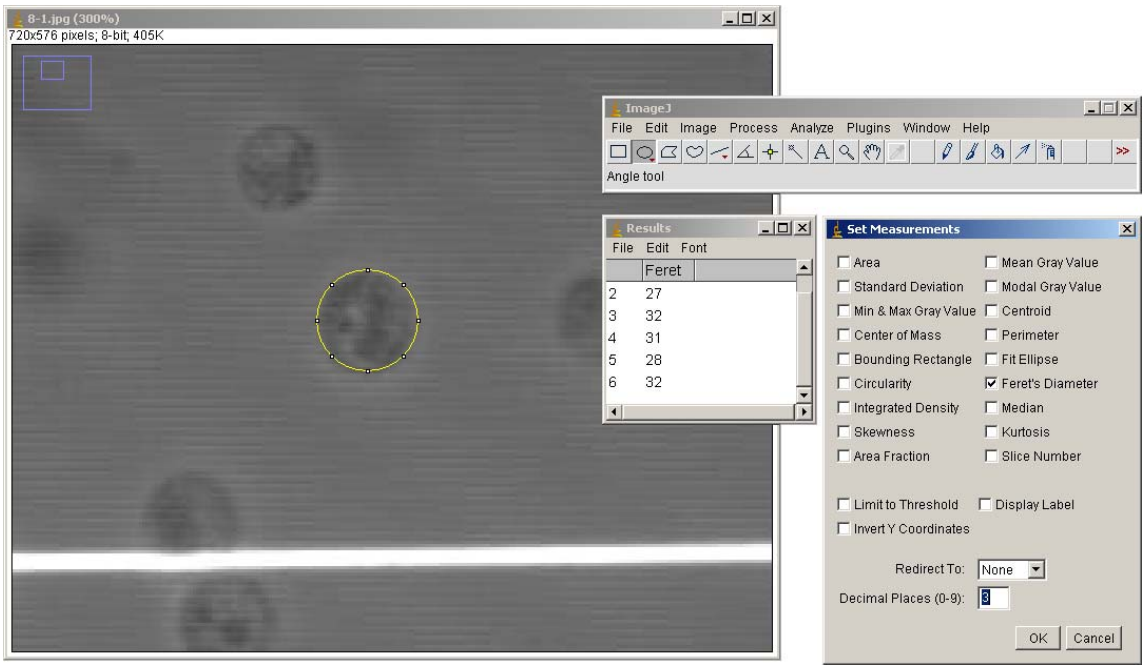

Figure 4-6 The first alternative method of measuring cell size using the Feret's diameter

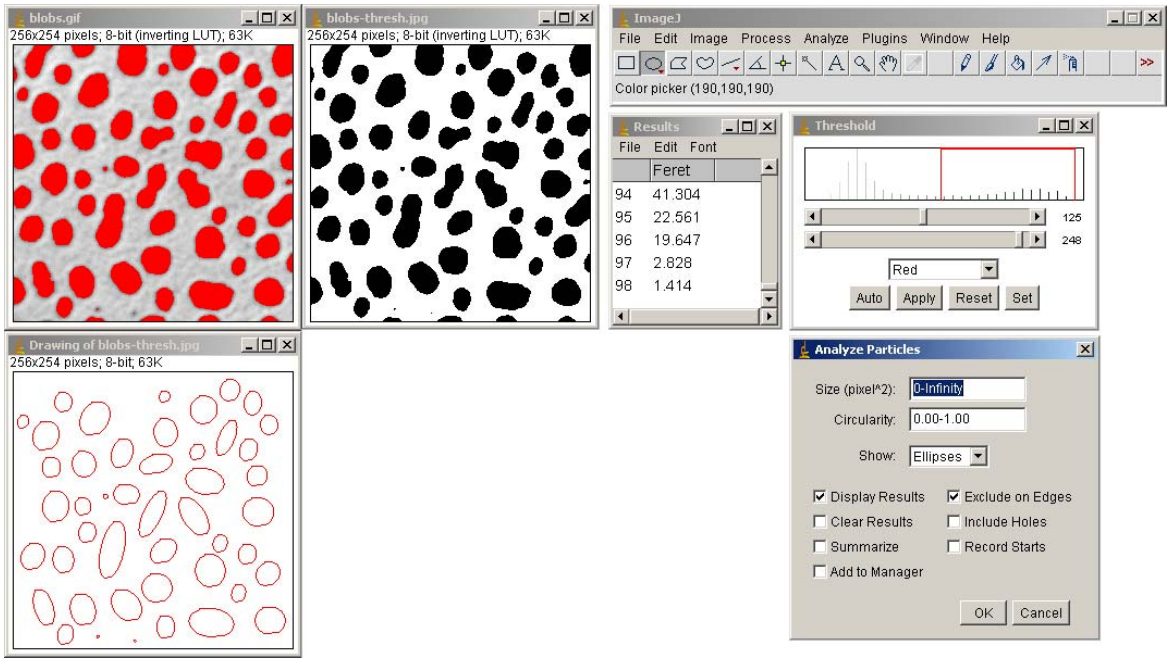

Figure 4-7 The second alternative method of measuring cell size using the 'Analyze Particles' menu (employing sample images from the program)

4.3.3 Serial 4-dot electrode system

The development of the microelectrode device started with the use of a planar microelectrode geometry that allowed the delivery of input signal in series, i.e. an electrical field of the same strength and gradient will be created over each of the dots. Images of the dots were then captured with 1 second temporal resolution, prior to the analysis of the light intensity within each of the dots.

Figures 4-8 and 4-9 show the images from a series of experiments using yeast cells, with KCl as the conductive medium prepared at 5 mS/m. The experiments were conducted within the range of 1 kHz to 2.154 MHz, supplied at 10 V_{p-p} for 20 seconds, using serial microelectrodes with 300 μm diameter dots. In Figure 4-8, the cells experienced negative DEP, and thus collected at the centre of the dots. Conversely, the cells were attracted towards the periphery of the dots if the generated electrical fields caused the cells to experience positive DEP (Figure 4-9). These observations were in accordance with the ones made by Fatoyinbo *et al.* (2008) when similar studies were made using single dots.

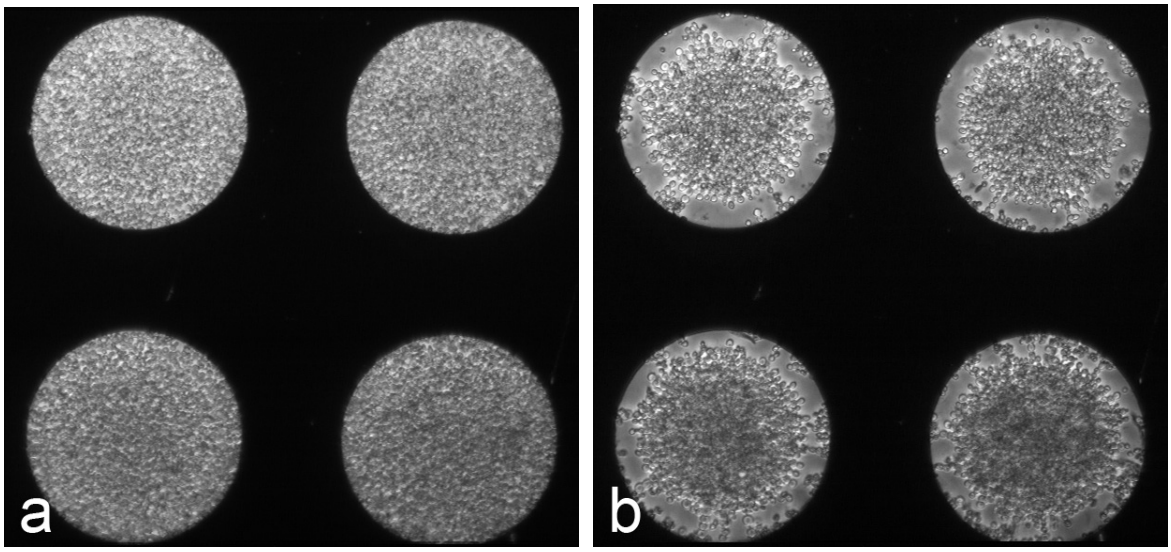

Figure 4-8 Collection of yeast cell suspension a) before and; b) after the electrical signal application, demonstrating negative DEP. Each of the dots received 10 kHz at 10V_{p-p}, applied for 20 seconds. The analysed light intensity values are represented in blue in Figure 4-13

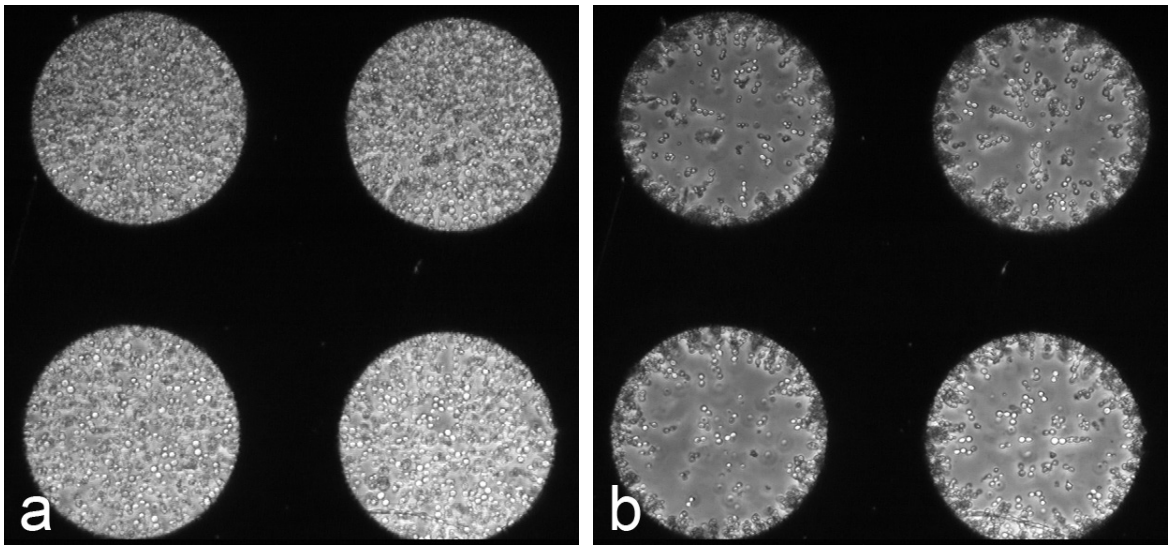

Figure 4-9 Collection of yeast cell suspension a) before and; b) after the electrical signal application, demonstrating positive DEP. Each of the dots received 1 MHz at $10V_{p-p}$, applied for 20 seconds. The analysed light intensity values are represented in red in Figure 4-13

Using the developed analysis program, which is an improvement of the one used by Fatoyinbo *et al.* (2008), the light intensity values over each of the dots were determined (Figure 4-10, with normalised values from dots shown in Figures 4-8 and 4-9). It can be seen that the dots that experience negative DEP displays negative intensity values, and vice versa for the ones experiencing positive DEP.

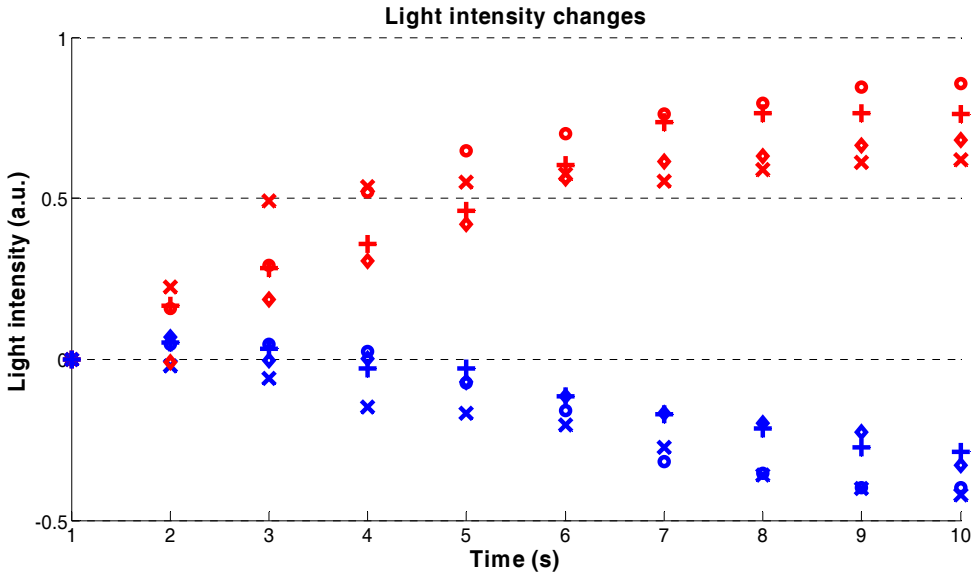

Figure 4-10 Light intensity changes over the course of conducting two experimental runs using a 4-dot serial set up. Blue datasets represent 10 kHz, the red datasets represent 1 MHz

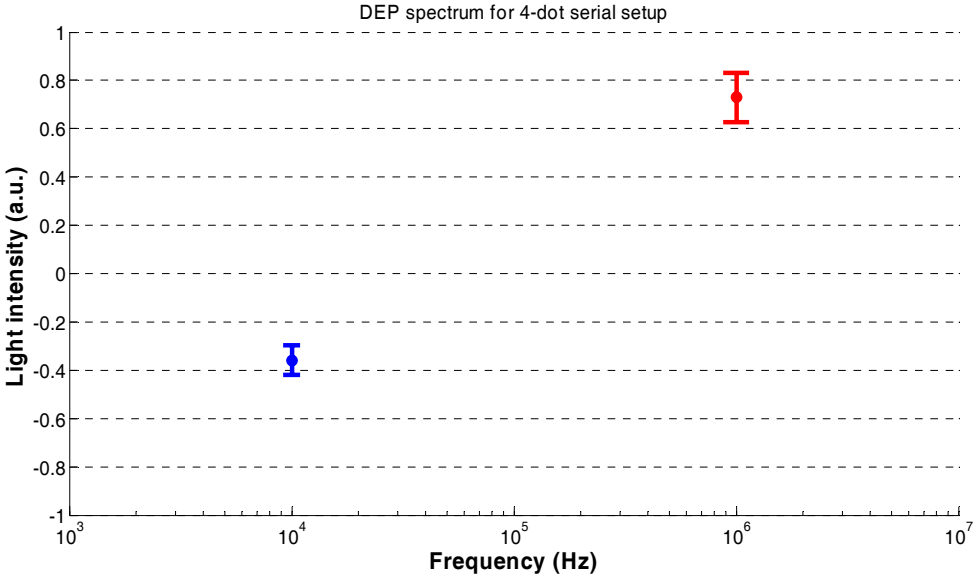

Figure 4-11 The DEP spectrum constructed from the datasets at the 10th second from Figure 4-10

The intensity value at the end of the signal application was used to construct a DEP spectrum, as shown in Figure 4-11. Obviously this is an incomplete spectrum as it was constructed from only two frequency sets; however it showed that the system, even when only four dots were used serially, is capable of significantly reducing the time it normally took to complete a DEP experiment. For example, a DEP spectrum consisting of eight data point, repeated five times for each frequency points, may be concluded in 40 minutes using this system. On the other hand, only one set of experiments may be conducted within the same time period when using the previous method employed at the Centre for Biomedical Engineering at the University of Surrey (e.g. Broche *et al.*, 2005; Labeed *et al.*, 2006).

Nevertheless, the system still cannot be used in the so-called real-time experiments, since it is incapable of capturing the movements of the cells experiencing different frequencies at the same point in time.

4.3.4 Parallel 4-dot electrode system

The primary objective in developing the parallel version of the microelectrode array used in Section 4.3.3 was to overcome the failure of the system in possibly conducting DEP experiments in real-time. If each of the electrodes is capable of receiving an input signal of differing frequency values, then there is a possibility of capturing the cellular movements at four different frequencies at the same point in time.

Figures 4-12(a) and 4-12(b) show the images captured by the system before and after, respectively, an experiment conducted using Jurkat cells, with RPMI as the conductive medium prepared at 10 mS/m. The experiments were conducted within the range of 1 kHz to 2.154 MHz, supplied at 10 V_{p-p} for 20 seconds, using parallel microelectrode with 300 µm diameter dots. As expected, all of the dots display positive DEP effects (cells attracted towards the electrode), except for the one dot that is receiving 100 kHz (dot 1 in Figure 4-12), indicating that the crossover frequency is most likely to occur between 100 kHz and 215.4 kHz.

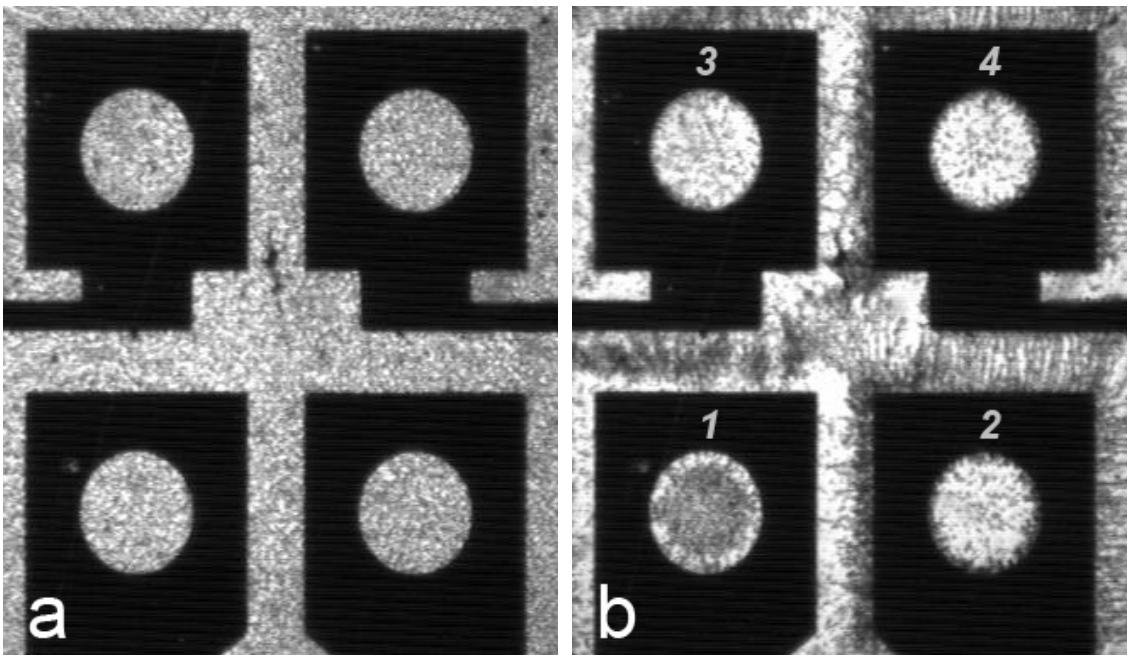

Figure 4-12 Collection of Jurkat cell suspension a) before and; b) after the experiment. The dots labelled 1, 2, 3, and 4 received 100 kHz, 215.4 kHz, 464.2 kHz, and 1 MHz, respectively. The measured light intensities for each of the dots are shown in Figure 4-13

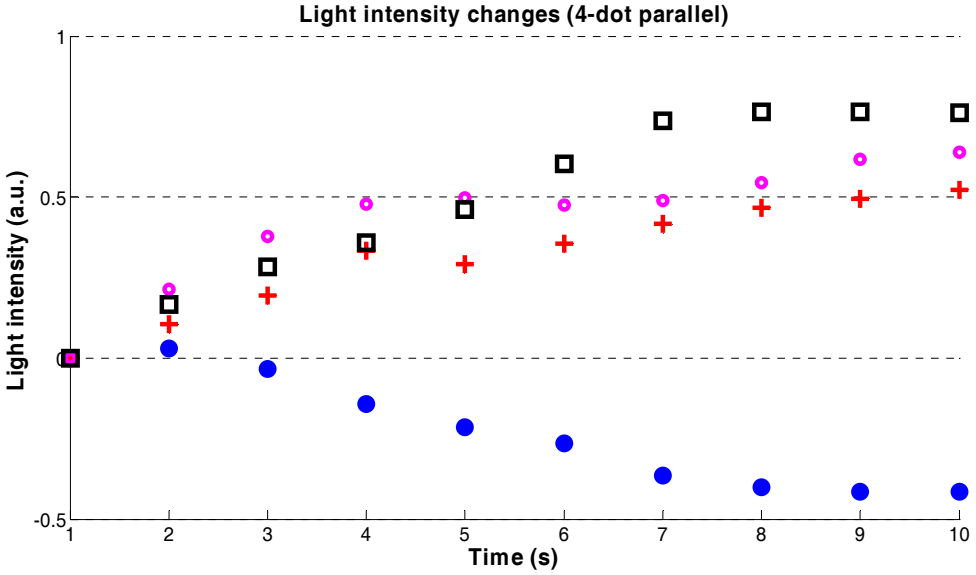

Figure 4-13 Light intensity changes over the course of conducting one experimental run using a 4-channel parallel set up

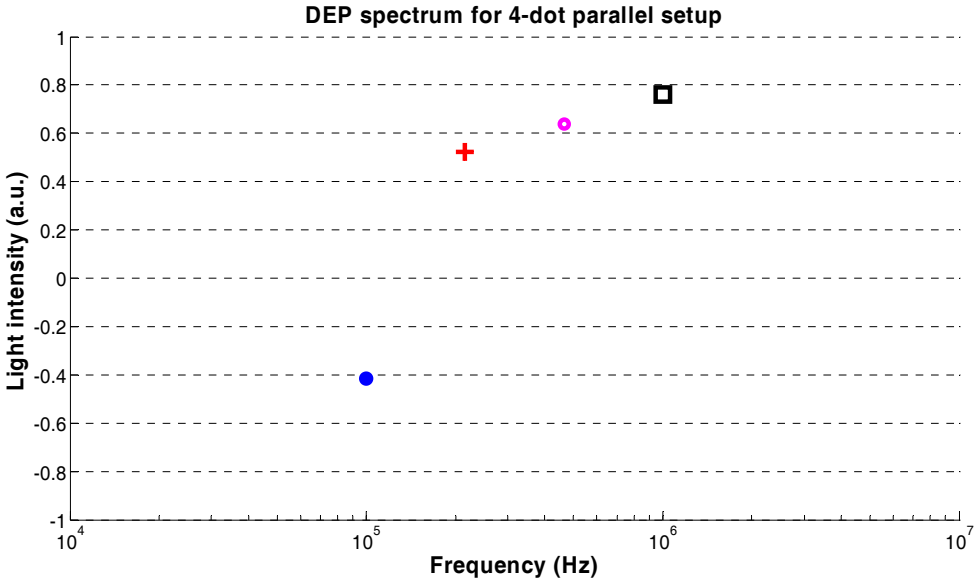

Figure 4-14 The DEP spectrum constructed from the datasets that were used in Figure 4-13

Using the available analysis system, the light intensity values can be determined (Figure 4-13, with normalised values), and a DEP spectrum with four data points may be constructed from a single run of experiment, lasting for about two minutes. In theory, this set up is capable of halving the time required to produce the same DEP spectra with eight data points, described in Section 4.3.3. In

addition, the time taken to complete the experiment may even be reduced further, since the light intensity values already reached a steady state at around 12 seconds (Figure 4-13). If a simple DEP spectrum consisting of only four data points is desired, then this set up is already capable of conducting real-time DEP experiments, since it is capable of recording the cellular movements at four different frequencies at the same point in time.

More importantly, the crossover frequency from the DEP spectrum produced by the system (Figure 4-14) appeared to be in accord with previously published data (e.g. Altomare *et al.*, 2003; Gascoyne and Vykoukal, 2004). Although crossover frequency by itself does not indicate the overall electrophysiological changes occurring on the cell population, it nevertheless showed that the change in relative polarisability of the membrane is occurring at a particular signal frequency.

4.3.5 Parallel 8-dot electrode system

By combining an additional board having four output channels, the waveform generator (Section 3.3) can now supply eight individually programmed input signals, thus opening up a real possibility of conducting real-time DEP experiments. Figure 4-15 shows the images captured by the system before and after an experiment conducted using K562 cells, with KCl as the conductive medium prepared at 10 mS/m. The experiments were conducted within the range of 10 kHz to 1 MHz, supplied at 8 V_{p-p} for 20 seconds, using parallel microelectrode with 200 µm diameter dots. Figures 4-16 and 4-17 showed the light intensity analysis and the resulting DEP spectrum, respectively; for the example image dataset shown in Figure 4-15. Again, the crossover frequency from the DEP spectrum appeared to be consistent with the outcome of the previously developed systems (Sections 4.3.3 and 4.3.4).

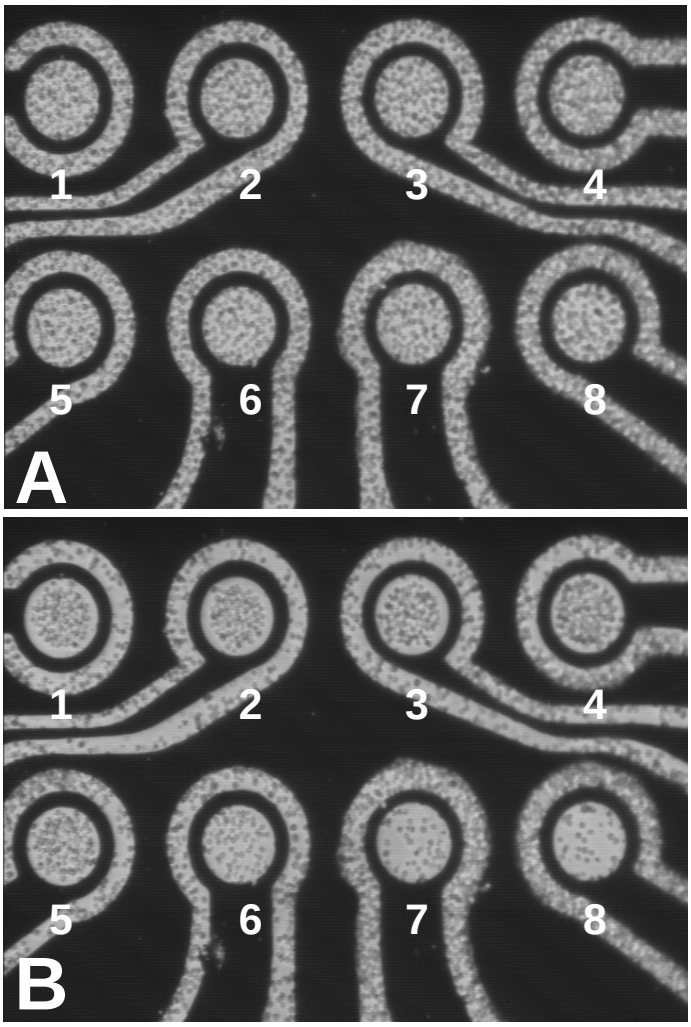

Figure 4-15 Collection of K562 cell suspension a) before and b) after the experiment. The dots receive a range of frequency between 10 kHz and 1 MHz at four points per decade. The measured light intensities for each of the dots are shown in Figure 4-16

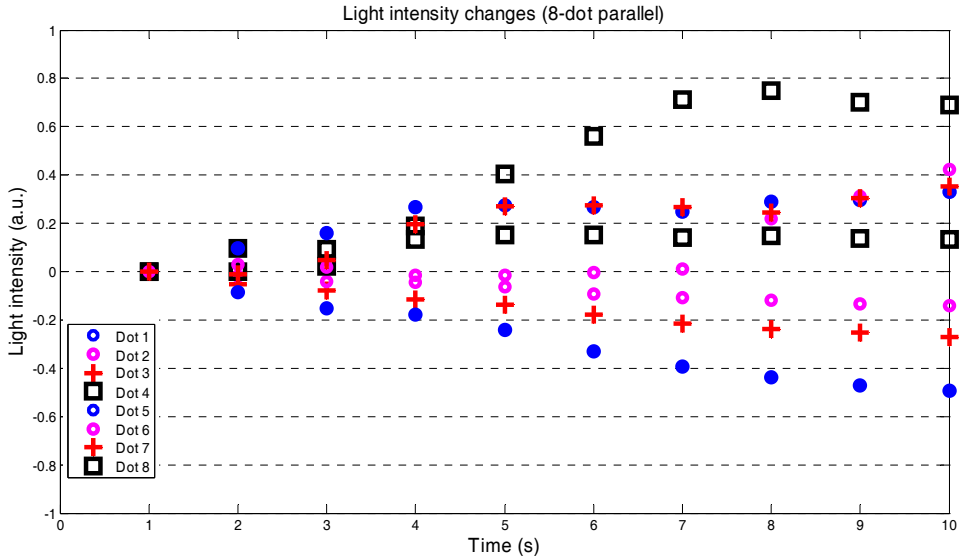

Figure 4-16 Light intensity changes over the course of conducting one experimental run using an 8-channel parallel set up

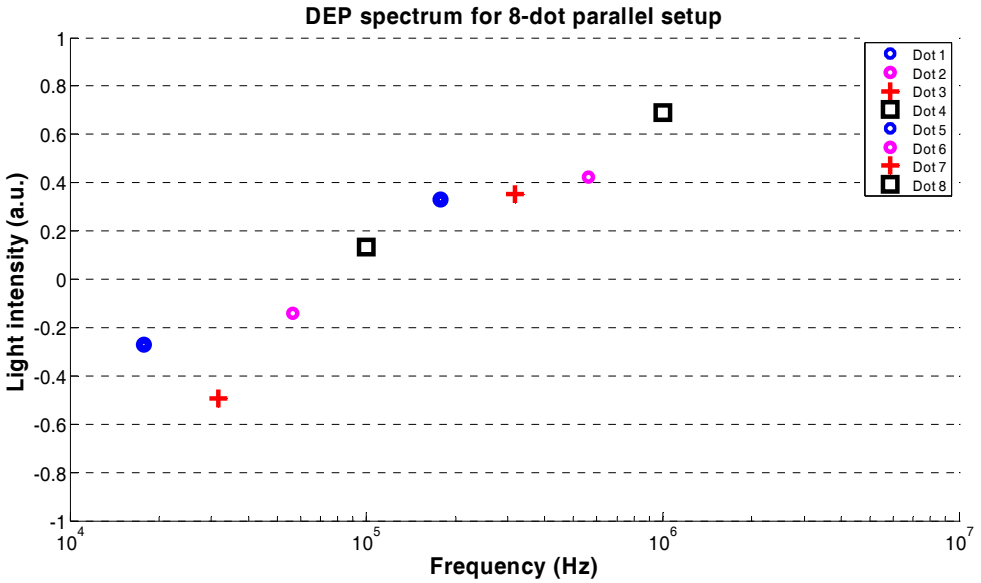

Figure 4-17 The DEP spectrum constructed from the datasets that were used in Figure 4-16

Using this set up, the time it took to complete the same experiments have been drastically reduced. Although technically, one will still require the same amount of time to complete an experiment using the 4-dot parallel system, the produced DEP spectrum will now have better resolution since it will

now have double the number of data points. A DEP spectrum having eight data points can be produced within two minutes using this set up.

This capability brings about the possibility of using the system to produce an additional dimension to the DEP spectrum, namely the time domain. Figure 4-18 shows an example of a typical set of DEP spectra of K562 cells over a period of 45 minutes, represented in 3D (1×10^7 cells per ml; 10 mS/m KCl conductive medium; 10 kHz-1.6 MHz; 8 V_{p-p}). The red regions represent positive DEP, while the blue regions represent negative DEP.

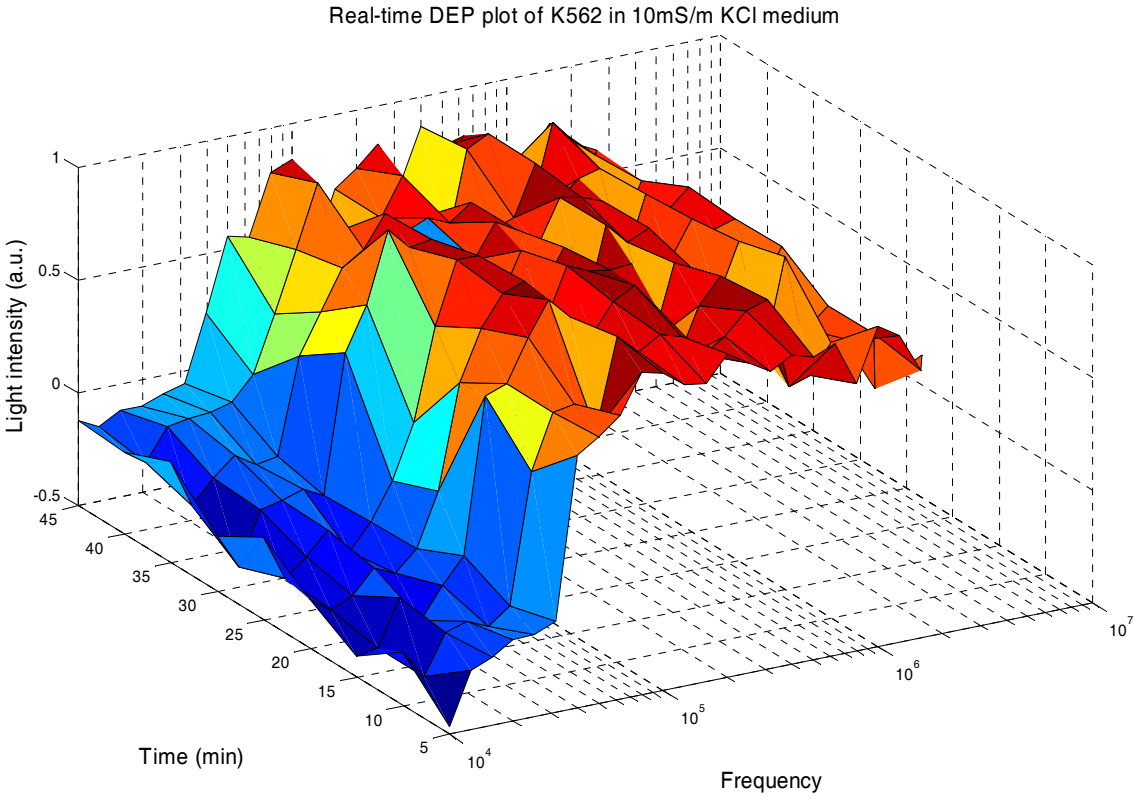

Figure 4-18 DEP spectra of K562 cells represented in 3D over 45 minutes

Therefore, any electrophysiological changes that affect the DEP spectrum occurring on the cell population should theoretically be observable as it happens over the course of an experiment. The changes observed in previous DEP-based studies (e.g. Johari *et al.*, 2003; Hübner *et al.*, 2005; Chin *et al.*, 2006), can now be measured close to real-time, and may provide a better and complete understanding towards the causes of the said changes in terms of the membrane electrophysiological make-up. The said DEP spectra changes can only be previously observed between an untreated cell

sample and a treated one, without the capability of observing the changes occurring in between these times, due to the long time required to complete a single set of DEP experiment. With the aid of the developed system, the gradual DEP changes can now be observed for the first time within a satisfactory temporal resolution that may be considered near real-time (Figure 4-18).

4.3.6 Effects of varying electric field intensity

In order to produce accurate DEP results, each of the microelectrode dots must produce a consistent electric field when the same input signal is applied. The variations, if any, must be sufficiently small enough to be produce a DEP spectrum with an acceptable margin of error. This may be determined by analysing the light intensity values of the dots when an input signal of similar frequency and voltage is applied to each of the dots.

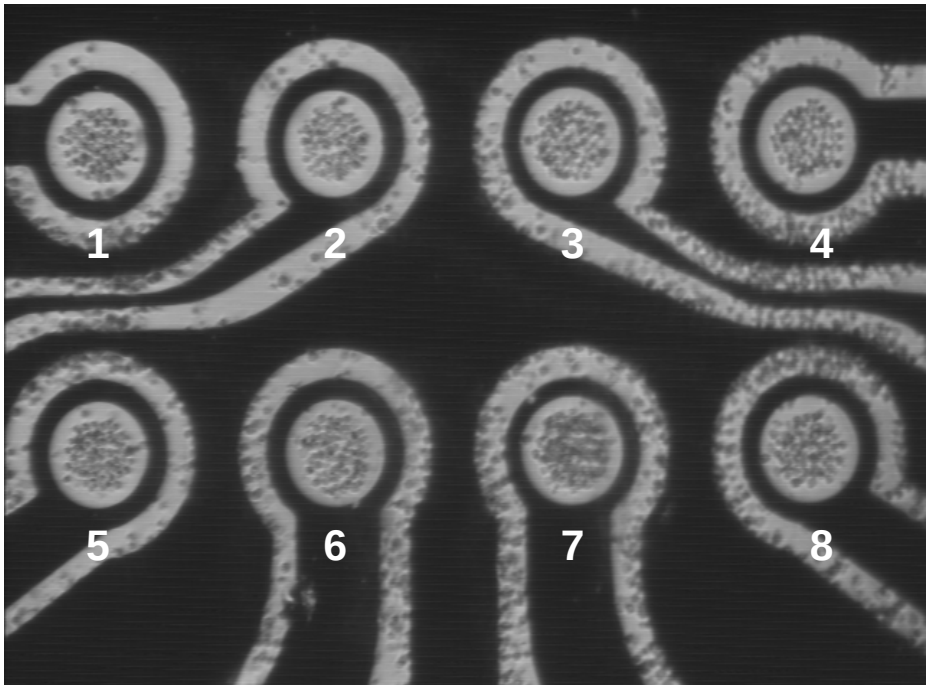

Figure 4-19 Collection of cells experiencing negative DEP following an experiment to determine the variation of the produced electrical field by each of the dots (K562 cells at 1×10^7 cells per ml, 10 mS/m medium using RPMI, 8 Vp-p input signal at 20 kHz)

It was found that the mean normalised light intensities for 10 kHz, 100 kHz, and 1 MHz were -0.03 (±0.04), 0.2 (±0.06), and 0.34 (±0.06), respectively. Since the standard deviation values remain constant over the course of these validation experiments, the system therefore has demonstrated repeatability and consistency in producing the electrical fields at the required gradient strength to be

used in actual DEP experiments. Figure 4-20 shows the overall light intensity change over the course of an experiment (15 s), for the particular dataset shown in Figure 4-19.

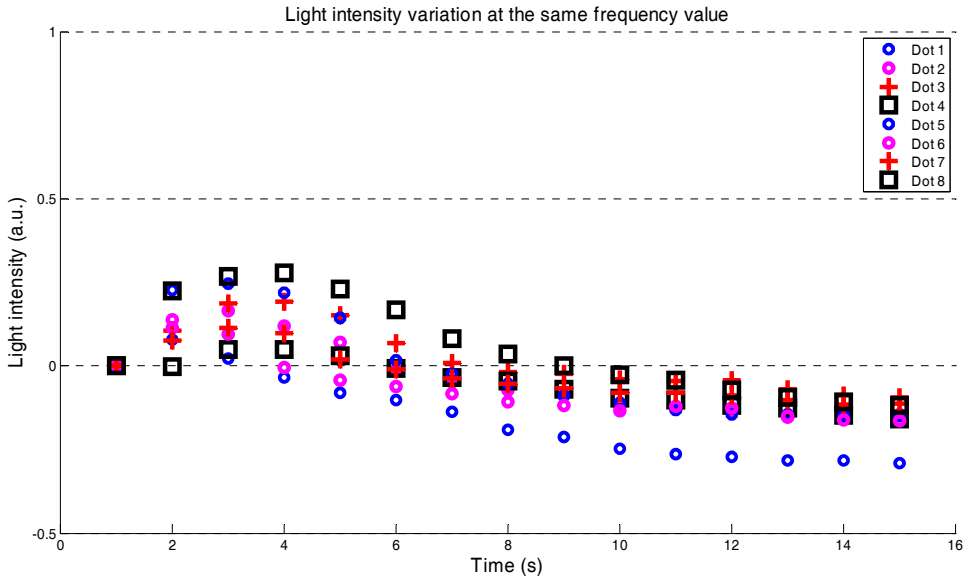

Figure 4-20 A typical example of light intensity changes over the course of an experiment (analysed from Figure 4-19) to determine the variation of the produced electrical field by each of the dots when similar input signal was applied

4.3.7 Effects of varying supply voltages

One of the important experimental settings is the voltage of the input signal, since it directly affects the gradient of the generated electric field. Due to the axisymmetrical nature of the electric field (Fatoyinbo *et al.*, 2008), there exists a limited range of suitable voltages to be used. A strong electric field may push out all of the cells before the intended DEP effect may take place (particularly for negative DEP), while a weak electric field may not generate sufficient gradient to affect any cellular movement (particularly for positive DEP). Figure 4-21 shows an example of the images taken from the same dot and time frame when an input signal of similar frequency but with different voltages was applied.

From the light intensity analysis (Figure 4-22), it is clear that the positive DEP effects (in this particular instance), is much better represented by an input signal with 8 $V_{p\text{-}p}$ amplitude, compared to the one with 2 $V_{p\text{-}p}$. This difference is better portrayed when the DEP spectrum is produced from the datasets (Figure 4-23). Clearly the DEP spectrum produced by having an input signal of 8 $V_{p\text{-}p}$ is more

representative of the cellular movements during the experiment, and lends itself well to be used in the subsequent electrophysiology analysis.

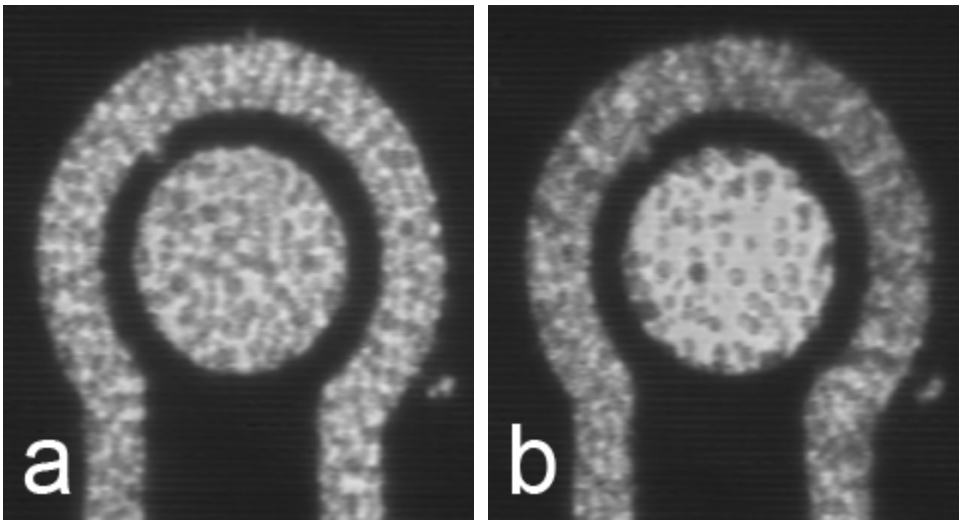

Figure 4-21 Original images taken from the same dot at 10 s supplied with a) 2 V_{p-p} and b) 8 V_{p-p} (K562 cells at 1×10^7 cells per ml, 10 mS/m KCl medium, 1 MHz input signal)

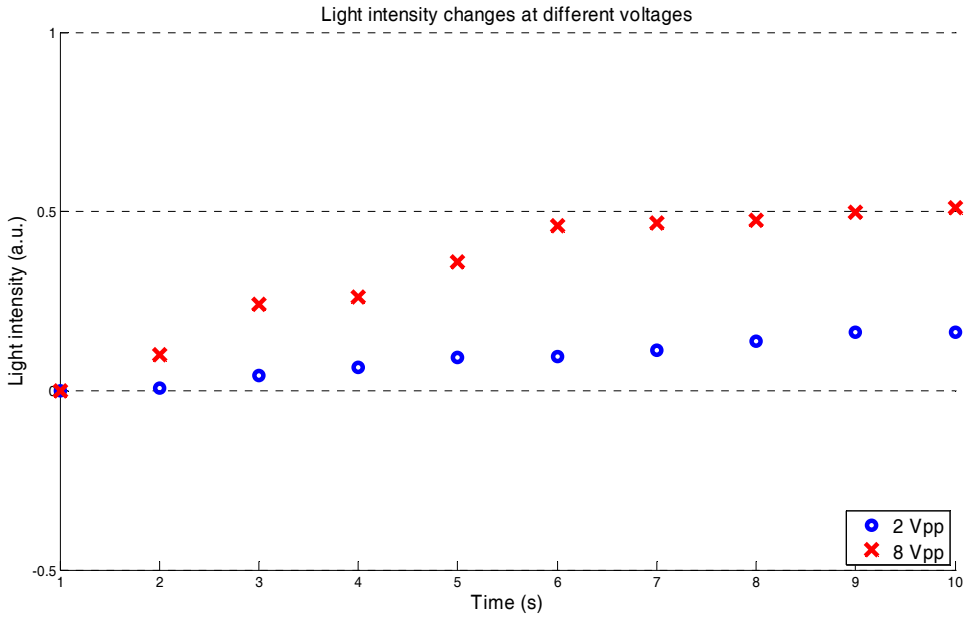

Figure 4-22 Light intensity analysis of the images shown in Figure 4-21

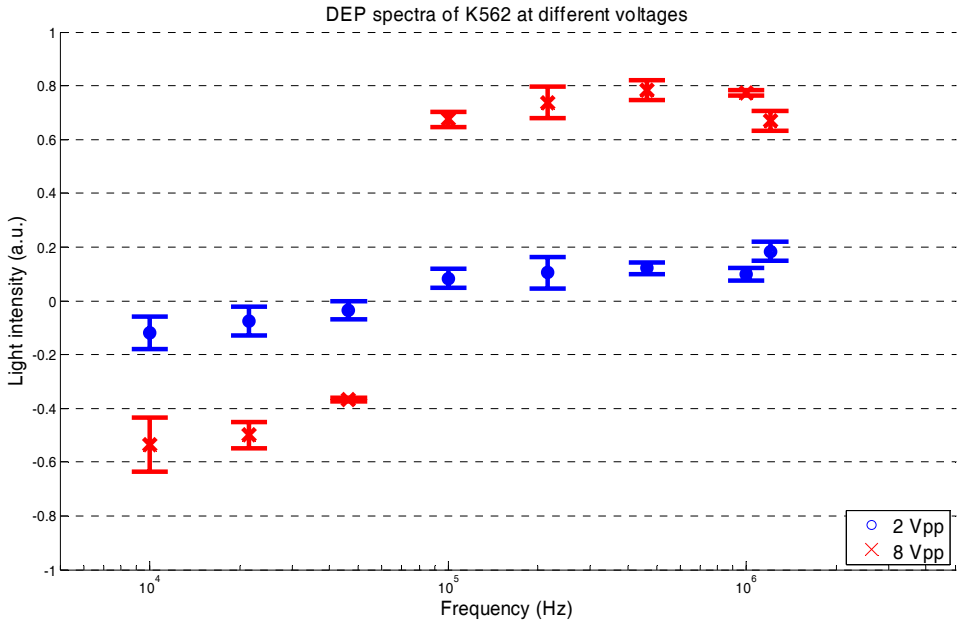

Figure 4-23 DEP spectra from two independent experiments conducted using K562 cells and supplied at different voltages

Nevertheless, it must be noted that the relationship between the light intensity change and the supplied voltage is not linear. Above a certain voltage threshold (depending on the diameter of the microelectrode dot used, the concentration of the cells, and time exposure), the initial strength of the produced electrical gradient is such that it may appear to push the cells away from the dots and the final captured image may not represent the true nature of the DEP effect on that particular dot. A dot that is expected to have negative DEP, for example, may not have enough cells at the centre of the dot to be analysed as having negative DEP, because most of the cells have been pushed out. In addition, these displaced cells may end up in neighbouring dots, and may further affect the final outcome of the analysis. Generally, very low voltage will not be able to produce the required DEP force to produce an accurate DEP spectrum, while very high voltage produced a high-gradient electric field that pushed the majority of cells out of the individual dots. This invariably caused incorrect negative DEP and very high positive DEP measurements.

In order to determine the optimal voltage supply to be used, a plot of light intensity change between the first and the last frames of the image is produced (Figure 4-24). The data were acquired from a set of experiment that was conducted using K562 cells, medium conductivity of 10 mS/m, dot size of 200 µm, and the supplied voltage was set at 20 kHz for 10 seconds. Since the cells were expected to experience negative DEP, a good supply voltage should then produce a sizeable difference in light

intensity but within the negative side. From Figure 4-24 it can be seen that between 1 to 5 V_{p-p} there is only a slight change of light intensity between the first and last images, meaning that the generated electric field do not have sufficient gradient to push the cells towards the centre of the dots. On the other hand, having an input signal between 12 to 15 V_{p-p} will either produce an incorrect light intensity value (e.g. at 12 V_{p-p}), or only a small change between the images, since a large proportion of the cells have been pushed out of the dots during the initial moments when the electric field was generated. In conclusion, the suitable range of input signal voltage to be used for DEP experiments using the microelectrode is between 6 to 11 V_{p-p}.

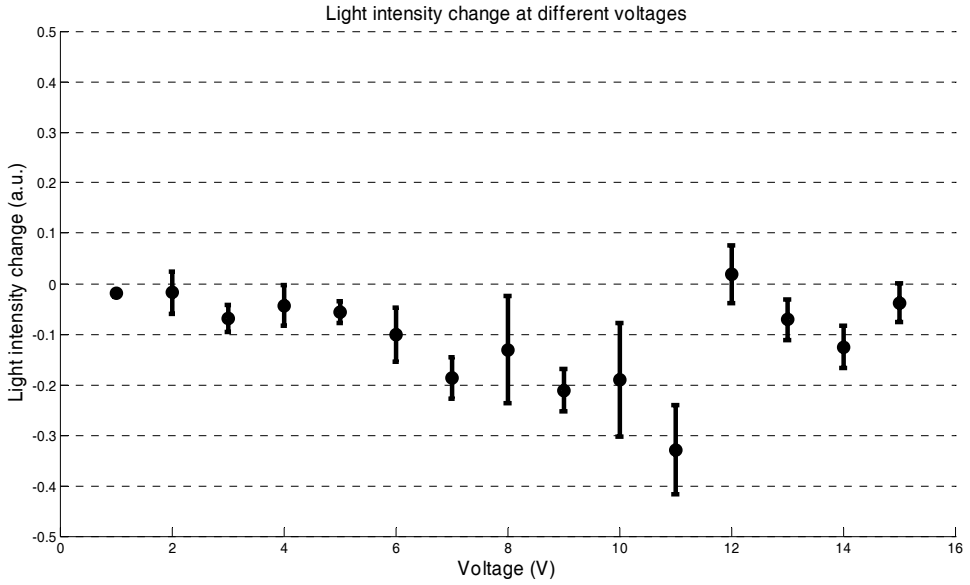

Figure 4-24 Light intensity changes between the first and the last frames of the captured image, at different supply voltages

4.3.8 Effects of varying cell concentrations

Another paramount factor to be considered in using the developed system is the effects of cell concentrations on the produced DEP spectrum. Ideally, the system should be able to consistently produce similar spectra, given two samples of cell populations with identical parameters, apart from the cell concentration. This should be easily determined by observing the crossover frequency from the spectra, apart from the analysis of the overall spectra to reveal the values of membrane electrophysiological parameters. The only difference would be the speed at which the experiments will take place: concentrated cells require higher electrical gradient since the cells will collectively create a larger dipole moment, thus theoretically requires higher voltage to produce a stronger electric

field gradient and will take longer to achieve the same DEP effect. Figure 4-25 shows the images taken from the same dot of the microelectrode, and at the same point in time (i.e. 10 s), of two independent DEP experiments having different cell concentrations. It can be seen that by using the same input supply voltage, the expected effect (i.e. positive DEP) on the sample with higher cell concentration have not yet reached the steady state, compared to the other sample.

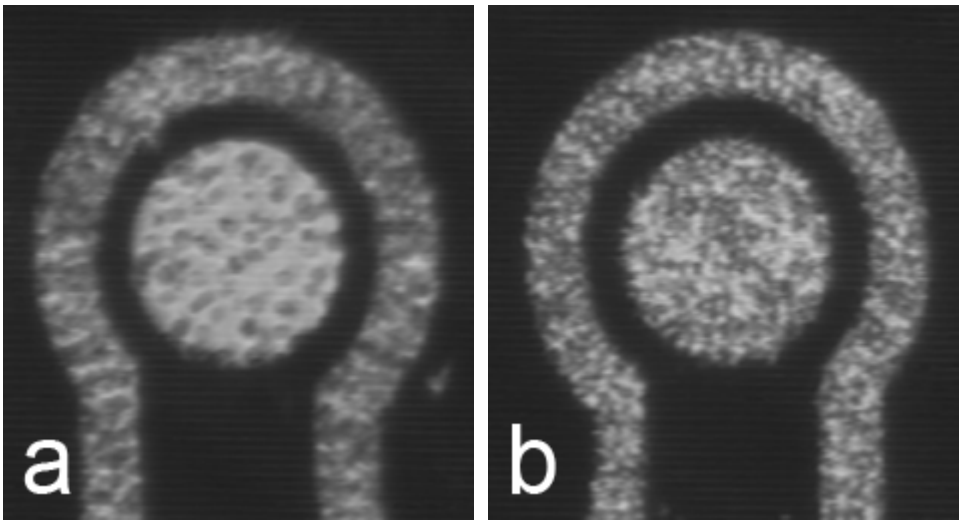

Figure 4-25 Original images from the experiments showing dots that experienced positive DEP at different cell concentrations of a) 0.7×10^7 cells per ml and b) 1.4×10^7 cells per ml, respectively; taken at the same frequency value (1 MHz) and image frame (10 s) (K562 cells, 10 mS/m KCl medium, 1 MHz input signal, $8V_{p\text{-}p}$ input signal)

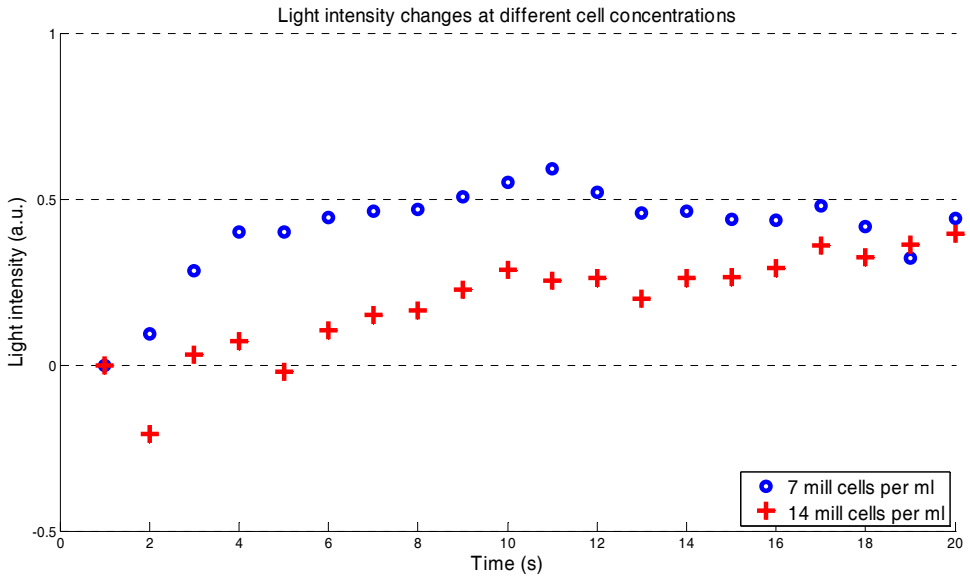

Figure 4-26 Light intensity changes for the dots depicted in Figure 4-25 over the course of an experiment. The frequency at which the data were taken is 1 MHz

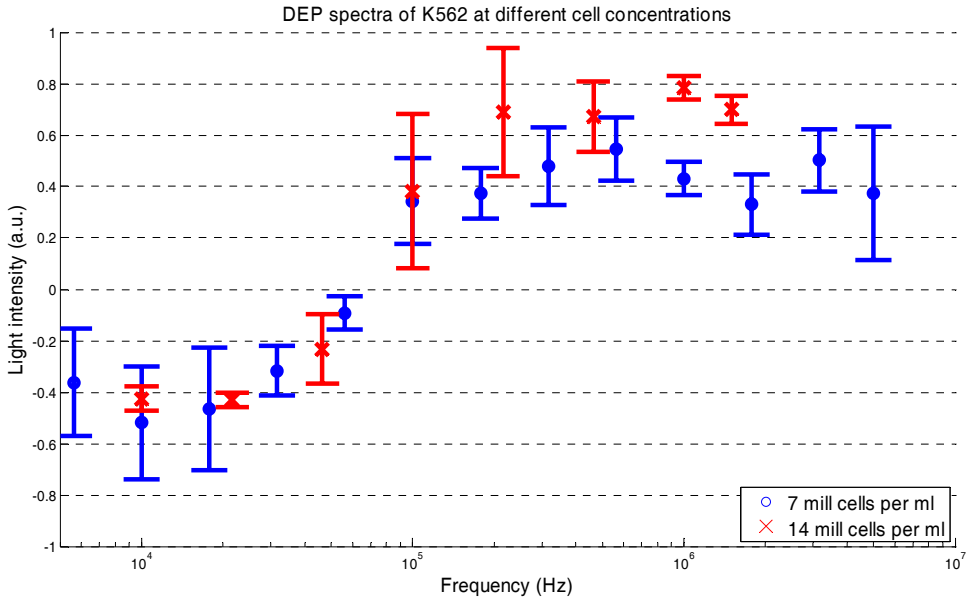

Figure 4-27 DEP spectra from two independent sets of experiments conducted with K562 cells at different cell concentrations, namely 0.7×10^7 (blue) and 1.4×10^7 (red) cells per ml

Figure 4-26 shows that the higher concentration sample still reached the same steady state level, albeit by taking a longer time. This proves that the system is capable of producing a consistent DEP spectra, despite the difference in cell concentrations (Figure 4-27). On the other hand, these sets of experiments also showed that a sample having a cell concentration in the range of 0.7 to 1×10^7 cells per ml will only take about 6 seconds to reach a steady state that is detectable by the system to be used in constructing the final DEP spectrum.

4.3.9 Effects of varying medium types

DEP-based experiments generally require the conductivity of the suspending media to be of specific value for the outcome to be of significant value. This is achieved by the titration of a certain ionic solution to the prepared isosmotic suspending medium to be used in the experiment, such that the desired conductivity value is achieved.

In this project, two types of solutions have been chosen to be used for the experiments, based on previous DEP-based studies conducted at the Centre for Biomedical Engineering at the University of Surrey, namely culture medium (i.e. RPMI 1640) and KCl. Of primary importance, however is whether the use of these solutions will be having a direct impact on the generation of the electric field, and thus the final DEP spectrum. Figure 4-31 shows the image captured by the system at the same

point in time of two independent experiments conducted using K562 cells, with KCl or RPMI as the conductive medium prepared at 10 mS/m. The experiments were conducted at 1 MHz, supplied with 8 V_{p-p} for 20 seconds, using parallel microelectrode with 200 μm diameter dots.

Figures 4-29 and 4-30 show the light intensity analysis and the produced DEP spectra for these experiments, respectively. Although there is a slight increase in the crossover frequency values when KCl was used as the conductive medium (Figure 4-30), the values are still within the range as reported in the literature (e.g. Altomare *et al.*, 2003; Labeed *et al.*, 2003). Therefore, both solutions may be satisfactorily used as the conductive medium of choice in conducting DEP-based experiments using the current system.

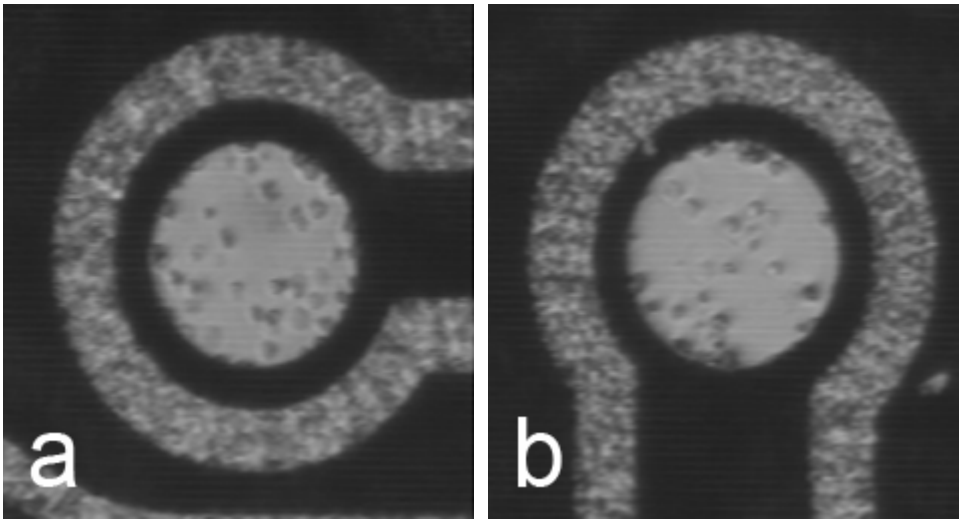

Figure 4-28 Original images from the experiments showing dots that experienced positive DEP using different conductive media of a) RPMI and b) KCl, respectively; taken at the same image frame (10 s) and signal frequency (1 MHz)

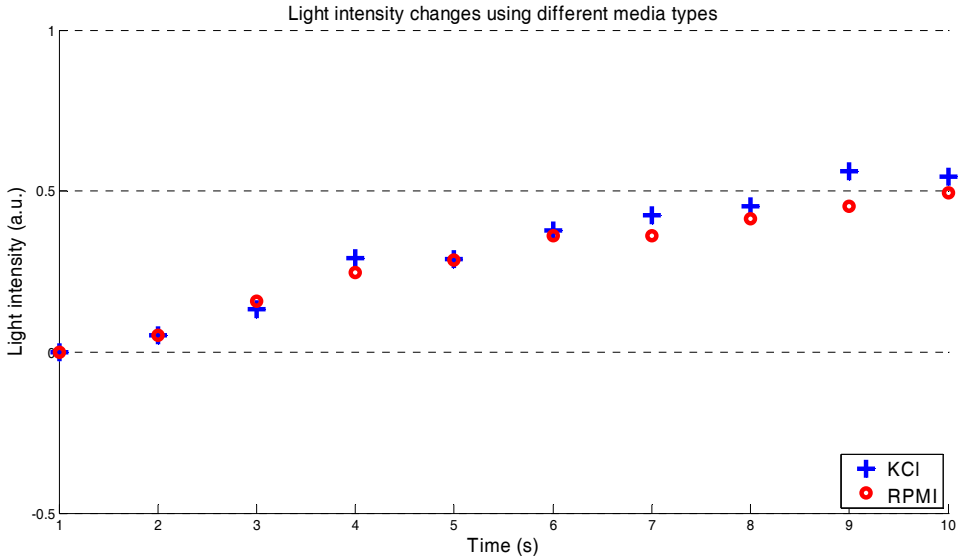

Figure 4-29 Light intensity changes for the dots depicted in Figure 4-28 over the course of an experiment. The frequency at which the data were taken is 300 kHz

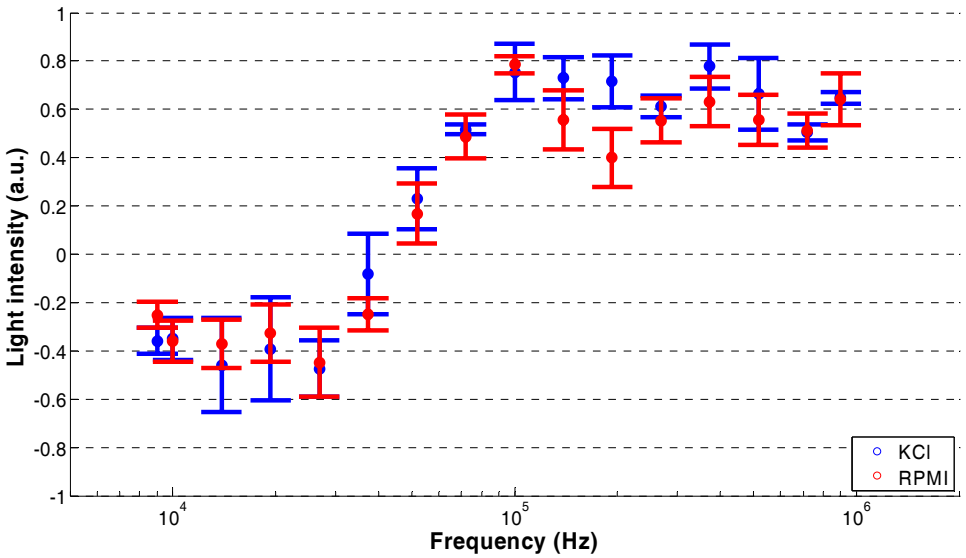

Figure 4-30 DEP spectra from two independent sets of experiments conducted with K562 cells using different conductive medium types, namely KCl (blue) and RPMI (red). The cell concentration is about 1×10^7 cells/ml, and the media had a conductivity of 10 mS/m

4.3.10 Effects of varying medium conductivities

Apart from the choice of solution used to increase the conductivity of the suspending media, the conductivity value of the medium is also an important consideration in determining the gradient of the

generated electric field and the accuracy of the experimental outcome. Although it is theoretically desirable to use the same medium used to culture the cells, so that any observed electrophysiological changes may be correlated with the changes occurring *in situ*, unfortunately DEP can only be practically occur and the cellular changes be observed at low conductivity values (Pohl 1958; Chen and Pohl, 1974). In addition, specific conductivity value directly affects the overall shape of the produced DEP spectra, and this change may be generally shown by the shift of the crossover frequency.

The crossover frequency of a given DEP spectrum over any range of conductivities may be modelled based on the DEP force function (Equation 2.1). As part of the validation process, a number of medium conductivities have been arbitrarily selected to be tested (Figure 4-31). Each of the error bars were constructed from the standard deviations of the crossover frequencies from at least three independent sets of experiments. The plot shows that the crossover frequency, and therefore the DEP spectra, will generally increase as the conductivity value of the medium increases. This can be mathematically deduced from the aforementioned DEP force equation (Equation 2.1) and its derivatives (Equations 2.2 and 2.3). For a given angular frequency, the resulting Clausius-Mossotti factor ($K(\omega)$) will be reduced if higher medium conductivity was used. In a typical DEP spectrum plot, a DEP spectrum will be expected to shift to the right as medium conductivity increased (Figure 4-32; data from three independent sets of experiments). Although DEP-based experiments may be conducted at any conductivity values, so long as the crossover frequency remained visible, in order for the subsequent electrophysiological analysis to be physically meaningful, the desired conductivity value for the suspending medium must be kept low. This is due to several undesirable phenomena that could be caused by high medium conductivity, including the killing of cells due to heating effects in the conductive medium (Ramos *et al.*, 1998), the disruption of DEP collection due to electrohydrodynamic effects, and the wearing off of electrodes due to high electrical field gradient differences (Hughes, 2002). Reported conductivity values that were used in previous studies ranged between 1 to 10 mS/m (e.g. Crane and Pohl, 1968; Gascoyne *et al.*, 1992; Labeed *et al.*, 2003), which should produce crossover frequencies in the range of 30-70 kHz. Figure 4-31 shows that the recorded crossover frequencies (red) for the selected medium conductivities generally conform to the expected values from the simulated model (black).

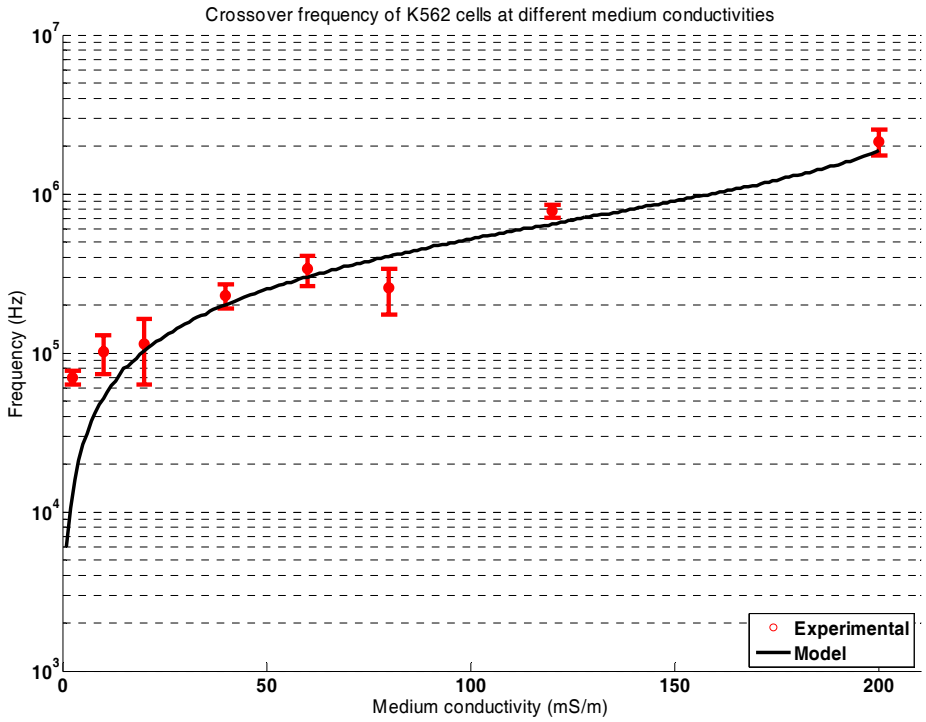

Figure 4-31 Crossover frequencies of K562 cells over a range of medium conductivity values

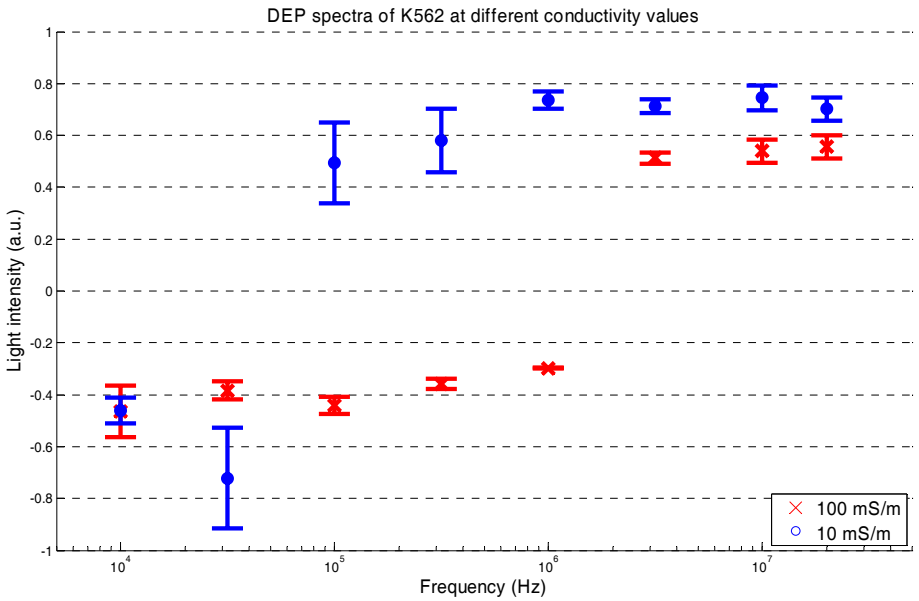

Figure 4-32 DEP spectra from two independent sets of experiments conducted using K562 cells at different media conductivity values. The cell concentration is about 1×10^7 cells/ml, the medium is RPMI, and the dot size is 300 µm

As part of the validation process, the project also set out to determine if the system is capable of handling cell samples suspended at very high medium conductivity. For this purpose, it was decided that the culture medium (RPMI 1640 with added penicillin, L-glutamine, FBS) to be used as the experimental medium. Figure 4-33 shows the DEP spectrum of K562 cells when conductive medium with very high conductivity value made up of pure culture medium (at 1.4 S/m) was used. An additional solution made to 0.5 S/m was also prepared and tested for comparison purposes. There are clearly no discernible DEP spectra of any significance, and subsequent electrophysiological analysis would therefore be meaningless. Nevertheless, this proves that the system is capable of handling DEP-related experiments at physiological conditions.

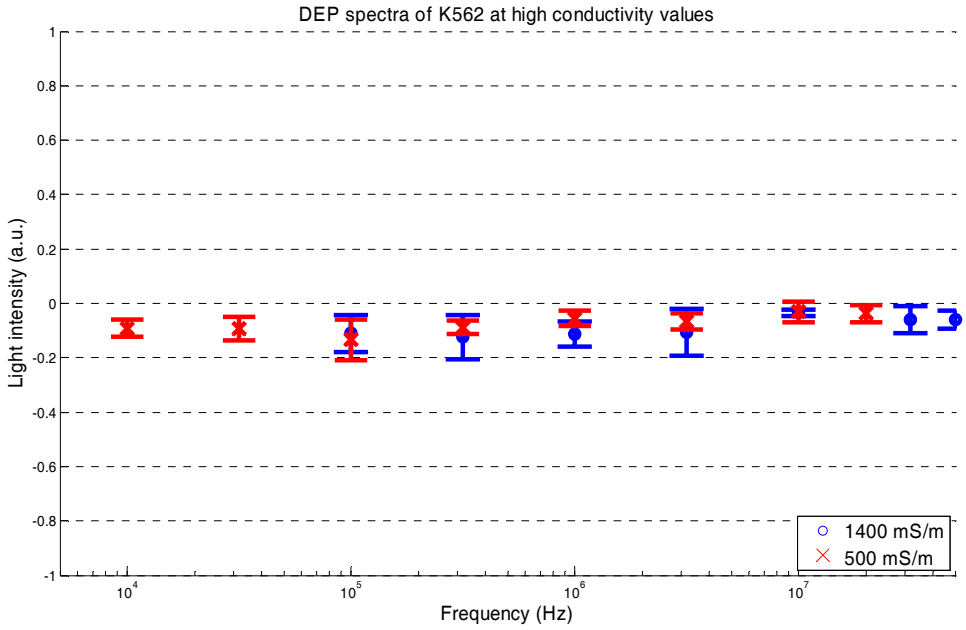

Figure 4-33 DEP spectrum of K562 cells at high conductivity values of 0.5 and 1.4 S/m.

4.4 Conclusion

The developed system seemed to be satisfactorily stable to be used in actual DEP experiments. The parameter values from the various feasibility and validation studies will be considered in designing the experimental protocol and optimising the settings of the subsequent near real-time DEP experiments.

5 Near real-time studies

5.1 Introduction

As alluded to in Chapter 4, the developed system should now be capable of conducting DEP experiments within a very short time (currently at a minimum of about 60 seconds for each experiment, including the required manual resuspension process), allowing changes to the DEP spectrum to be observed and recorded at the same temporal resolution. Since the changes to the DEP spectrum may be directly related to the changes occurring to the membrane and cytoplasmic electrophysiological properties, the system may act as a complimentary tool in predicting the causes of these changes, apart from other conventional biochemical measures. This is of particular importance since the knowledge of the mechanism of action of any reagents on the membrane surface, and the subsequent cytoplasmic effects, will determine its overall effect on the cell.

This section will document the outcome of selected experiments in observing the changes occurring to small samples of K562 cells (about 8 μl) when treated with 30 μM valinomycin.

5.2 Materials and methods

Human myelogeneous leukemic K562 cell lines used were sourced from LGC Standards (Teddington, UK), and were cryogenically frozen in 1 ml aliquots containing the culture medium in 5% DMSO at a concentration of 1×10^6 cells per ml. Each aliquot will be thawed and cultured before being used in experiments. All reagents and solutions are sourced from Sigma Aldrich Co., (St. Louis, USA), unless stated otherwise.

5.2.1 Cell culture

The K562 cells require a culture medium consisting of RPMI solution (GIBCO® RPMI Media 1640, Invitrogen Ltd., Paisley, UK), supplemented with 10% heat-inactivated fetal bovine serum (FBS) (PAA, Pasching, Austria), 1% L-glutamine, and 1% penicillin-streptomycin solution. The cells are cultured in the humidified incubator (CO-150, New Brunswick Scientific, Edison, NJ, USA) set at 37

degrees Celsius and 5.0% CO_2. The cell population in each culture flask were considered confluent when the concentration reached around 5×10^6 cells per ml. Doubling time was reached after 24 hours.

5.2.2 Cell sample preparation

Once confluence was reached, the cells may be used for DEP experiments; and needs to be transferred to a DEP conductive medium of a certain conductivity value. The protocol for preparing the conductive medium was presented in Table 4-2. The medium was made of 8.5% sucrose and 0.3% dextrose, and the final conductivity value was adjusted to the desired value by addition of 150 mM KCl solution. The conductivity was routinely set at 10 mS/m, to provide a crossover frequency at the centre of the 10 to 100 kHz frequency decade (based on previous findings by e.g. Altomare *et al.*, 2003; and Labeed *et al.*, 2003), and was verified with a Jenway 470 conductivity meter (Bibby Scientific Ltd., Staffordshire, UK).

Cell samples were washed twice by centrifugation set at 180 g for a period of five minutes, and resuspended in the DEP conductive medium at a cell concentration of 1×10^7 cells per ml. The protocol for estimating the cell count and viability (using Trypan blue exclusion test) was as presented in Sections 4.2.4 and 4.2.5.

5.2.3 Valinomycin preparation

A 30 µM valinomycin solution was prepared, by measuring 1.7 mg of valinomycin and made up to 50 mL with 5% DMSO and 95% deionised water. The solution is divided into 1 mL aliquots and stored in a freezer at -80 degrees Celsius until needed. The molar concentration was arbitrarily chosen to ensure the reduction in cell viability to about 10% within 60 minutes, based on previous findings by e.g. Dise and Goodman (1984); Inai *et al.* (1997). Valinomycin have also been used in previous studies conducted at the Centre for Biomedical Engineering at the University of Surrey, e.g. Hübner *et al.* (2007).

5.2.4 DEP experimental procedures

The experiments were conducted using the multiple waveform generator and microelectrode device developed earlier in Sections 3.3 and 3.4, respectively. The microelectrode dot size of choice was 200 µm, which was suited for cells having diameters of about 15-20 µm (based on findings from Chapter 4, data not shown). DEP experiments were conducted for an arbitrarily chosen number of frequencies (in multiples of eight, depending on the desired resolution of data points) between 1 kHz

and 1 MHz. A complete experimental protocol for conducting a DEP experiment, starting from cell preparation is presented in Table 5-1.

Table 5-1 Summary of DEP experimental procedures for K562 cells

Step 1	Take 20 ml each of cultured cells from two T75 flasks (commonly the day after cell passaging to maximise cell viability)
Step 2	Place cell suspension in 50 ml tubes, and centrifuge each at 180 g for five minutes. Remove supernatant when completed.
Step 3	Add 10 ml of conductive medium (10 mS/m) to each tube, and gently mix the suspension using a pipettor.
Step 4	Centrifuge each tube at 115 g for five minutes. Remove supernatant when completed.
Step 5	Repeat Steps 3 and 4.
Step 6	Depending on the cell concentration required, appropriate amount of conductive medium is added. Typically, add 1 ml of medium to achieve 1×10^7 cells per ml.
Step 7	Pipette the solutions into two Eppendorf tubes: one each for control and drug-treated samples.
Step 8	Conduct cell counting (Section 4.2.4) and cell viability estimations (Section 4.2.5) from the control tube.
Step 9	Set up the microelectrode device (preferably completed prior to conducting an experiment): fabricate the gasket (Section 3.4.2) and attach it to the electrode (Section 3.4.1).
Step 10	Set up the microscope: 4x magnification, and ensure uniform amount of light shining through the dots of the electrode.
Step 11	Set up the program: number of electrodes to be used (multiples of 4), start and end frequency, duration of signal and image capture, peak-to-peak voltage, dot diameter, and other information. The typical steps and values used for conducting an experiment are detailed below.
Step 12	Using a syringe, push a small amount of cell suspension through the inlet to completely cover the chamber created by the gasket. Avoid bubbles and/or over spilling of cell suspension out of the outlet.
Step 13	Start applying the signal.
Step 14	Re-suspend the cell suspension at the end of an experimental run, either by lightly tapping the electrode or pushing another small amount of cell suspension through the inlet.
Step 15	Repeat Steps 13 and 14 as necessary (routinely five) for control samples.
Step 16	Clean the microelectrode device thoroughly using 70% ethanol and deionised water.
Step 17	Add the required amount of drug to the sample tube. Start the stopwatch. Deliver a small sample of drug treated cells to the inlet of the device using a syringe.
Step 18	Start applying the signal. Record the stopwatch time at the moment that the signal is switched on from the waveform generator.
Step 19	Repeat Steps 13 and 14 as necessary (routinely for 60 minutes).

The control for the delivery of the input signals and the subsequent production and analysis of the DEP spectra was achieved using a MATLAB program (an improvement from a previously developed program used in Fatoyinbo *et al.* (2008) that was described in Section 3.3.3). The electrophysiological properties of the cell membrane were extracted from the DEP spectra by the fitting of the plot to the single-shell model data (Benguigui and Lin, 1982; Broche *et al.*, 2005). The required cell radius for the calculation was measured from at least 150 cells using ImageJ (outlined in Section 4.3.2). The whole experiment was repeated 15 times, conducted on different days. The results presented in the following section were from a single experiment day, but were representative of the rest of the experimental results.

5.3 Results and discussion

The main objective of these near real-time studies was to assess how the system could measure the electrophysiological changes occurring on the membrane when a population of K562 cells were treated with valinomycin, a known apoptotic agent (Inai *et al.*, 1997; Dallaporta *et al.*, 1999). As such, this section will cover the three important components to the analysis, namely the cell size (required in order determine the correct radius values needed for the modelling data), the DEP spectra (from which the model data will be fitted and the electrophysiological properties will be extracted), and the electrophysiological properties (namely the membrane conductance and capacitance values).

5.3.1 Cell size

Images of K562 cells, seen under the microscope at 10× magnification, were captured at a certain period of time to reproduce the different times at which the experimental data were recorded during actual DEP experiments. Depending on the cell concentrations, the number of captured images varied, but a total of at least 150 cells were captured and later analysed using ImageJ (Section 4.3.2). For the purpose of calibration, some of the captured images contained the borders of the smallest hemocytometer grids, which are known to be 0.05 mm in width.

Figure 5-1 shows the average size of the K562 cells and the corresponding variance at intervals of around 5 minutes. Although there is not much change in the average cell radii before and after valinomycin delivery, there is a considerable increase in the standard deviations of the cell radii following the introduction of valinomycin. This could indicate that there are significant number of cell subpopulations having smaller and larger radii, most probably caused by the different stages of apoptosis that the cells were experiencing.

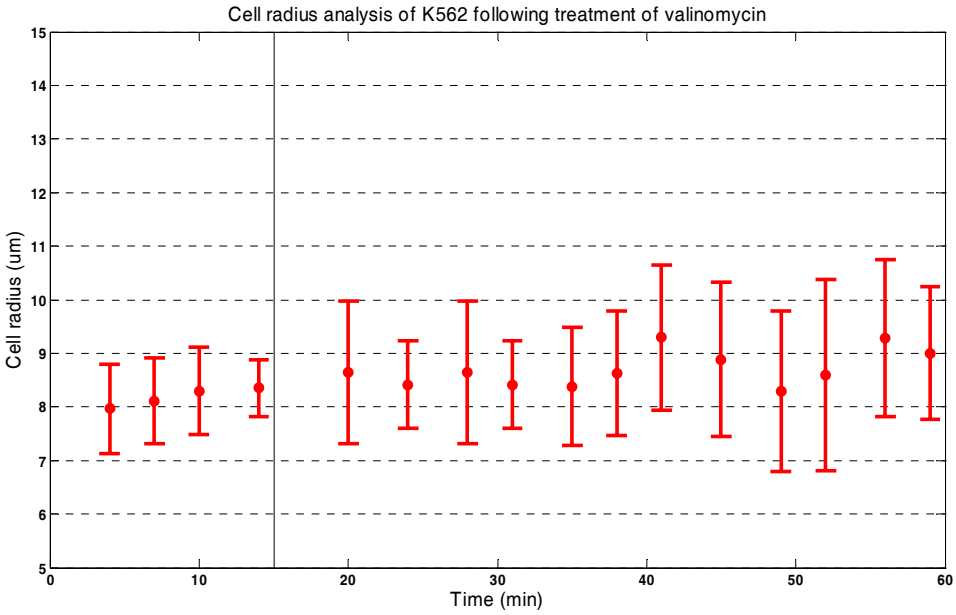

Figure 5-1 Cell size analysis of K562 cells when treated with 30µM valinomycin over a period of about 70 minutes (cell concentration 1×10^7 cells per ml, conductive medium 10 mS/m made from KCl). Error bars indicate standard deviation of radii measurements

5.3.2 DEP spectra

The DEP spectra were constructed based on the image analysis algorithm developed in Section 3.5.8. Several near real-time studies of K562 being treated with valinomycin were conducted, and a typical DEP spectra from these studies is shown in Figure 5-2. The rather large variance of the values was attributed to the difference in the light intensity values as the course of the experiment progressed, and the DEP spectra shifted. Figure 5-3 shows a representation of the DEP spectra in 3D (with only time and frequency axes shown). It can be seen that the crossover frequency has shifted slightly to the right (the starting point of the reddish areas, indicating positive DEP, has shifted to the right), as the incubation period progresses. Figure 5-4, which plots the change in crossover frequency values, illustrates this finding well. The vertical line indicates the delivery of valinomycin into the cell sample at the 15th minute. Figures 5-2 to 5-4 show the representative outcomes from all of the experiments involving the treatment of K562 cells with valinomycin.

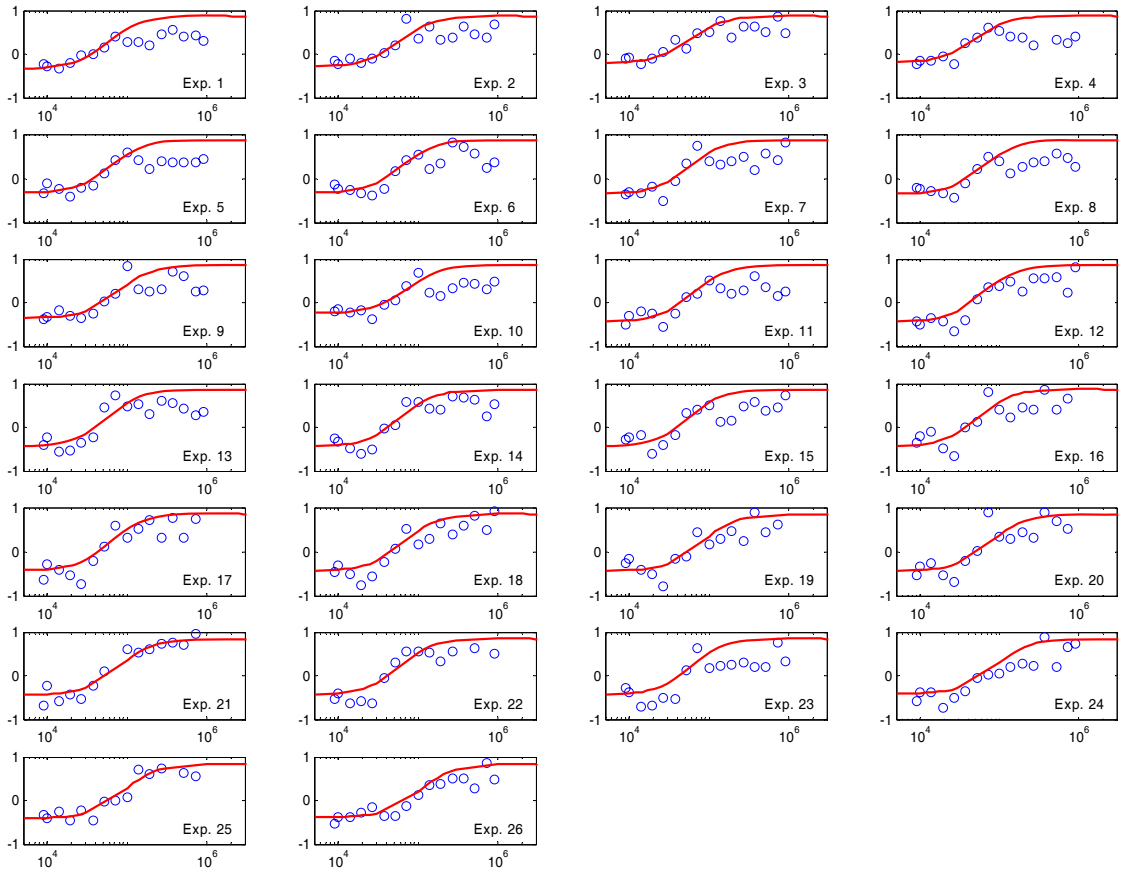

Figure 5-2 DEP spectra for experiments using K562 cells (1×10^7 cells per ml, 10mS/m KCl conductive medium) taken for a period of 75 minutes. Valinomycin (30 µM) was added at the 15th minute (between Experiment no. 4 and 5). The blue dots indicate the raw data points from the light intensity analysis, while the red line show the model fit data for the corresponding curve. The horizontal axes are for frequency (in Hz), and the vertical axes are for light intensity (in arbitrary units)

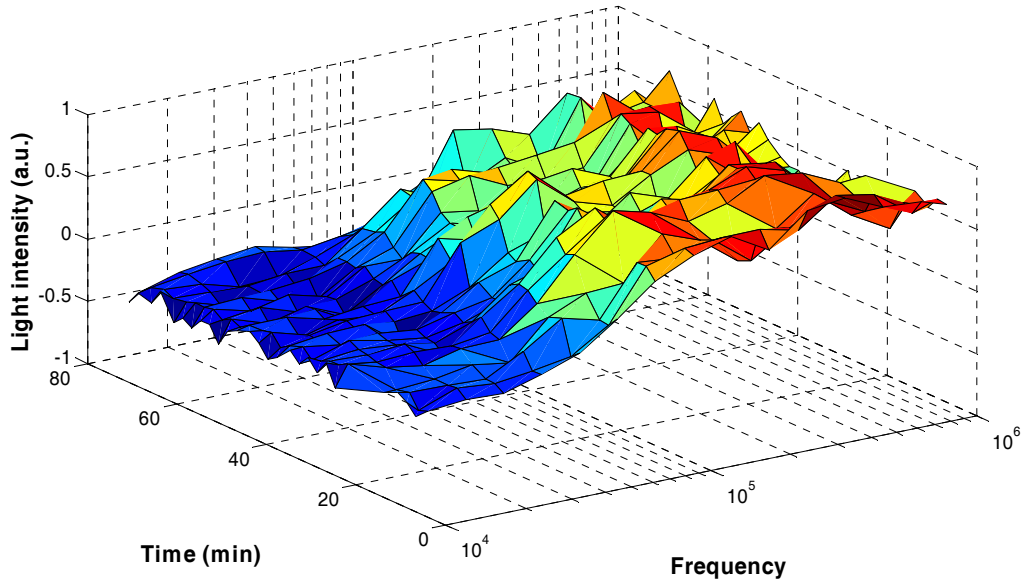

(a)

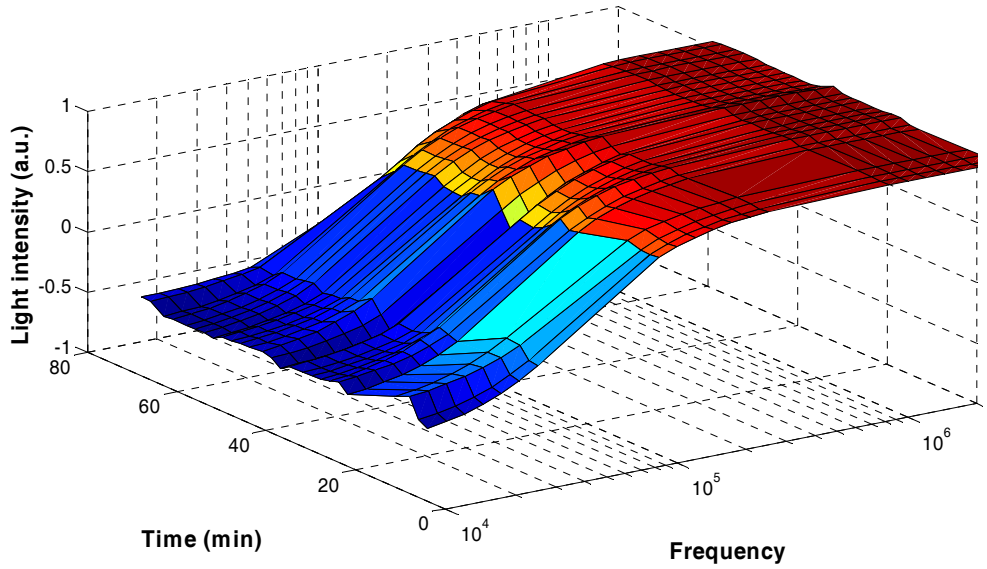

(b)

Figure 5-3 Three-dimensional representation of DEP spectra from Figure 5-2, constructed from a) raw data, and b) model fit data, showing a slight shift of the crossover frequency to the right. Reddish areas indicate positive DEP; bluish areas indicate negative DEP. Valinomycin is added at the 15th minute

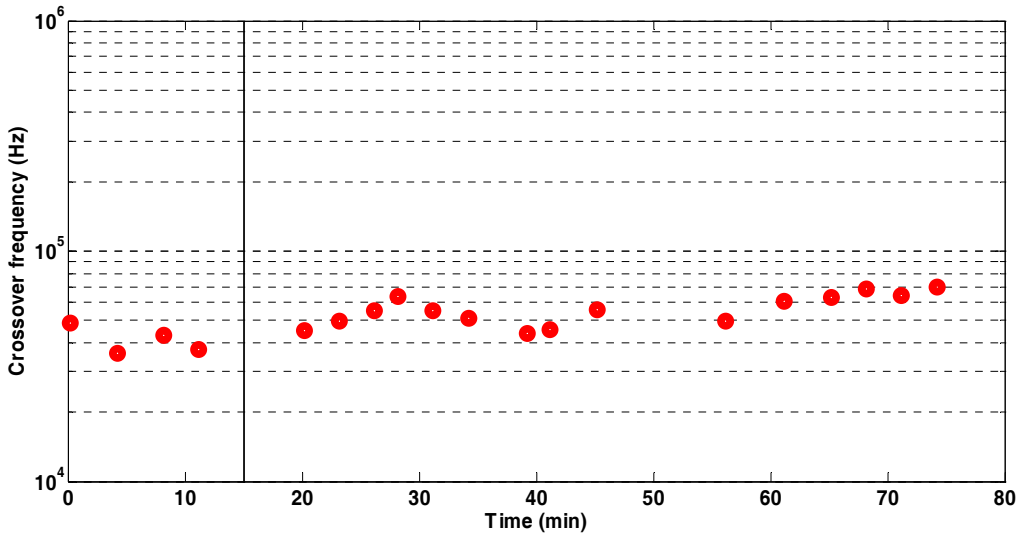

Figure 5-4 Crossover frequency changes of K562 cells over the course of an experiment. Straight line at the 15th minute indicate the time valinomycin is added

5.3.3 Electrophysiological properties

In order to observe the electrophysiological changes over the course of an experiment, a single-shell DEP model data will be fitted onto each of the individual DEP spectra, and the values will be plotted over the same time points used in Figure 5-4. The change in membrane capacitance and conductance is shown in Figure 5-5(a) and 5-5(b), respectively. A declining trend is observed for both parameters, indicating the effect of valinomycin on the membrane surface, confirming it as an ionophore as was first described by Finkelstein and Cass in 1968. This observation may compliment the currently known apoptotic mechanisms of action for valinomycin on a living mammalian cell, namely its effect on the lipid deposition on the membrane surface (Thompson and Krull (1982); Dise and Goodman (1984)), and the subsequent cell apoptosis caused by its action on the mitochondrial membrane (Inai *et al.*, 1997; Dallaporta *et al.*, 1999).

Lipid deposition may directly alter the physiological make-up of the cellular surface; and since DEP effects are primarily a function of the cell surface dipole moments in a given AC electric field, any change towards the distribution of ions (in this case caused by both the uncontrolled transport of K^+ ions and deposition of inert lipid molecules) over the cell surface will inherently affect the DEP values. Presumably this effect is compounded as the number of cells undergoing apoptosis increases over the course of the experiment, reducing both the membrane capacitance and conductance values even further, as more and more cells shrivel and die. This may be inferred from the increasing deviation of cell sizes (Figure 5-1) following the addition of valinomycin.

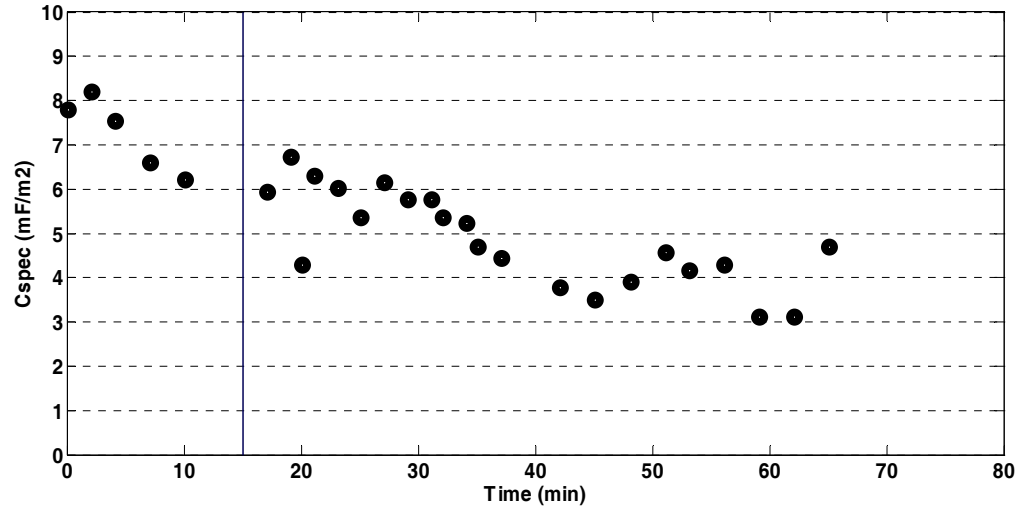

(a)

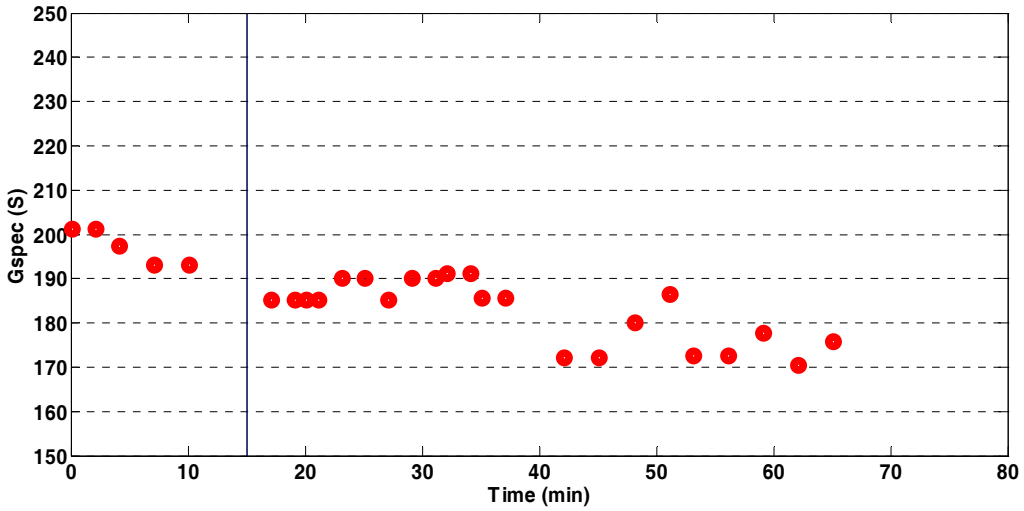

(b)

Figure 5-5 Observed electrophysiological properties for the DEP spectra from Figure 5-2 over the course of the experiment, a) membrane capacitance, b) membrane conductance

There are however, two related limitations that may be attributed to the developed system, namely the temporal resolution limit and the lack of precision in determining the said resolution. The limit on the temporal resolution is due to the currently required manual resuspension process following the completion of each DEP experiments. As mentioned in Chapter 2, the currently used CMIS analysis algorithm requires a uniform cell distribution over each of the dots at the start of each DEP experiment, since it depends on the change of light intensity values when compared with the first captured image. The cellular distribution uniformity within each of the dots may be achieved by

manually pushing a small amount of cell suspension through the inlet of the microelectrode device prior to commencing the subsequent experiment, which is currently limited to a period between 70 to 100 seconds. This period is the time it took to physically push the syringe through the inlet and running the main control program. This is an obvious disadvantage if the expected cellular electrophysiological changes were to occur during these resuspension processes, and thus missed when the DEP spectra were analysed.

These manual interventions were also the reason why the temporal resolution may not be ascertained exactly for the system. Although this may not be regarded as a disadvantage by itself, it nevertheless made it difficult to benchmark the developed system against previously developed systems. Hölzel (1998) for example, developed an automated DEP-based system to track the electrical changes occurring on single yeast cells with an exact temporal resolution of 3 minutes, which allowed the system to produce DEP spectra at consistent time intervals. Although the system developed in the project may achieve better temporal resolution, it relied heavily on the dexterity and expertise of the user in handling the microelectrode device and the control program.

It must be noted however, that the said system developed by Hölzel is specifically designed using the electrorotation technique to track the movement of a single cell, which obviously did not involve any resuspension processes. The algorithm used only relied on the difference of axial positions of the cell within the captured images. Although this allowed a precise DEP profile to be constructed for that particular cell based on its electrorotation spectra, it does not represent an overall picture of the DEP effects that would be expected if the said cells were present in a homogenous solution of a certain concentration. In addition, the said system would only be useful when used within a lab on a chip application that was equipped with a highly focused separation and trapping components. The current developed system however, is capable to characterise a given small quantity cellular suspension (about 8 μl) based on its DEP spectra alone, without the need of additional components. Although the resulting plot may not be desirably smooth and recorded at consistent time intervals (Figures 5-3 and 5-5), it is nonetheless capable of recording trending changes over the course of an experiment, close enough for the recorded changes to be considered near real-time. The recorded changes in the yeast cells treated with nystatin in Hölzel's study at 7th and 75th minutes should be similarly detectable using the currently developed system.

5.4 Conclusion

The developed system is capable of recording near real-time electrophysiological changes occurring on the cellular membrane at a temporal resolution of about 2 minutes. The reduction in membrane conductance and capacitance may help to affirm the currently held knowledge of apoptotic effects of valinomycin on mammalian cells, particularly involving the morphological changes occurring on the membrane surface and the changes in cytoplasmic conductivity.

6 Conclusion and future work

6.1 Conclusion

DEP-based AC electrokinetic cell manipulation techniques, introduced as early as the 1960s, have been shown to be capable in detecting, sorting and collecting desired particles in a given sample of homogeneous and heterogeneous mixtures. The technique is particularly advantageous, since it works for non-polar particles (including cells), and does not require any chemical-based tagging or markers, thus making it useful in drug interaction analyses. Nevertheless, the technique has been constantly plagued by its inability to conduct large batch cell assays, and as a consequence the technique is almost always left in the realm of academic research centres. A number of recent studies however, have tried to address the said problem through a variety of techniques, and the Centre for Biomedical Engineering at the University of Surrey has chosen to explore the possibility of increasing the throughput of DEP experiments by means of conducting parallel experiments using small samples of cell populations (Hoettges *et al.*, 2008; Fatoyinbo *et al.*, 2008).

This project was set out with the objective of developing a system that is capable of conducting parallel DEP experiments, based on the planar microelectrode geometry used by Fatoyinbo *et al.* (2008). The general strategy of achieving this goal is by first developing a programmable, multiple output waveform generator; and subsequently to test the said generator with the parallel version of the dot microelectrode. The geometry of the microelectrode dot array is such that each of the dot will receive a signal at an individually programmed frequency, and thus allows a set of DEP experiment to be conducted in a very short period of time. The outcomes from several feasibility studies (Chapter 3) indicated that the system is capable of fulfilling the initial objective of conducting parallel DEP experiments using a planar microelectrode.

Following a series of validation and optimisation (Chapter 4), and near real-time (Chapter 5) studies, it was found that the developed system is capable of producing consistent DEP spectra that may be used in the subsequent model fitting to determine the electrophysiological properties of the chosen cell population. Because of the speed at which a single experiment can be conducted (currently at around 2 minutes, which includes the required manual resuspension process in between experiment sets), a temporal domain may be included in the DEP spectra and allowed any real-time changes

occurring over the experimental period to be observed. These changes have been observed for K562 cell populations when treated with valinomycin, and the outcome of the electrophysiological properties from these experiments may suggest the effect that valinomycin has on the cellular membrane.

In conclusion, the developed system is capable of conducting parallel DEP experiments that allows electrophysiological changes to the final DEP spectrum to be recorded with a temporal resolution of about 2 minutes. The resolution of the observed changes is currently limited to the speed at which a satisfactory DEP spectrum may be produced, which included the manual resuspension process.

6.2 Future work

The following is a list of desirable improvements to be incorporated into the current developed system, covering both the software and hardware aspects.

6.2.1 Automatic cell redispersion

At the moment, the microelectrode device set up was an improvement from a previous design; and as such there is a need for manual resuspension of cells prior to conducting each set of experiments. The resuspension process is necessary, since a uniform distribution of cells is needed for the first image in order to produce a smooth histogram, from which the histogram of the final image will be compared with. Non-uniformly distributed cells within a dot will directly affect the outcome of the analysis, since it will skew the light intensity calculation, and the subsequent relative polarisability measurement. An automatic cell redispersion following the completion of a single experiment, particularly one that only requires a period of time in the region of seconds, is highly desirable, since it allows multiple experiments to be conducted in one go without any manual intervention. More importantly, it allows the recording of DEP spectra at smaller temporal resolution. The current temporal resolution limit of about 2 minutes, as mentioned in Chapter 5, is primarily due to the time taken to manually push a small amount of cell suspension through the inlet using a syringe to resuspend the cells following a single experiment. This is currently the preferred resuspension method, as it will not significantly affect the light intensity settings of the microscope, as opposed to manually shaking the microelectrode device.

Although there is a possibility of automatic redispersion of cells following an experiment as seen previously in the single dot set up (Fatoyinbo *et al.*, 2008) following the turning off of the input signal, this has not been adequately looked at for the current system, particularly with regards to its

efficacy in conducting real-time experiments using cancer cells that are generally larger. In addition, the said redispersion was only satisfactorily observed for yeast cells experiencing positive DEP following 60 seconds of the signal being turned off. The time lag may not be appropriate for a system that was intended for observing so-called real-time effects. Furthermore, redispersion for yeast cells experiencing negative DEP only reached a third of its original light intensity values after 60 seconds.

A possibility of addressing the problem is by having an additional microfluidics system to aid in the resuspension of cells following a set of experiment. The outlet (or inlet) of the chamber may be connected to an additional system that automatically pushes the cell suspension around the chamber. This additional module may be directly programmed in the microprocessor, or could be added to the GUI of the main control program.

6.2.2 Improvement of graphical user interface

The initial inspiration behind the development of the main control program for the system is to allow a user to control the waveform generator to be used on its own or in conjunction with a DEP experiment, and to control the various parameters of the digital camera used to capture the images, and to analyse the captured images and produce the desired DEP spectrum, along with the fitting of the model. Although developing a versatile program like this is not necessarily a problem by itself, but this inadvertently demands the creation of a crowded and disorganised graphical user interface (GUI) design (Figure 6-1). In addition, the step-by-step guide in conducting a single experiment (attached in Appendix A) is quite tedious, and may prove to be confusing for a novice user. A major drawback to the functioning and GUI of the program is the inability to display and analyse saved data. Once the image data have been loaded into the program and processed, the user may choose to analyse the produced DEP spectrum and fit a model dataset to extract the electrophysiological properties. But since the program cannot reload the saved data, a user is required to re-process all images in order to view or conduct any analyses in the future.

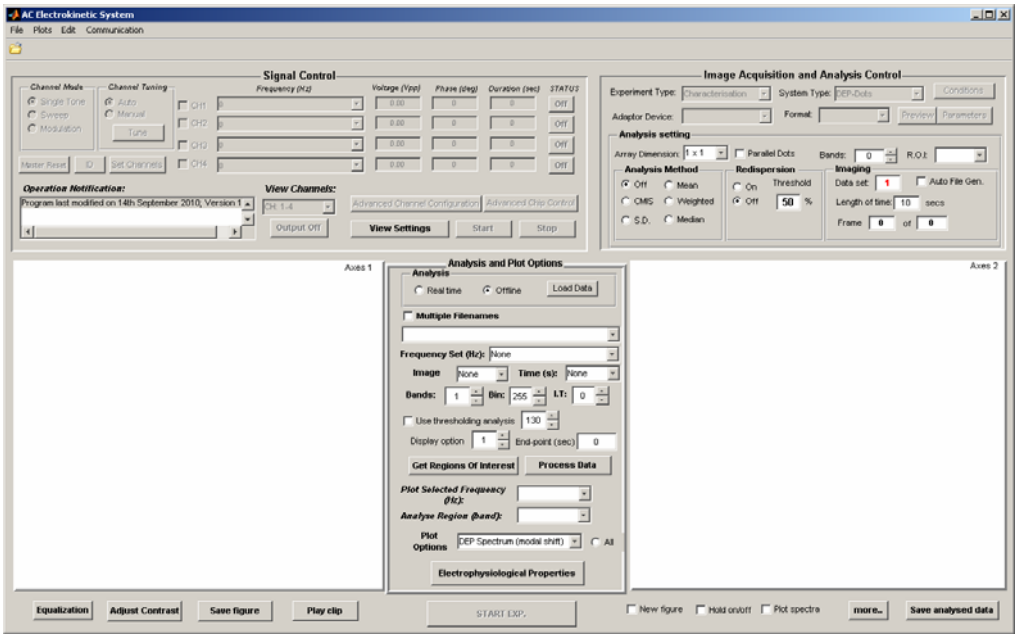

Figure 6-1 The graphical user interface of the program (as of 8 December 2010)

Therefore it is proposed that a simpler GUI be designed for the program, preferably using a tabbed interface to accommodate the various functions of the program; and the ability to reload all previously saved data be incorporated into future versions of the program.

6.2.3 Improvement of microelectrode geometry

The microelectrode used in the current system was designed in a 4×4 array, in such a way that all of the dots will fit into view when viewed using a typical light microscope at low magnifications (i.e. 4 to 10× magnifications). Nevertheless, since each of the dots will receive input signals of different frequencies, the generated electric field over each of these dots will also have different gradients. This in turn will produce DEP forces of differing strengths in moving the cells within each of the dots, and localised collections of cells on certain areas of the microelectrode may occur and overflowed into adjacent dots (Figure 6-2). Depending on the overall cell concentration, this phenomenon may affect the analysis of the actual DEP effect that was expected to be seen on that particular dot. Therefore it is proposed that a new and better microelectrode geometry be designed for the future versions of the system to overcome the said problem.

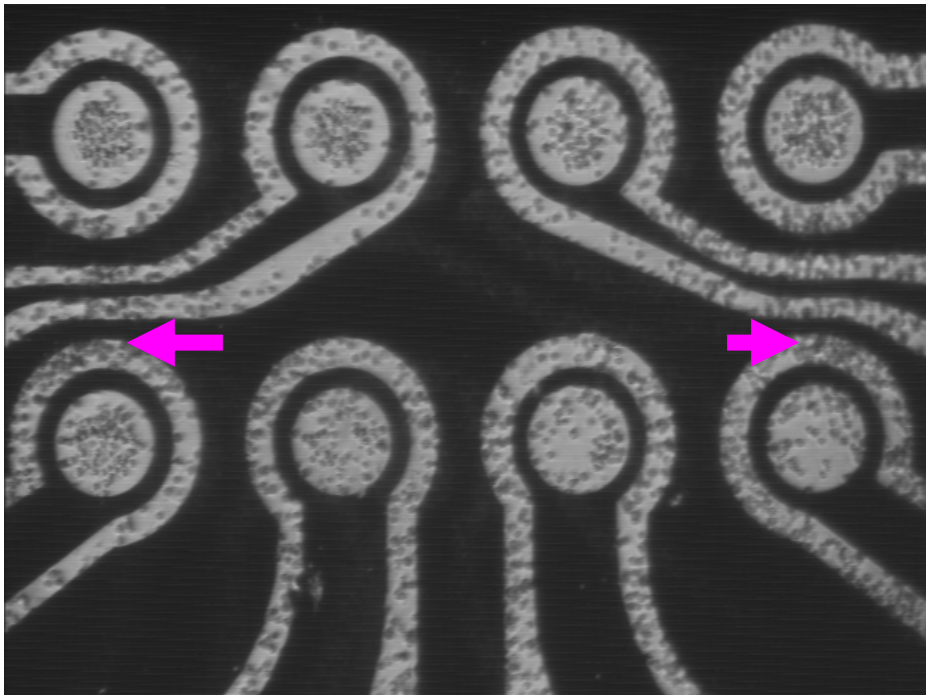

Figure 6-2 An example of experiment where the cells overflowed into adjacent dots (arrows), causing an incorrect DEP analysis

6.2.4 Improvement of image processing during analysis

As mentioned in Section 3.5.8, the use of image processing may produce a better image for the analysis algorithm to work with; and this has been proven to a certain extent by the proposed bitmapped image analysis algorithm. The DEP spectra produced by this algorithm have proven to be more consistent and may be completed automatically, without the need of additional tweaking of the parameter variables. The advantage of this algorithm however, lies in its capability of handling imperfect lighting conditions. Experiments having slightly different background light intensity can still be processed with acceptable outcomes.

Nevertheless, this proposed algorithm only employed a single image processing technique, namely the thresholding, which have only been tested using a limited number of experimental conditions (i.e. cell types and sizes, microscope magnification, and microelectrode dot diameter and design geometry). Other types of image processing, notably those with movement registration capabilities and segmentation of subpopulations within a heterogeneous population, would be a desirable addition to the analysis algorithm.

Bibliography

Abdalah, R.; Wei, L.; Francis, K. & Yu, S. (2006), 'Valinomycin-induced apoptosis in Chinese hamster ovary cells', *Neuroscience letters* **405**(1-2), 68–73.

Alberts, B. (1998), *Essential cell biology: an introduction to the molecular biology of the cell*, Garland.

Alberts, K.; Johnson, A.; Lewis, J.; Raff, M. (2008), *Molecular Biology of the Cell* (5th ed.), Garland Science.

Alexopoulos, C. J., M. C. W. B. M. (1996), *Introductory mycology*, Wiley.

Altman, S.; Randers, L. & Rao, G. (1993), 'Comparison of trypan blue dye exclusion and fluorometric assays for mammalian cell viability determinations', *Biotechnology progress* **9**(6), 671–674.

Altomare, L.; Borgatti, M.; Medoro, G.; Manaresi, N.; Tartagni, M.; Guerrieri, R. & Gambari, R. (2003), 'Levitation and movement of human tumor cells using a printed circuit board device based on software-controlled dielectrophoresis', *Biotechnology and bioengineering* **82**(4), 474–479.

An, J.; Lee, J.; Lee, S.; Park, J. & Kim, B. (2009), 'Separation of malignant human breast cancer epithelial cells from healthy epithelial cells using an advanced dielectrophoresis-activated cell sorter (DACS)', *Analytical and Bioanalytical Chemistry* **394**(3), 801–809.

Andersson, L.; Nilsson, K. & Gahmberg, C. (1979), 'K562–a human erythroleukemic cell line', *Int J Cancer* **23**(2), 143–147.

Archer, G.; Betts, W. & Haigh, T. (1993), 'Rapid differentiation of untreated, autoclaved and ozone-treated Cryptosporidium parvum oocysts using dielectrophoresis.', *Microbios* **73**(296), 165.

Archer, S.; Morgan, H. & Rixon, F. (1999), 'Electrorotation studies of baby hamster kidney fibroblasts infected with herpes simplex virus type 1', *Biophysical journal* **76**(5), 2833–2842.

Arnold, W. & Zimmermann, U. (1982), 'Rotating-field-induced rotation and measurement of the membrane capacitance of single mesophyll cells of Avena sativa [oat]', *Zeitschrift fuer Naturforschung. Section C. Biosciences (Germany, FR)*.

Asami, K.; Hanai, T. & Koizumi, N. (1976), 'Dielectric properties of yeast cells', *Journal of Membrane Biology* **28**(1), 169–180.

Auerswald, J. & Knapp, H. (2003), 'Quantitative assessment of dielectrophoresis as a micro fluidic retention and separation technique for beads and human blood erythrocytes', *Microelectronic Engineering* **67**, 879–886.

Becker, F.; Wang, X.; Huang, Y.; Pethig, R.; Vykoukal, J. & Gascoyne, P. (1995), 'Separation of human breast cancer cells from blood by differential dielectric affinity', *Proceedings of the National Academy of Sciences* **92**(3), 860.

Becker, F.; Wang, X.; Huang, Y.; Pethig, R.; Vykoukal, J. & Gascoyne, P. (1994), 'The removal of human leukaemia cells from blood using interdigitated microelectrodes', *Journal of Physics D: Applied Physics* **27**, 2659–2662.

Becker, H. & Gertner, C. (2000), 'Polymer microfabrication methods for microfluidic analytical applications', *Electrophoresis* **21**(1), 12–26.

Benguigui, L. & Lin, I. (1982), 'More about the dielectrophoretic force', *Journal of Applied Physics* **53**, 1141.

Broche, L.; Bhadal, N.; Lewis, M.; Porter, S.; Hughes, M. & Labeed, F. (2007), 'Early detection of oral cancer-Is dielectrophoresis the answer?', *Oral oncology* **43**(2), 199–203.

Broche, L.; Labeed, F. & Hughes, M. (2005), 'Extraction of dielectric properties of multiple populations', *Physics in Medicine and Biology* **50**, 2267–2274.

Burt, J.; Al-Ameen, T. & Pethig, R. (1989), 'An optical dielectrophoresis spectrometer for low-frequency measurements on colloidal suspensions', *Journal of Physics E: Scientific Instruments* **22**, 952–957.

Burt, J.; Pethig, R.; Gascoyne, P. & Becker, F. (1990), 'Dielectrophoretic characterisation of Friend murine erythroleukaemic cells as a measure of induced differentiation.', *Biochimica et biophysica acta* **1034**(1), 93.

Cen, E.; Dalton, C.; Li, Y.; Adamia, S.; Pilarski, L. & Kaler, K. (2004), 'A combined dielectrophoresis, traveling wave dielectrophoresis and electrorotation microchip for the manipulation and characterization of human malignant cells', *Journal of microbiological methods* **58**(3), 387–401.

Chan, K.; Gascoyne, P.; Becker, F. & Pethig, R. (1997), 'Electrorotation of liposomes: verification of dielectric multi-shell model for cells', *Biochimica et Biophysica Acta (BBA)-Lipids and Lipid Metabolism* **1349**(2), 182–196.

Chen, C. & Pohl, H. (1974), 'BIOLOGICAL DIELECTROPHORESIS: THE BEHAVIOR OF LONE CELLS IN A NONUNIFORM ELECTRIC FIELD*', *Annals of the New York Academy of Sciences* **238**(Electrically Mediated Growth Mechanisms in Living Systems), 176–185.

Cheng, J.; Sheldon, E.; Wu, L.; Heller, M. & O'Connell, J. (1998), 'Isolation of cultured cervical carcinoma cells mixed with peripheral blood cells on a bioelectronic chip', *Anal. Chem* **70**(11), 2321–2326.

Chin, S.; Hughes, M.; Coley, H. & Labeed, F. (2006), 'Rapid assessment of early biophysical changes in K562 cells during apoptosis determined using dielectrophoresis', *International Journal of Nanomedicine* **1**(3), 333.

Christopoulos, A. (2002), 'Allosteric binding sites on cell-surface receptors: novel targets for drug discovery', *Nature Reviews Drug Discovery* **1**(3), 198–210.

Coley, H.; Labeed, F.; Thomas, H. & Hughes, M. (2007), 'Biophysical characterization of MDR breast cancer cell lines reveals the cytoplasm is critical in determining drug sensitivity', *BBA-General Subjects* **1770**(4), 601–608.

Crane, J. & Pohl, H. (1972), 'Theoretical models of cellular dielectrophoresis.', *Journal of theoretical biology* **37**(1), 15.

Crane, J. & Pohl, H. (1968), 'A study of living and dead yeast cells using dielectrophoresis', *Journal of the Electrochemical Society* **115**, 584.

Cristofanilli, M.; De Gasperis, G.; Zhang, L.; Hung, M.; Gascoyne, P. & Hortobagyi, G. (2002), 'Automated electrorotation to reveal dielectric variations related to HER-2/neu overexpression in MCF-7 sublines', *Clinical Cancer Research* **8**(2), 615.

Cristofanilli, M.; Krishnamurthy, S.; Das, C.; Reuben, J.; Spohn, W.; Noshari, J.; Becker, F. & Gascoyne, P. (2008), 'Dielectric cell separation of fine needle aspirates from tumor xenografts', *Journal of High Resolution Chromatography* **31**(21), 3732–3739.

Cummings, E. & Singh, A. (2003), 'Dielectrophoresis in microchips containing arrays of insulating posts: theoretical and experimental results', *Anal. Chem* **75**(18), 4724–4731.

Dallaporta, B.; Marchetti, P.; de Pablo, M.; Maisse, C.; Duc, H.; Metivier, D.; Zamzami, N.; Geuskens, M. & Kroemer, G. (1999), 'Plasma membrane potential in thymocyte apoptosis', *The Journal of Immunology* **162**(11), 6534.

Dalton, C.; Goater, A.; Drysdale, J. & Pethig, R. (2001), 'Parasite viability by electrorotation', *Colloids and Surfaces A: Physicochemical and Engineering Aspects* **195**(1-3), 263–268.

Devices, A. (2004), 'AD9850 CMOS, 125 MHz Complete DDS Synthesizer', Analog Devices, One Technology Way, P.O. Box 9106, Norwood, MA 02062-9106, U.S.A..

Devices, A. (2003), 'AD8007/8008 Ultralow Distortion High Speed Amplifiers', Analog Devices, One Technology Way, P.O. Box 9106, Norwood, MA 02062-9106, U.S.A..

Devices, A. (2003), 'AD9833 Low Power 20 mW 2.3 V to 5.5 V Programmable Waveform Generator', Analog Devices, One Technology Way, P.O. Box 9106, Norwood, MA 02062-9106, U.S.A..

Dise, C. & Goodman, D. (1985), 'The relationship between valinomycin-induced alterations in membrane phospholipid fatty acid turnover, membrane potential, and cell volume in the human erythrocyte.', *Journal of Biological Chemistry* **260**(5), 2869.

Doll, R. & Peto, R. (1981), 'The causes of cancer: quantitative estimates of avoidable risks of cancer in the United States today.', *Journal of the National Cancer Institute* **66**(6), 1191.

Duffy, D.; McDonald, J.; Schueller, O. & Whitesides, G. (1998), 'Rapid prototyping of microfluidic systems in poly (dimethylsiloxane)', *Anal. Chem* **70**(23), 4974–4984.

Duncan, L.; Shelmerdine, H.; Hughes, M.; Coley, H.; Hübner, Y. & Labeed, F. (2008), 'Dielectrophoretic analysis of changes in cytoplasmic ion levels', *Physics in Medicine and Biology* **53**, N1–N7.

Eisenberg, R. & Mathias, R. (1980), 'Structural analysis of electrical properties of cells and tissues', *Crit Rev Bioeng* **4**(3), 203–232.

Ermolina, I. & Morgan, H. (2005), 'The electrokinetic properties of latex particles: comparison of electrophoresis and dielectrophoresis', *Journal of Colloid and Interface Science* **285**(1), 419–428.

Faris, M.; Kokot, N.; Latinis, K.; Kasibhatla, S.; Green, D.; Koretzky, G. & Nel, A. (1998), 'The c-Jun N-terminal kinase cascade plays a role in stress-induced apoptosis in Jurkat cells by up-regulating Fas ligand expression', *The Journal of Immunology* **160**(1), 134.

Fatoyinbo, H.; Hoettges, K. & Hughes, M. (2008), 'Rapid-on-chip determination of dielectric properties of biological cells using imaging techniques in a dielectrophoresis dot microsystem', *Electrophoresis* **29**(1), 3–10.

Fatoyinbo, H.; Hughes, M.; Martin, S.; Pashby, P. & Labeed, F. (2007), 'Dielectrophoretic separation of Bacillus subtilis spores from environmental diesel particles', *Journal of Environmental Monitoring* **9**(1), 87–90.

Fatoyinbo, H.; Kamchis, D.; Whattingham, R.; Ogin, S. & Hughes, M. (2005), 'A high-throughput 3-D composite dielectrophoretic separator', *Biomedical Engineering, IEEE Transactions on* **52**(7), 1347–1349.

Fiedler, S.; Shirley, S.; Schnelle, T. & Fuhr, G. (1998), 'Dielectrophoretic sorting of particles and cells in a microsystem', *Anal. Chem* **70**(9), 1909–1915.

Finkelstein, A. & Cass, A. (1968), 'Permeability and electrical properties of thin lipid membranes', *The Journal of general physiology* **52**(1), 145.

Fuhr, G.; Arnold, W.; Hagedorn, R.; Müller, T.; Benecke, W.; Wagner, B. & Zimmermann, U. (1992), 'Levitation, holding, and rotation of cells within traps made by high-frequency fields.', *Biochimica et biophysica acta* **1108**(2), 215.

Fuhr, G.; Muller, T.; Baukloh, V. & Lucas, K. (1998), 'High-frequency electric field trapping of individual human spermatozoa', *Human Reproduction* **13**(1), 136.

Furlong, I.; Lopez, M.; Ascaso, R.; Lopez, R. & Collins, M. (1998), 'Induction of apoptosis by valinomycin: mitochondrial permeability transition causes intracellular acidification.', *Cell death and differentiation* **5**(3), 214.

Gascoyne, P. & Becker, F. (1990), 'Alterations in electrophoretic mobility, diaphorase activity, and terminal differentiation induced in murine erythroleukemia lines by differentiating agents', *Journal of Cellular Physiology* **142**(2), 309–315.

Gascoyne, P.; Huang, Y.; Pethig, R.; Vykoukal, J. & Becker, F. (1992), 'Dielectrophoretic separation of mammalian cells studied by computerized image analysis', *Measurement Science and Technology* **3**, 439–445.

Gascoyne, P.; Mahidol, C.; Ruchirawat, M.; Satayavivad, J.; Watcharasit, P. & Becker, F. (2002), 'Microsample preparation by dielectrophoresis: isolation of malaria', *Lab on a Chip* **2**(2), 70–75.

Gascoyne, P.; Noshari, J.; Anderson, T. & Becker, F. (2009), 'Isolation of rare cells from cell mixtures by dielectrophoresis', *Electrophoresis* **30**(8), 1388–1398.

Gascoyne, P.; Noshari, J.; Becker, F. & Pethig, R. (1994), 'Use of dielectrophoretic collection spectra for characterizing differences between normal and cancerous cells, Industry Applications', *IEEE Transactions on Industry Applications* **30**, 829–834.

Gascoyne, P.; Pethig, R.; Burt, J. & Becker, F. (1993), 'Membrane changes accompanying the induced differentiation of Friend murine erythroleukemia cells studied by dielectrophoresis', *Biochimica et biophysica acta. Biomembranes* **1149**(1), 119–126.

Gascoyne, P.; Pethig, R.; Satayavivad, J.; Becker, F. & Ruchirawat, M. (1997), 'Dielectrophoretic detection of changes in erythrocyte membranes following malarial infection', *Biochimica et Biophysica Acta (BBA)-Biomembranes* **1323**(2), 240–252.

Gascoyne, P. & Vykoukal, J. (2004), 'Dielectrophoresis-based sample handling in general-purpose programmable diagnostic instruments', *Proceedings of the IEEE. Institute of Electrical and Electronics Engineers* **92**(1), 22.

Gascoyne, P.; Vykoukal, J.; Schwartz, J.; Anderson, T.; Vykoukal, D.; Current, K.; McConaghy, C.; Becker, F. & Andrews, C. (2004), 'Dielectrophoresis-based programmable fluidic processors', *Lab on a Chip* **4**(4), 299–309.

Gascoyne, P.; Wang, X.; Huang, Y. & Becker, F. (1997), 'Dielectrophoretic separation of cancer cells from blood', *IEEE Transactions on Industry Applications* **33**(3), 670–678.

Gasperis, G.; Wang, X.; Yang, J.; Becker, F. & Gascoyne, P. (1998), 'Automated electrorotation: dielectric characterization of living cells by real-time motion estimation', *Measurement Science and Technology* **9**, 518.

Gasperis, G.; Yang, J.; Becker, F.; Gascoyne, P. & Wang, X. (1999), 'Microfluidic cell separation by 2-dimensional dielectrophoresis', *Biomedical Microdevices* **2**(1), 41–49.

Gimsa, J.; Marszalek, P.; Loewe, U. & Tsong, T. (1991), 'Dielectrophoresis and electrorotation of neurospora slime and murine myeloma cells', *Biophysical journal* **60**(4), 749–760.

Gimsa, J.; Schnelle, T.; Zechel, G. & Glaser, R. (1994), 'Dielectric spectroscopy of human erythrocytes: investigations under the influence of nystatin', *Biophysical journal* **66**(4), 1244–1253.

Goater, A.; Pethig, R.; Paton, C. & Smith, H. (1999), 'Single Cryptosporidium oocyst Isolation and Capture using a Travelling-Wave Dielectrophoresis Device."Electrostatics 1999: proceedings of the 10th international conference, Cambridge, 28-31 March 1999', Taylor Francis, 69.

Gonzalez, R. & Woods, R. (1992), 'Digital image processing', *MA: Addison-Wesley*.

Gonzalez, R.; Woods, R. & Eddins, S. (2004), *Digital image processing using MATLAB*, Prentice Hall Upper Saddle River, NJ.

Gottlieb, R.; Nordberg, J.; Skowronski, E. & Babior, B. (1996), 'Apoptosis induced in Jurkat cells by several agents is preceded by intracellular acidification', *Proceedings of the National Academy of Sciences* **93**(2), 654.

Gravesen, P.; Branebjerg, J. & Jensen, O. (1993), 'Microfluidics-a review', *Journal of Micromechanics and Microengineering* **3**, 168–182.

Green, N. & Morgan, H. (1999), 'Dielectrophoresis of submicrometer latex spheres. 1. Experimental results', *J. Phys. Chem. B* **103**(1), 41–50.

Green, N. & Morgan, H. (1997), 'Dielectrophoretic separation of nano-particles', *Journal of Physics D: Applied Physics* **30**, L41–L44.

Green, N.; Ramos, A. & Morgan, H. (2000), 'AC electrokinetics: a survey of sub-micrometre particle dynamics', *Journal of Physics D: Applied Physics* **33**, 632–641.

Heida, T.; Rutten, W. & Marani, E. (2002), 'Dielectrophoretic trapping of neuronal cells', *Journal of Physics D: Applied Physics* **35**, 1592–1602.

Heida, T.; Rutten, W. & Marani, E. (2001), 'Dielectrophoretic trapping of dissociated fetal cortical rat neurons', *IEEE transactions on biomedical engineering* **48**(8), 921–930.

Hoettges, K.; Hubner, Y.; Broche, L.; Ogin, S.; Kass, G. & Hughes, M. (2008), 'Dielectrophoresis-Activated Multiwell Plate for Label-Free High-Throughput Drug Assessment', *Anal. Chem* **80**(6), 2063–2068.

Huang, C.; Chen, A.; Guo, M. & Yu, J. (2007), 'Membrane dielectric responses of bufalin-induced apoptosis in HL-60 cells detected by an electrorotation chip', *Biotechnology letters* **29**(9), 1307–1313.

Huang, C.; Chen, A.; Wang, L.; Guo, M. & Yu, J. (2007), 'Electrokinetic measurements of dielectric properties of membrane for apoptotic HL-60 cells on chip-based device', *Biomedical Microdevices* **9**(3), 335–343.

Huang, Y.; Holzel, R.; Pethig, R. & Wang, X. (1992), 'Differences in the AC electrodynamics of viable and non-viable yeast cells determined through combined dielectrophoresis and electrorotation studies', *Physics in medicine and biology* **37**, 1499–1517.

Huang, Y. & Pethig, R. (1991), 'Electrode design for negative dielectrophoresis', *Measurement Science and Technology* **2**, 1142–1146.

Huang, Y.; Wang, X.; Becker, F. & Gascoyne, P. (1996), 'Membrane changes associated with the temperature-sensitive P85gag-mos-dependent transformation of rat kidney cells as determined by dielectrophoresis and electrorotation', *Biochimica et Biophysica Acta (BBA)-Biomembranes* **1282**(1), 76–84.

Hughes, M. (2002), *Nanoelectromechanics in engineering and biology*, CRC.

Hughes, M. (2002), 'Strategies for dielectrophoretic separation in laboratory-on-a-chip systems.', *Electrophoresis* **23**(16), 2569.

Hughes, M. (2000), 'AC electrokinetics: applications for nanotechnology', *Nanotechnology* **11**, 124–132.

Hughes, M. (1998), 'Computer-aided analysis of conditions for optimizing practical electrorotation', *Physics in medicine and biology* **43**, 3639.

Hughes, M. & Morgan, H. (1998), 'Dielectrophoretic trapping of single sub-micrometre scale bioparticles', *Journal of Physics D: Applied Physics* **31**, 2205.

Hughes, M.; Morgan, H.; Rixon, F.; Burt, J. & Pethig, R. (1998), 'Manipulation of herpes simplex virus type 1 by dielectrophoresis', *BBA-General Subjects* **1425**(1), 119–126.

Hughes, M.; Wang, X. & others (1994), 'Computer-aided analyses of electric fields used in electrorotation studies', *Journal of Physics D: Applied Physics* **27**, 1564.

Hölzel, R. (1998), 'Nystatin-induced changes in yeast monitored by time-resolved automated single cell electrorotation', *Biochimica et Biophysica Acta (BBA)-General Subjects* **1425**(2), 311–318.

Hölzel, R. & Lamprecht, I. (1992), 'Dielectric properties of yeast cells as determined by electrorotation', *Biochimica et Biophysica Acta (BBA)-Biomembranes* **1104**(1), 195–200.

Hübner, Y.; Hoettges, K. & Hughes, M. (2003), 'Water quality test based on dielectrophoretic measurements of fresh water algae Selenastrum capricornutum', *Journal of Environmental Monitoring* **5**(6), 861–864.

Hübner, Y.; Hoettges, K.; Kass, G.; Ogin, S. & Hughes, M. (2005), 'Parallel measurements of drug actions on erythrocytes by dielectrophoresis, using a three-dimensional electrode design"IEE Proceedings-Nanobiotechnology', 150.

Hübner, Y.; Mulhall, H.; Hoettges, K.; Kass, G.; Ogin, S. & Hughes, M. (2007), 'Dielectrophoresis: A new in vitro approach to measure drug-induced cytotoxicity', *Toxicology* **240**(3), 183–184.

Inai, Y.; Yabuki, M.; Kanno, T.; Akiyama, J.; Yasuda, T. & Utsumi, K. (1997), 'Valinomycin induces apoptosis of ascites hepatoma cells (AH-130) in relation to mitochondrial membrane potential', *Cell structure and function* **22**(5), 555–563.

Inoue, T.; Pethig, R.; Al-Ameen, T.; Burt, J. & Price, J. (1988), 'Dielectrophoretic behaviour of Micrococcus lysodeikticus and its protoplast', *Journal of Electrostatics* **21**(2-3), 215–223.

Irimajiri, A.; Hanai, T. & Inouye, A. (1979), 'A dielectric theory of 'multistratified shell' model with its application to a lymphoma cell', *Journal of Theoretical Biology* **78**(2), 251–269.

Jaber, F.; Labeed, F. & Hughes, M. (2009), 'Action potential recording from dielectrophoretically positioned neurons inside micro-wells of a planar microelectrode array', *Journal of neuroscience methods* **182**(2), 225–235.

Jemal, A.; Clegg, L.; Ward, E.; Ries, L.; Wu, X.; Jamison, P.; Wingo, P.; Howe, H.; Anderson, R. & Edwards, B. (2004), 'Annual report to the nation on the status of cancer, 1975-2001, with a special feature regarding survival.', *cancer* **101**(1), 3.

Jemal, A.; Siegel, R.; Ward, E.; Hao, Y.; Xu, J.; Murray, T. & Thun, M. (2008), 'Cancer statistics, 2008', *CA: a cancer journal for clinicians* **58**(2), 71.

Johari, J.; Hübner, Y.; Hull, J.; Dale, J. & Hughes, M. (2003), 'Dielectrophoretic assay of bacterial resistance to antibiotics', *Physics in Medicine and Biology* **48**, N193–N198.

Jones, K. & Senft, J. (1985), 'An improved method to determine cell viability by simultaneous staining with fluorescein diacetate-propidium iodide', *Journal of histochemistry and cytochemistry* **33**(1), 77.

Jones, T. (2009), 'Basic theory of dielectrophoresis and electrorotation', *Engineering in Medicine and Biology Magazine, IEEE* **22**(6), 33–42.

Jones, T. (1995), *Electromechanics of particles*, Cambridge Univ Pr.

Jones, T. (1979), 'Dielectrophoretic force calculation', *Journal of Electrostatics* **6**(1), 69–82.

Jones, T. & Kallio, G. (1979), 'Dielectrophoretic levitation of spheres and shells', *Journal of Electrostatics* **6**(3), 207–224.

Jones, T. & Kraybill, J. (1986), 'Active feedback-controlled dielectrophoretic levitation', *Journal of Applied Physics* **60**, 1247.

Kadri, N.; Hoettges, K. & Hughes, M. (2009), 'Development of a generic multiple frequency signal generator for BioMEMS"World Congress on Medical Physics and Biomedical Engineering, September 7-12, 2009, Munich, Germany', Springer, 120–123.

Kadri, N.; Hoettges, K. & Hughes, M. (2008), 'Microelectrode Fabrication Using Indium Tin Oxide (ITO) For Microfluidic Devices Employing Dielectrophoresis"4th Kuala Lumpur International Conference on Biomedical Engineering 2008', Springer, 719–722.

Kaler, K. & Jones, T. (1990), 'Dielectrophoretic spectra of single cells determined by feedback-controlled levitation', *Biophysical journal* **57**(2), 173–182.

Kaler, K. & Pohl, H. (1983), 'Dynamic dielectrophoretic levitation of living individual cells', *Industry Applications, IEEE Transactions on* **IA-19**(6), 1089–1093.

Kaler, K.; Xie, J.; Jones, T. & Paul, R. (1992), 'Dual-frequency dielectrophoretic levitation of Canola protoplasts', *Biophysical journal* **63**(1), 58–69.

Kang, Y. & Li, D. (2009), 'Electrokinetic motion of particles and cells in microchannels', *Microfluidics and Nanofluidics* **6**(4), 431–460.

Kang, Y.; Li, D.; Kalams, S. & Eid, J. (2008), 'DC-Dielectrophoretic separation of biological cells by size', *Biomedical Microdevices* **10**(2), 243–249.

Kerr, J.; Wyllie, A. & Currie, A. (1972), 'Apoptosis: a basic biological phenomenon with wide-ranging implications in tissue kinetics', *Br J Cancer* **26**(4): 239–257

Kim, Y.; Lee, J.; An, J.; Lee, S. & Kim, B. (2009), 'Effect of a blind spot in a dielectrophoretic field on the separation of human breast cancer cells (MCF 7)', *Journal of Mechanical Science and Technology* **23**(11), 3132–3139.

Klein, E.; Ben-Bassat, H.; Neumann, H.; Ralph, P.; Zeuthen, J.; Polliack, A. & Vanky, F. (1976), 'Properties of the K562 cell line, derived from a patient with chronic myeloid leukemia', *Int J Cancer* **18**(4), 421–431.

Konopka, J.; Watanabe, S. & Witte, O. (1984), 'An alteration of the human c-abl protein in K562 leukemia cells unmasks associated tyrosine kinase activity', *Cell* **37**(3), 1035–1042.

Krishna, G.; ANWAR ALI, A.; RAM MOHAN, D. & Ahmad, A. (1989), 'Dielectrophoretic study of human erythrocytes', *Journal of biomedical engineering* **11**(5), 375–380.

Labeed, F.; Coley, H. & Hughes, M. (2006), 'Differences in the biophysical properties of membrane and cytoplasm of apoptotic cells revealed using dielectrophoresis', *BBA-General Subjects* **1760**(6), 922–929.

Labeed, F.; Coley, H.; Thomas, H. & Hughes, M. (2003), 'Assessment of multidrug resistance reversal using dielectrophoresis and flow cytometry', *Biophysical journal* **85**(3), 2028–2034.

Lapizco-Encinas, B.; Simmons, B.; Cummings, E. & Fintschenko, Y. (2004), 'Insulator-based dielectrophoresis for the selective concentration and separation of live bacteria in water', *Electrophoresis* **25**(10-11), 1695–1704.

Lehmann, J.; McKee, D.; Watson, M.; Willson, T.; Moore, J. & Kliewer, S. (1998), 'The human orphan nuclear receptor PXR is activated by compounds that regulate CYP3A4 gene expression and cause drug interactions.', *Journal of Clinical Investigation* **102**(5), 1016.

Lin, C.; Li, S.; Sheu, B. & Chang, H. (2009), 'Rapid characterization and separation of isogenic mutants of H. pylori by dielectrophoresis', *Biomedical Engineering-Applications Basis Communications* **21**(6), 433-436.

Lozzio, C. & Lozzio, B. (1975), 'Human chronic myelogenous leukemia cell-line with positive Philadelphia chromosome', *Blood* **45**(3), 321.

Mahaworasilpa, T.; Coster, H. & George, E. (1994), 'Forces on biological cells due to applied alternating (AC) electric fields. I. Dielectrophoresis', *Biochimica et Biophysica Acta (BBA)-Biomembranes* **1193**(1), 118–126.

Markx, G.; Dyda, P. & Pethig, R. (1996), 'Dielectrophoretic separation of bacteria using a conductivity gradient', *Journal of biotechnology* **51**(2), 175–180.

Markx, G.; Huang, Y.; Zhou, X. & Pethig, R. (1994), 'Dielectrophoretic characterization and separation of micro-organisms', *Microbiology* **140**(3), 585–591.

Markx, G. & Pethig, R. (1995), 'Dielectrophoretic separation of cells: continuous separation', *Biotechnology and bioengineering* **45**(4), 337–343.

Markx, G.; Talary, M. & Pethig, R. (1994), 'Separation of viable and non-viable yeast using dielectrophoresis', *Journal of biotechnology* **32**(1), 29–37.

Marszalek, P.; Zielinsky, J.; Fikus, M. & Tsong, T. (1991), 'Determination of electric parameters of cell membranes by a dielectrophoresis method', *Biophysical journal* **59**(5), 982–987.

Mason, B. & Townsley, P. (1971), 'Dielectrophoretic separation of living cells.', *Canadian journal of microbiology* **17**(7), 879.

McDonald, J.; Duffy, D.; Anderson, J.; Chiu, D.; Wu, H.; Schueller, O. & Whitesides, G. (2000), 'Fabrication of microfluidic systems in poly (dimethylsiloxane)', *Electrophoresis* **21**(1), 27–40.

McDonald, J. & Whitesides, G. (2002), 'Poly (dimethylsiloxane) as a material for fabricating microfluidic devices', *Acc. Chem. Res* **35**(7), 491–499.

Microchip (1999), 'PIC16F87X 28/40-pin 8-bit CMOS FLASH Microcontrollers', Microchip Technology Inc., Microchip Technology Inc., 2355 West Chandler Blvd., Chandler, Arizona, USA 85224-6199.

Mischel, M.; Rouge, F.; Lamprecht, I.; Aubert, C. & Prota, G. (1983), 'Dielectrophoresis of malignant human melanocytes', *Archives of Dermatological Research* **275**(3), 141–143.

Morgan, H.; Green, N.; Hughes, M.; Monaghan, W. & Tan, T. (1997), 'Large-area travelling-wave dielectrophoresis particle separator', *Journal of Micromechanics and Microengineering* **7**, 65–70.

Morgan, H.; Hughes, M. & Green, N. (1999), 'Separation of submicron bioparticles by dielectrophoresis', *Biophysical Journal* **77**(1), 516–525.

Müller, T.; Gerardino, A.; Schnelle, T.; Shirley, S.; Bordoni, F.; De Gasperis, G.; Leoni, R. & Fuhr, G. (1996), 'Trapping of micrometre and sub-micrometre particles by high-frequency electric fields and hydrodynamic forces', *Journal of Physics D: Applied Physics* **29**, 340–349.

Müller, T.; Gradl, G.; Howitz, S.; Shirley, S.; Schnelle, T. & Fuhr, G. (1999), 'A 3-D microelectrode system for handling and caging single cells and particles', *Biosensors and Bioelectronics* **14**(3), 247–256.

Otsu, N. (1979), 'A threshold selection method from gray-level histograms', *IEEE Transactions on Systems, Man and Cybernetics* **9**(1), 62–66.

Park, K.; Suk, H.; Akind, D. & Bashir, R. (2009), 'Dielectrophoresis-based cell manipulation using electrodes on a reusable printed circuit board', *DEP* **9**, 2224–2229.

Patel, P.; Bhat, A. & Markx, G. (2008), 'A comparative study of cell death using electrical capacitance measurements and dielectrophoresis', *Enzyme and Microbial Technology* **43**(7), 523–530.

Patel, P. & Markx, G. (2008), 'Dielectric measurement of cell death', *Enzyme and Microbial Technology* **43**(7), 463–470.

Pethig, R. (2010), 'Dielectrophoresis: Status of the theory, technology, and applications', *Biomicrofluidics* **4**, 022811.

Pethig, R. (1996), 'Dielectrophoresis: using inhomogeneous AC electrical fields to separate and manipulate cells', *Critical reviews in biotechnology* **16**(4), 331–348.

Pethig, R. (1985), 'Dielectric and Electrical Properties of Biological Materials', *Electromagnetic Biology and Medicine* **4**(2), 7–9.

Pethig, R.; Lee, R. & Talary, M. (2004), 'Cell physiometry tools based on dielectrophoresis', *Journal of the Association for Laboratory Automation* **9**(5), 324–330.

Pethig, R. & Markx, G. (1997), 'Applications of dielectrophoresis in biotechnology', *Trends in biotechnology* **15**(10), 426–432.

Pohl, H. (1978), *Dielectrophoresis: the behavior of neutral matter in nonuniform electric fields*, Cambridge University Press Cambridge.

Pohl, H. (1958), 'Some effects of nonuniform fields on dielectrics', *Journal of Applied Physics* **29**, 1182.

Pohl, H. (1951), 'The motion and precipitation of suspensoids in divergent electric fields', *Journal of Applied Physics* **22**, 869.

Pohl, H. & Crane, J. (1971), 'Dielectrophoresis of cells', *Biophysical Journal* **11**(9), 711–727.

Pohl, H. & Hawk, I. (1966), 'Separation of Living and Dead Cells by Dielectrophoresis.', *Science (New York, NY)* **152**(3722), 647.

Pohl, H.; Kaler, K. & Pollock, K. (1981), 'The continuous positive and negative dielectrophoresis of microorganisms', *Journal of Biological Physics* **9**(2), 67–86.

Pohl, H. & Pethig, R. (1977), 'Dielectric measurements using non-uniform electric field (dielectrophoretic) effects', *Journal of Physics E: Scientific Instruments* **10**, 190–193.

Pohl, H.; Pollock, K. & Crane, J. (1978), 'Dielectrophoretic force: A comparison of theory and experiment', *Journal of Biological Physics* **6**(3), 133–160.

Polevaya, Y.; Ermolina, I.; Schlesinger, M.; Ginzburg, B. & Feldman, Y. (1999), 'Time domain dielectric spectroscopy study of human cells II. Normal and malignant white blood cells', *BBA-Biomembranes* **1419**(2), 257–271.

Pommer, M.; Zhang, Y.; Keerthi, N.; Chen, D.; Thomson, J.; Meinhart, C. & Soh, H. (2008), 'Dielectrophoretic separation of platelets from diluted whole blood in microfluidic channels', *Electrophoresis* **29**(6), 1213–1218.

Prasad, B.; Du, S.; Badawy, W. & Kaler, K. (2005), 'A real-time multiple-cell tracking platform for dielectrophoresis (DEP)-based cellular analysis', *Measurement Science and Technology* **16**, 909–924.

Prasad, S.; Zhang, X.; Yang, M.; Ni, Y.; Parpura, V.; Ozkan, C. & Ozkan, M. (2004), 'Separation of individual neurons using dielectrophoretic alternative current fields', *Journal of neuroscience methods* **135**(1-2), 79–88.

Price, J.; Burt, J. & Pethig, R. (1988), 'Applications of a new optical technique for measuring the dielectrophoretic behaviour of micro-organisms', *Biochimica et Biophysica Acta (BBA)-General Subjects* **964**(2), 221–230.

Qian, L.; Scott, M.; Kaler, K. & Paul, R. (2002), 'Integrated planar concentric ring dielectrophoretic (DEP) levitator', *Journal of Electrostatics* **55**(1), 65–79.

Qiu, Z.; Markarian, N.; Khusid, B. & Acrivos, A. (2002), 'Positive dielectrophoresis and heterogeneous aggregation in high-gradient ac electric fields', *Journal of Applied Physics* **92**, 2829.

Ramos, A.; Morgan, H.; Green, N. & Castellanos, A. (1998), 'AC electrokinetics: a review of forces in microelectrode structures', *Journal of Physics D: Applied Physics* **31**, 2338–2353.

Ratanachoo, K.; Gascoyne, P. & Ruchirawat, M. (2002), 'Detection of cellular responses to toxicants by dielectrophoresis', *BBA-Biomembranes* **1564**(2), 449–458.

Rhoads, J.; Pohl, H. & Buckner, R. (1976), 'The dielectrophoresis of blood platelets as affected by hemophilic traits', *Journal of Biological Physics* **4**(3), 93–108.

Russ, J. (1995), 'The handbook of image processing', CRC Press, New York.

Samali, A.; Cai, J.; Zhivotovsky, B.; Jones, D. & Orrenius, S. (1999), 'Presence of a pre-apoptotic complex of pro-caspase-3, Hsp60 and Hsp10 in the mitochondrial fraction of jurkat cells.', *The EMBO journal* **18**(8), 2040.

Scarlett, J.; Sheard, P.; Hughes, G.; Ledgerwood, E.; Ku, H. & Murphy, M. (2000), 'Changes in mitochondrial membrane potential during staurosporine-induced apoptosis in Jurkat cells', *FEBS letters* **475**(3), 267–272.

Schneider, U.; Schwenk, H. & Bornkamm, G. (1977), 'Characterization of EBV-genome negative "null" and "T" cell lines derived from children with acute lymphoblastic leukemia and leukemic transformed non-Hodgkin lymphoma', *Int J Cancer* **19**(5), 621–626.

Schnelle, T.; Hagedorn, R.; Fuhr, G.; Fiedler, S. & Müller, T. (1993), 'Three-dimensional electric field traps for manipulation of cells–calculation and experimental verification', *Biochimica et Biophysica Acta (BBA)-General Subjects* **1157**(3), 127–140.

Schnelle, T.; Muller, T.; Gradl, G.; Shirley, S. & Fuhr, G. (1999), 'Paired microelectrode system: dielectrophoretic particle sorting and force calibration', *Journal of Electrostatics* **47**(3), 121–132.

Schwartz, J.; Vykoukal, J. & Gascoyne, P. (2004), 'Droplet-based chemistry on a programmable micro-chip', *Lab on a Chip* **4**(1), 11–17.

Shapiro, L. & Stockman, G. (2001), 'Computer Vision', Prentice Hall.

Sonka, M.; Hlavac, V. & Boyle, R. (1999), 'Image processing, analysis, and machine vision second edition', *International Thomson*.

Suehiro, J.; Noutomi, D.; Shutou, M. & Hara, M. (2003), 'Selective detection of specific bacteria using dielectrophoretic impedance measurement method combined with an antigen-antibody reaction', *Journal of Electrostatics* **58**(3-4), 229–246.

Suehiro, J. & Pethig, R. (1998), 'The dielectrophoretic movement and positioning of a biological cell using a three-dimensional grid electrode system', *Journal of Physics D: Applied Physics* **31**, 3298.

Sukas, S.; Elif Erson, A.; Sert, C. & Kulah, H. (2008), 'A parylene-based dual channel micro-electrophoresis system for rapid mutation detection via heteroduplex analysis', *Electrophoresis* **29**(18), 3752–3758.

Tai, C.; Hsiung, S.; Chen, C.; Tsai, M. & Lee, G. (2007), 'Automatic microfluidic platform for cell separation and nucleus collection', *Biomedical Microdevices* **9**(4), 533–543.

Talary, M. & Pethig, R. (1994), 'Optical technique for measuring the positive and negative dielectrophoretic behaviour of cells and colloidal suspensions', *IEE Proceedings-Science, Measurement and Technology* **141**, 395.

Thompson, M. & Krull, U. (1982), 'The electroanalytical response of the bilayer lipid membrane to valinomycin: membrane cholesterol content', *Analytica Chimica Acta* **141**, 33–47.

Thorsen, T.; Maerkl, S. & Quake, S. (2002), 'Microfluidic large-scale integration', *Science* **298**(5593), 580.

Thummel, K. & Wilkinson, G. (1998), 'In vitro and in vivo drug interactions involving human CYP3A', *Annual review of pharmacology and toxicology* **38**(1), 389–430.

Walton, W. (1948), 'Feret's statistical diameter as a measure of particle size', *Nature* **162**(4113), 329–330.

Wang, X.; Becker, F. & Gascoyne, P. (2002), 'Membrane dielectric changes indicate induced apoptosis in HL-60 cells more sensitively than surface phosphatidylserine expression or DNA fragmentation', *BBA-Biomembranes* **1564**(2), 412–420.

Wang, X.; Huang, Y.; Burt, J.; Markx, G. & Pethig, R. (1993), 'Selective dielectrophoretic confinement of bioparticles in potential energy wells', *Journal of Physics D: Applied Physics* **26**, 1278–1285.

Wang, X.; Huang, Y.; Gascoyne, P.; Becker, F.; Hölzel, R. & Pethig, R. (1994), 'Changes in Friend murine erythroleukaemia cell membranes during induced differentiation determined by electrorotation.', *Biochimica et biophysica acta* **1193**(2), 330.

Wang, X.; Huang, Y.; Wang, X.; Becker, F. & Gascoyne, P. (1997), 'Dielectrophoretic manipulation of cells with spiral electrodes', *Biophysical journal* **72**(4), 1887–1899.

Wang, X.; Pethig, R. & Jones, T. (1992), 'Relationship of dielectrophoretic and electrorotational behaviour exhibited by polarized particles', *Journal of Physics D: Applied Physics* **25**, 905.

Wang, X.; Yang, J. & Gascoyne, P. (1999), 'Role of peroxide in AC electrical field exposure effects on Friend murine erythroleukemia cells during dielectrophoretic manipulations', *BBA-General Subjects* **1426**(1), 53–68.

Wang, X.; Yang, J.; Huang, Y.; Vykoukal, J.; Becker, F. & Gascoyne, P. (2000), 'Cell separation by dielectrophoretic field-flow-fractionation', *Anal. Chem* **72**(4), 832–839.

Washizu, M.; Kurahashi, Y.; Iochi, H.; Kurosawa, O.; Aizawa, S.; Kudo, S.; Magariyama, Y. & Hotani, H. (1993), 'Dielectrophoretic measurement of bacterial motor characteristics', *IEEE Transactions on Industry Applications* **29**(2), 286–294.

Washizu, M.; Kurosawa, O.; Arai, I.; Suzuki, S. & Shimamoto, N. (1995), 'Applications of electrostatic stretch-and-positioning of DNA', *IEEE Transactions on industry applications* **31**(3), 447–456.

Washizu, M.; Suzuki, S.; Kurosawa, O.; Nishizaka, T. & Shinohara, T. (1994), 'Molecular dielectrophoresis of biopolymers', *IEEE Transactions on Industry Applications* **30**(4), 835–843.

Whitesides, G. (2006), 'The origins and the future of microfluidics', *NATURE-LONDON-* **442**(7101), 368.

Yang, J.; Huang, Y.; Wang, X.; Becker, F. & Gascoyne, P. (2000), 'Differential analysis of human leukocytes by dielectrophoretic field-flow-fractionation', *Biophysical journal* **78**(5), 2680–2689.

Yang, J.; Huang, Y.; Wang, X.; Wang, X.; Becker, F. & Gascoyne, P. (1999), 'Dielectric properties of human leukocyte subpopulations determined by electrorotation as a cell separation criterion', *Biophysical journal* **76**(6), 3307–3314.

Yang, M. & Zhang, X. (2007), 'Electrical assisted patterning of cardiac myocytes with controlled macroscopic anisotropy using a microfluidic dielectrophoresis chip', *Sensors & Actuators: A. Physical* **135**(1), 73–79.

Yang, Q. (2005), 'Design of a Four-Phase High Frequency Amplitude-Stable Power Supply', *Biomedical Microdevices* **7**(3), 243–246.

Zimmermann, U. & Neil, G. (1996), *Electromanipulation of cells*, CRC.

Appendix

Appendix A

User's manual

The following is a brief step-by-step guide in both conducting an experiment and analysing the captured images. Note that this guide may change in the future as the program is further developed.

A.1 Conducting an experiment

Step 1: Run the program (currently named as `Syscontrol.exe`)

Step 2: Select 'Real Time Analysis' on the Program Mode window

Step 3: Select the COM Port that the RS-232 cable is attached. Select the number of waveform generator output channels to be used for the experiments (currently limited to 8 parallel output channels).

Step 4: 'Signal Control' panel:

- Click the 'Master Reset' button to reset the system prior to conducting an experiment
- Click the 'ID' button
- Click the 'Output On' button to test the output channels. Attach each of the output cables to an oscilloscope to verify the outputs that were set at 10 V_{p-p} with 10 kHz frequency. Click 'Output Off' once the outputs have been checked
- Click on the 'Tune' button on the Channel Tuning subpanel to set the output frequencies of the input signals
- Select the appropriate number of channels, the starting and ending frequency values, and the desired number of points per decade
- Click on the 'Set Channels' button (should be red in colour)

Step 5: 'Image Acquisition and Analysis Control' panel:

- Select the appropriate Experiment and System Types from the drop-down menu.
- Click on the 'Conditions' menu. Enter appropriate parameter values for the experiment.

- Select a video camera to use by selecting from the 'Adaptor Device' drop-down menu. Select the desirable size format for the captured images to be saved in the 'Format' drop-down menu.

- Click the 'Preview' button to preview the video camera. The output should appear on Axes 1. Click on the 'Parameters' button to set the output to greyscale format.

Step 6: Cell sample preparation:

- Connect all cables to the corresponding SMB connectors on the microelectrode device

- Adjust the position of the device such that the desired dots appear at the centre of the microscope view

- Push a small amount of cell suspension to fill up the experimental chamber using a syringe

Step 7: Click on the 'START EXP.' button to start the experiment.

Step 8: Once the signal has been turned off, click on the 'Conditions' button. Enter any new parameter values that are different than the previous experiment.

Step 9: Re-disperse the cell suspension within the experimental chamber by pushing in and out a small amount of the solution

Step 10: Repeat Step 7

A.2 Analysing captured images

Step 1: Run the program (currently named as `Syscontrol.exe`)

Step 2: Select 'Offline Analysis' on the Program Mode window

Step 3: 'Analysis and Plot Options' panel:

- Click on the 'Load Data' button. Select the desired file to be analysed. Click OK.

- Click on the 'Get Regions of Interest' button. Enter the appropriate number of dots in the horizontal and vertical axes

- If an error is produced, change the value of the intensity threshold by changing the number in the 'I.T.' field

- Once the ROI segmentation is completed, click on the 'Process Data' button.

- Once the processing is completed, the results may be plotted in Axes 2 by selecting the desired plot types in the 'Plot Options' drop-down menu

Step 4: Analysed data may be saved by clicking on the 'Save analysed data' button

Appendix B

Electronic files

The following is a list of files that were included in the attached CD-ROM:

- Circuit diagram for the multiple output waveform generator (Versions 1 and 2)
- Printed circuit board footprint for the multiple output waveform generator (Versions 1 and 2)
- Microprocessor program in assembler language to be used within the multiple output waveform generator (Version 1)
- Main control program to conduct DEP experiments and analyse captured images (Version 2)
- Selected DEP experimental data (NB. Total file size of all experimental data is more than 20 GB)